UNIVERSIDAD DE MURCIA

FACULTAD DE MEDICINA

Methods to Measure Intraocular Scattering
and Its Impact in Vision

Metodos de Medida de la Difusión Intraocular
y su Impacto en la Visión

D. Alexandros Valentinos Pennos

2017

Universidad de Murcia

Departamento de Física

Laboratorio de Óptica

METHODS TO MEASURE INTRAOCULAR SCATTERING AND ITS IMPACT IN VISION

METODOS DE MEDIDA DE LA DIFUSIÓN INTRAOCULAR Y SU IMPACTO EN LA VISION

Thesis presented at the Faculty of Medicine

of the University of Murcia by:

Alexandros Valentinos Pennos

To attain the degree of PhD from the University of Murcia.

Laboratorio de Óptica. Departamento de Física. Universidad de Murcia.
April 2017

Dedicated to my parents, Panagiotis and Evangelia and especially to my brother Christos.

TABLE OF CONTENTS.

LIST OF FIGURES.

LIST OF TABLES.

LIST OF ABBREVIATIONS.

VF:	Visual Function
VA:	Visual Acuity
CDVA:	Corrected Distance Visual Acuity
D:	Diopters
OCT:	Optical Coherence Tomography
LCA:	Longitudinal Chromatic Aberrations
TCA:	Transverse Chromatic Aberrations
RPE:	Retinal Pigment Epithelium
ILM:	Inner Limiting Membrane
PSF:	Point Spread Function
MLB:	Multi-Lamellar Bodies
IOL:	Intraocular Lens
S:	Straylight Parameter
CS:	Contrast Sensitivity
PCO:	Posterior Capsule Opacification
CSF:	Contrast Sensitivity Function
VCTS:	Vision Contrast Test System
CCD:	Charged Coupled Device
DLP:	Digital Light Processing
CMOS:	Complementary Metal Oxide Sensor
IDE:	Integrated Development Environment
ROI:	Region of Interest
GUI:	Graphical User Interface
PSF_{dp}	Double Pass Point Spread Function
FWHM:	Full Width Half Maximum
AULCSF:	Area Under Logarithmic Contrast Sensitivity Function
DAQ:	Data Acquisition Card
MPOD:	Macular Pigment Optical Density
MP:	Macular Pigment
HFP:	Heterochromatic Flicker Photometry
SiPM:	Silicon Photo-Multiplier

RESUMEN

Objetivos

En esta tesis se han desarrollado varios de estudios sobre la luz difundida en el ojo, o "scattering" intraocular. Este fenómeno, debido principalmente a la interacción de la luz con variaciones del índice de refracción en las estructuras oculares, reduce la calidad de la visión y sus efectos aumentan con el envejecimiento o algunas patologías relacionadas, tal como las cataratas. Así, el objetivo inicial de esta tesis ha sido investigar y establecer nuevos métodos para una evaluación precisa del scattering generado por materiales similares a los que componen el ojo humano, como una primera aproximación a la medida del scattering intraocular.

Los efectos del scattering en la calidad de la visión no han sido examinados a profundidad. Por esta razón, un segundo objetivo de la tesis fue la evaluación precisa de la influencia del scattering sobre la función visual en términos de una métrica física ampliamente entendida, tal como lo es la cantidad de luz disfundida, o parámetro S.

La evaluación de la cantidad precisa de scattering intraocular, el entendimiento de su naturaleza y sus efectos en la calidad de la visión, requieren métodos precisos e innovadores. Por tanto, con los objetivos anteriormente mencionados se contribuye a la mejora de la visión.

Métodos.

En general, la función que representa la distribución de luz en la imagen de un punto (PSF; del inglés Point Spread Function) describe la propagación a través de las componentes de un sistema óptico. Se desarrolló un método para reconstruir la PSF ocular, incrementando la sensibilidad para detectar la luz dispersada en ángulos amplios. La principal ventaja de este método es el uso de un detector convencional sin requerimientos avanzados de rango dinámico. El método, llamado de integración óptica, se basa en la medida de la intensidad en un área específica, la cual es entendida como la suma de las contribuciones provenientes de las fuentes puntuales de luz ubicadas alrededor. Inicialmente, este método fue implementado para caracterizar la cantidad de luz dispersada por algunos elementos ópticos y biomateriales. En particular, se caracterizaron varios diseños de lentes intraoculares. Además, este método fue aplicado para cuantificar el scattering de los edemas inducidos en muestras de córneas de cerdo cuya hidratación fue alterada de manera controlada.

Seguidamente, el método de integración óptica se adaptó para la medida in vivo del parámetro S en ojos humanos. El montaje óptico para esta tarea está basado en una configuración de doble paso. El procedimiento consiste en la proyección de discos con intensidad uniforme sobre la retina y el posterior registro de la intensidad central en las imágenes reflejadas en el fondo del ojo. Un primer resultado de este método es la estimación de la PSF ocular con un rango angular

(diámetro) de 16 grados. Además, varias longitudes de onda fueron usadas para las para examinar su efecto en la distribución angular de la luz dispersa en el fondo del ojo.

Tras la validación experimental en banco óptico, un prototipo del dispositivo basado en el método de integración óptica fue desarrollado para la medida rápida de la cantidad de scattering en el ojo. Este instrumento fue diseñado para ser usado en entornos clínico. Por lo tanto, sus dimensiones son reducidas y la fuente de iluminación de la retina fue simplificada usando LEDs (del inglés Light Emitting Diode) cuasi-monocromáticos para proyectar un disco central y un anillo, en lugar de varios discos. Así, el tiempo total requerido para una medida es 300 milisegundos, lo cual es un similar al tiempo de contracción de la pupila debido a la iluminación percibida durante el examen. En consecuencia, las medidas pueden ser realizadas sin la necesidad de dilatar la pupila, evitando las molestias que tal procedimiento conlleva.

Posteriormente, el prototipo se usó en un estudio clínico para la estimación objetiva del nivel de transparencia del medio ocular en pacientes con cataratas. Para ello, el instrumento fue instalado en el departamento de oftalmología del hospital universitario Virgen de la Arrixaca en Murcia. El parámetro S, la métrica proporcionada por el instrumento, se comparó con otros resultados de valoraciones subjetivas sobre el estado de las cataratas de los pacientes evaluados.

El scattering intraocular tiene un impacto significativo en la calidad visual, el cual no siempre es evidente en las pruebas de agudeza visual convencionales. Por otra parte, se ha reportado que la valoración de la sensibilidad al contraste (SC) para diferentes frecuencias espaciales, aunque es una prueba psicofísica, permite valorar el impacto del scattering intraocular. Sin embargo, se ha demostrado que, en general, los valores resultantes de la SC no pueden compararse directamente con otras métricas que describen la transparencia de los medios ocular y sus efectos. Es así como se documenta un vínculo directo entre los valores de SC y el parámetro S. Se estableció la medida diferencial de la SC mediante el uso de una fuente de deslumbramiento. Se evaluó una métrica para la valoración del scattering intraocular mediante la comparación de los valores del parámetro S medido con dos instrumentos. Los resultados de un estudio piloto empleando filtros difusores para simular los efectos de las cataratas, mostraron que todas las métricas se correlacionaron entre sí. Un paso adelante en el mismo objetivo fue el aprovechamiento de los dispositivos portátiles de uso cotidiano, tal como los teléfonos inteligentes o tabletas, para la estimación rápida del parámetro S. Estos dispositivos han evolucionado para tener grandes prestaciones en su capacidad de procesamiento y calidad de video. De esta forma, se programó una rutina para la medición diferencial de la SC en una tableta comercial (iPad, Apple Inc., California, U.S.A.) combinada con el uso de un anillo de LEDs como fuente externa de deslumbramiento. Esta metodología, la caracterización previa de la intensidad luminosa de la pantalla y la comparación de los resultados obtenidos de S con otro instrumento, se describen en este trabajo.

Una nueva aplicación fue desarrollada a partir de las nuevas metodologías y dispositivos para la cuantificación del scattering intraocular. Se trata de la cuantificación de la densidad óptica de pigmento macular (MPOD, del inglés

Macular Pigment Optical Density). Este instrumento está basado en el diseño del dispositivo compacto para la medida del parámetro S pero con la introducción de diversas modificaciones. Por ejemplo, la incorporación de dos fuentes LED, con luz verde (528 ± 10 nm) y azul (465± 15 nm), que simultáneamente iluminan el fondo del ojo. Por cada fuente, la iluminación que se proyecta en la retina está dividida en dos partes: un disco central y un anillo sobre la zona periférica. Finalmente, se desarrolló un estudio piloto en una población de ojos sanos, con edad promedio 31 ± 9 años, para la valoración de la precisión y sensibilidad del dispositivo.

Resultados.

Caracterización de la cantidad de luz dispersada por difusores, materiales y tejidos biológicos

El método de integración óptica fue usado para la evaluación del scattering producido por filtros fotográficos comerciales, los cuales son comúnmente usados para la simulación de los efectos de las cataratas. Los resultados obtenidos están en concordancia con la densidad indicada por el fabricante y con los valores absolutos reportados previamente. Posteriormente, este mismo montaje experimental fue usado para caracterizar la cantidad de luz difundida por lentes intraoculares (LIOs) monofocales y multifocales comercialmente disponibles. Se encontró una mayor generación de scattering en las lentes multifocales que en las lentes monofocales. Sin embargo, los efectos en la función visual debido al scattering adicional presente en las LIO multifocales, en comparación a las monofocales, deben ser evaluados en vivo. Esta experiencia demuestra la capacidad del método para detectar pequeños incrementos en el parámetro S, como los debidos al tipo de LIO.

Con esta metodología se confirmó que el edema corneal produce un incremento del scattering intraocular, midiendo el parámetro S en muestras de córneas porcinas con diferentes niveles de hidratación. Finalmente, se explica el mecanismo responsable del incremento de luz dispersada, el cual está basado en la pérdida de la organización de las fibras de colágeno en el estroma, debido a la creación de burbujas de agua.

Medidas in vivo del scattering intraocular con el método de integración óptica

La metodología anteriormente descrita, ahora aplicada en un sistema de doble paso, reveló la posibilidad de realizar medidas en vivo del scattering intraocular de forma objetiva. El sistema experimental fue inicialmente probado en un ojo artificial y el scattering fue inducido usando filtros fotográficos. Posteriormente, se llevaron a cabo medidas en vivo, donde el efecto de las cataratas fue reproducido mediante el uso de lentes de contacto especialmente diseñadas. El scattering intraocular medido fue similar al reportado previamente en la literatura. Además, fueron registrados los incrementos de la luz dispersada debido al uso de las lentes de contacto.

Dependencia del scattering intraocular con la longitud de onda

Las medidas del scattering intraocular con diferentes longitudes de onda revelaron el efecto de las capas en el fondo del ojo sobre la dispersión de la luz. Según los

resultados, mientras la dispersión de la luz con longitudes de onda menor se puede explicar desde la interacción de la luz con las fuentes de scattering, la dispersión de la luz con longitudes de onda mayores obedece principalmente a un fenómeno de difusión en las capas profundas del fondo ocular.

Prototipo del dispositivo para medidas clínicas del scattering intraocular

Se llevó a cabo un estudio piloto en un entorno clínico usando el prototipo de un dispositivo compacto basado en el método de integración óptica. Los resultados fueron comparados con medidas hechas con otros dispositivos disponibles comercialmente, como el instrumento C-Quant (Oculus, Wetzlar, Alemania). El resultado más importante fue la alta correlación encontrada entre las medidas objetivas y subjetivas realizadas usando el prototipo y el C-Quant, respectivamente. En el estudio se identificaron las siguientes ventajas ofrecidas por el prototipo desarrollado para el uso clínico: i) la posibilidad de realizar mediciones precisas del parámetro S sin la necesidad de dilatar la pupila, ii) portabilidad y iii) examinación rápida del paciente a través de una operatividad simple.

Sensibilidad al contraste diferencial: Un método psicofísico para la estimación del scattering intraocular

Un estudio en una pequeña población reveló la alta correlación encontrada entre el método propuesto y dos dispositivos empleados para la estimación directa del scattering intraocular. En el estudio se usaron filtros fotográficos para simular los efectos de las cataratas. Además, las medidas aportadas por el método son repetibles.

Aplicación de la sensibilidad al contraste diferencial en dispositivos portátiles (teléfonos o tabletas)

El método desarrollado fue aplicado a un dispositivo portátil fácilmente accesible como una propuesta para la detección temprana de las cataratas (u otras patologías que afecten la sensibilidad al contraste) en países en desarrollo. Los procedimientos para su implementación, al igual que los resultados de un estudio en una pequeña población, son describen en detalle. Este es un método subjetivo eficaz para la evaluación del scattering intraocular y su seguimiento temporal.

Mediciones de la densidad óptica dekl pigmento macular usando un prototipo compacto de doble paso

Los resultados de un estudio piloto indicaron que el dispositivo puede medir la densidad de pigmento macular correspondiente a cada sujeto, los cuales se encontraron en los rangos normales (en promedio 0.43 con una desviación estándar de 0.10). Además, estos resultados fueron comparados con estudios reportados, sobre poblaciones de mayor tamaño, donde se emplearon otras metodologías.

Conclusiones.

- Fue establecido un nuevo método para la reconstrucción de la PSF en un amplio rango angular, permitiendo evaluar el scattering presente en los sistemas ópticos y sus componentes.

- Inicialmente, el método se implementó en un sistema de paso simple con el que se caracterizaron difusores comercialmente disponibles, los cuales han sido ampliamente usados anteriormente para simular los efectos de las cataratas.
- Este método se usó para estimar la cantidad de luz difundida por lentes intraoculares de diferentes diseños y procesos de fabricación.
- Se esclareció la relación entre el scattering generado y el nivel de hidratación del estroma corneal. El scattering se genera por la pérdida de la organización entre las fibras de colágeno por la ocupación del agua.
- El método para la reconstrucción de la PSF fue adaptado en un sistema de doble paso para la medida in vivo del scattering intraocular en el ojo humano.
- La dependencia del scattering con la longitud de onda de iluminación fue medida y explicada. Se evidenció que la propagación de la luz con longitudes de onda corta está afectada por su interacción con los dispersores, cuyo tamaño es similar a la longitud de onda. Por otra parte, los fenómenos de absorción y difusión en el fondo del ojo son predominantes en la dispersión de la luz con longitudes de onda mayor, incluyendo el infrarrojo cercano.
- Las metodologías y los conocimientos adquiridos en los estudios anteriores fueron aplicados en el desarrollo de un dispositivo para la medida rápida y precisa del scattering intraocular en un entorno clínico. Un estudio piloto evaluó la repetitividad y eficacia de los resultados obtenidos mediante la comparación con los aportados por otro dispositivo.
- Por otra parte, se desarrolló una nueva metodología para la estimación subjetiva del scattering intraocular a partir de la medida diferencial de la sensibilidad al contraste. Se basa en la comparación de los valores de sensibilidad al contraste cuando una fuente de deslumbramiento, con una geometría e intensidad determinadas, está presente o no. Los resultados obtenidos con este método se compararon con los proporcionados por dos dispositivos, cuya medición del scattering intraocular se realiza subjetivamente (C-Quant) y objetivamente (el prototipo desarrollado con la técnica de doble paso).
- La metodología diferencial se implementó en un dispositivo portátil y compacto (iPad), cuyas propiedades de iluminación fueron previamente caracterizadas. La aplicación desarrollada es intuitiva y accesible, posibilitando la evaluación rápida del scattering intraocular sin la necesidad de dispositivos costosos. Los resultados de un estudio piloto confirmaron la repetitividad de las mediciones subjetivas hechas con este desarrollo.
- Finalmente, la experiencia y conocimiento adquiridos sobre la estimación del scattering intraocular permitieron el desarrollo de un prototipo para la medida de la densidad óptica de pigmento macular. Una comparación cuantitativa mostró que este dispositivo basado en la reflectancia y

absorción de las zonas retinianas centrales y periféricas, puede estimar objetivamente las densidades del pigmento macular de manera simple.

SUMMARY

A very comprehensive way to characterize an optical system, such as the human eye, concerning its optical quality, is to obtain its Point Spread Function; a function that describes the angular re-distribution of the light, deriving from a point source and propagated through the optical system.

Optical phenomena, like diffraction or refraction have been thoroughly studied and described in the past two, or more, decades. An additional phenomenon that significantly affects the performance of an optical system, is scattering. This refers to the deviation of light as it is being propagated through a medium containing refractive index irregularities. The exact effect on the course or other characteristics of light, is defined by the size of these optically irregular areas and depends on their distribution and number. The effect of light scattering is not limited to the higher spatial frequencies of an image, but also affects the lower ones, degrading the imaging performance by decreasing the contrast. This loss of contrast depends also on the dynamic range of the imaged scene both locally and globally, as scattered intensity can be spread to a wide angular range.

One of the purposes of this thesis was to establish a method that would be able to extract the Point Spread Function of any given optical system, being less vulnerable to cases where a wide dynamic range detector is needed to pick up the intensity re-distribution even at wide angles. Initially, this methodology was used to characterize scattered light by materials, lenses and biological tissues.

Later this was applied to characterize, in vivo, the human eye. For this attempt, special methodology and instrumentation was developed and applied. We first studied the possible wavelength dependence of the intraocular scattering. Additionally, a compact clinical device was developed.

In parallel, a new method to evaluate the effect of intraocular scatter on visual performance was developed. This was compared with other established metrics for the quantification of intraocular scatter. To make the method even more intuitive and accessible, a portable, low-cost version of it was proposed by using a tablet.

Finally, the experience and the know-how from the modalities and methods developed to measure scattering in the human eye, by depicting a pattern on the retina and imaging it simultaneously, where applied for the development of a compact optical setup to evaluate the density of the macular pigment, a centrally localized area of the fundus where high concentration of specific pigments is observed, with an important role in the ocular function and in the potential prevention of some retinal diseases.

1. INTRODUCTION

For many years, the visual function (VF) was described only by visual acuity (VA); the quantification of the perception of fine detail. The Corrected Distance Visual Acuity (CDVA) is routinely tested by clinicians, where VA charts and appropriate trial lenses are used. In some particular cases, although CDVA scores are adequately high, the VF remains poor, mainly because natural scenes comprise of a large combination of contrasts, luminance and spatial frequencies.

In this chapter, a brief description of the complexity of VF is presented. It is explained which part of it is described by VA and the necessity of a more well-rounded descriptor of the visual function, containing the missing information of the quantity of intraocular straylight.

Finally, the state of the art methods for the complete description of the VF are documented, both for the measurements of the intraocular scattering (see sub-chapter 1.7.2) and for the quantification of its impact on contrast sensitivity (see sub-chapter 1.7.1).

1.1 The Eye as an Optical System

The human eye is a light sensory organ that captures visual information from the environment and transfers it to the brain to complete crucial living tasks. As demonstrated in Figure 1, it consists of a spherical, composite structure with an external diameter of 24-mm approximately, held in position by six muscles giving it the ability to perform an almost perfect rotation. The elements with a key role in the eye's function as an optical system, are the cornea, the lens (mutually responsible for the image formation) and the retina (responsible for the image detection and transmission of the signal to the brain). A number of structures, such as the iris, the choroid, the vitreous and the sclera, have a supportive role in the eye's function, i.e. providing protection, nutrition or adjusting the amount of light that reaches the retina (Nickla & Wallman, 2010; Trier, 2005).

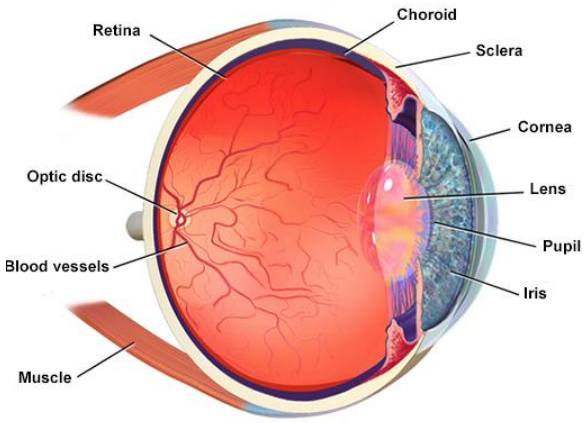

Figure 1. Schematic of the human eye (Source: Bruce Blaus/Wikimedia commons).

As for its optical functionality, the human eye, compared to its resulting imaging capabilities, is far from being complex. The formation of the image of an object is being done through two lens-like components; the cornea and the crystalline lens. Between them, the pigmented iris separates the eye chamber filled with aqueous humor and provides the supportive optical role of regulating the light that reaches the retina, similarly to a circular diaphragm. Due to a slight misalignment of the cornea and the lens the visual axis and the visual axis do not coincide and therefore the image of an object lying on the optical axis will be created at about 4 degrees off-axis, on a location on the retina called the fovea (Artal & Tabernero, 2008).

The cornea is a transparent, avascular meniscus-shaped lens, with an outer surface curvature of approximately 8-mm and an average of about 0.5-mm central thickness, responsible for roughly one third of the total refractive power of the eye. In particular, its refractive power is about 48 D, when surrounded by air, with a refractive index of 1.376. Behind the posterior surface of the cornea the chamber formed by the posterior cornea and the anterior lens is filled with aqueous humor, a water-like liquid, with a refractive index of 1.336, that reduces the effective refractive power of the cornea to about 42 D (Asbell & Brocks, 2010; Cox, 2001). The cornea consists of five layers (Figure 2): The epithelium, the Bowman's membrane, the stroma, Descemet's Membrane and the endothelium (Bron, Tripathi, Tripathi, & Wolff, 1997). The stroma, which makes up for about 90% of the total volume of the cornea, has a very tightly organized structure, necessary for maintaining the cornea's transparency.

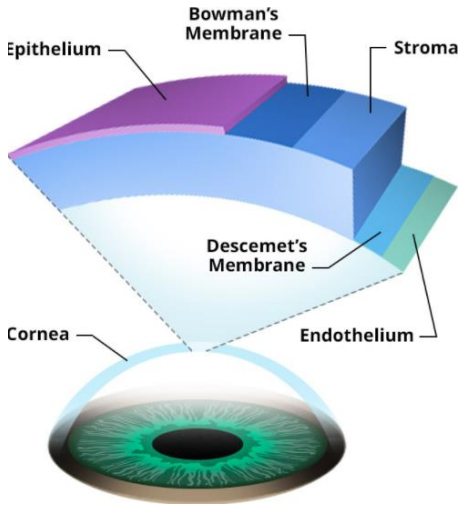

Figure 2. Corneal layers (Source: Vance Thompson).

A thin tear film is covering the external surface of the cornea. Produced continuously by the lacrimal gland, the tear film's function is to buffer any corneal irregularities thus playing an important role in the quality of the retinal image.

The second refractive element of the eye, the lens, is a transparent, biconvex structure, positioned right behind the iris (Figure 3). Given the fact that the lens has no blood supply after fetal development, its metabolic requirements and waste disposal are covered entirely from the aqueous humor. It lies posteriorly to the iris

and anteriorly to the vitreous body. The zonules of Zinn that are responsible for its mechanical support and attachment to the ciliary body, consist of fine but mechanically strong fibers. The lens is composed of the capsule, lens epithelium, cortex, and nucleus. The imaginary line that connects the anterior and posterior poles of the lens is called the optic axis, whereas the imaginary axes crossing the surface of the crystalline lens, connecting the two poles are its meridians. The equator of the lens is its greatest circumference. The refractive index of the lens is around 1.4 centrally and 1.36 peripherally (Cox, 2001), significantly different from that of the aqueous and vitreous that surround it. In its non-accommodative state, the lens contributes about 15–20 D of the approximately total 60-D of refractive power of the average eye. Throughout life, the size of the lens is continuously growing. Initially, its size is limited to about 6.4 mm equatorially and 3.5 mm anteroposteriorly and weighing only 90 mg, with the adult lens becoming approximately 9 mm equatorially and 5 mm anteroposteriorly and increasing its mas at approximately 255 mg. The relative thickness of the cortex increases with age as well. Additionally, the shape of the lens also changes throughout life, adopting a curved shape, offering more refractive power to older lenses. On the other hand, the refractive index is decreasing with age, as a result of the increasing presence of particles consisted of proteins (www.aao.org).

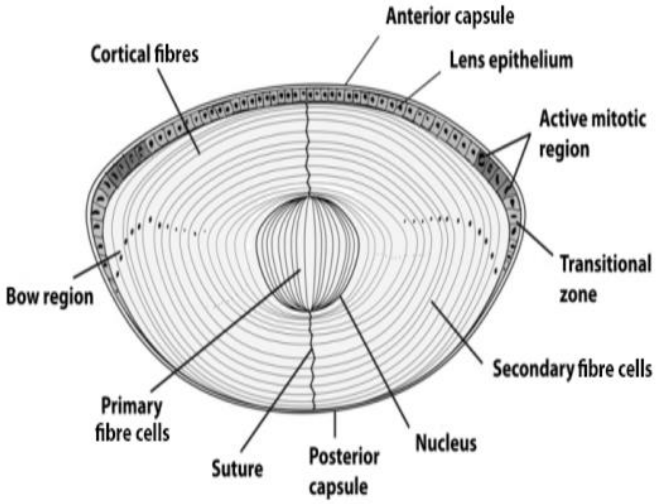

Figure 3. Schematic od the crystalline lens of an adult human (Source: adapted from Openi).

Posteriorly to the lens lies the vitreous body consisting of the vitreous humor, as mentioned previously, with identical optical properties to the aqueous humor.

The retina has an average thickness of about 0.5 mm. Surprisingly, the photoreceptors do not come first in the light path in the retina, but rather last, with the light traveling the entire retina before being detected. This "inverted" structure has been the subject of many studies and has been considered a major imperfection of the human eye. Recently, a study has shown, however, that Muller cells in the retina act as waveguides for the mid-long wavelengths and scatter the

shorter wavelengths, improving this way vision (Labin, Safuri, Ribak, & Perlman, 2014).

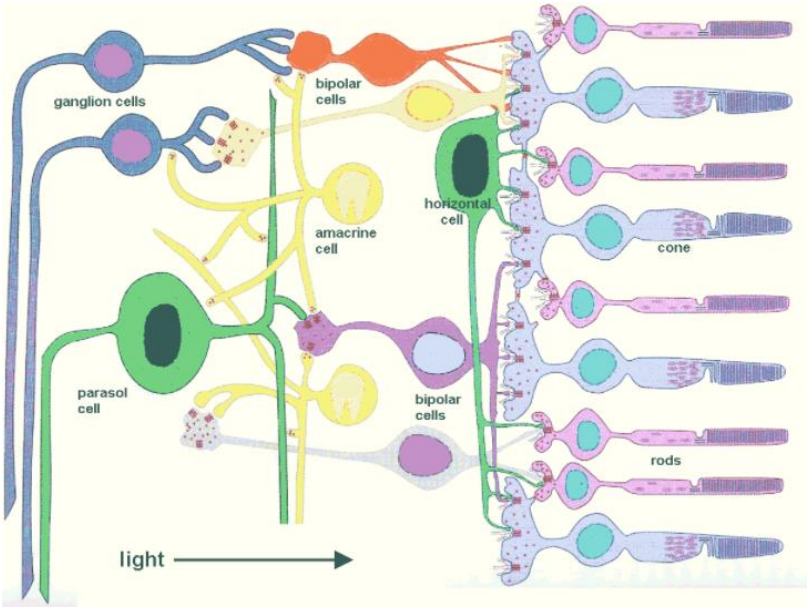

Figure 4. Simplified diagram of the position of photoreceptors (Source: adapted from Dowling (1997) Encyclopedia of Human Biology)

The retinal function can be described briefly and simply as: first, the detection at the photoreceptors then transmission to the bipolar cells and from there to the ganglion cells concluding to transmission through the optic nerve(Figure 4). The retina, apart from the elements related to light detection, is also comprised of layers that have a protective role, namely the Inner Limiting Membrane (ILM), Bruch's Membrane and the Retinal Pigment Epithelium (RPE). The RPE is a melanin-containing mono-layer that lies between the photoreceptors and choroid and, though it doesn't participate directly in vision, has an essential role in the correct function of the retina. Firstly, due to its highly melanin content, it absorbs light exiting the photoreceptors, thus reducing scattering (Bok, 1993). Additionally, it controls the flow of fluid and nutrients from the blood to the retina and vice versa (Steinberg, 1985) and it participates in the regeneration of the pigment (Figure 5).

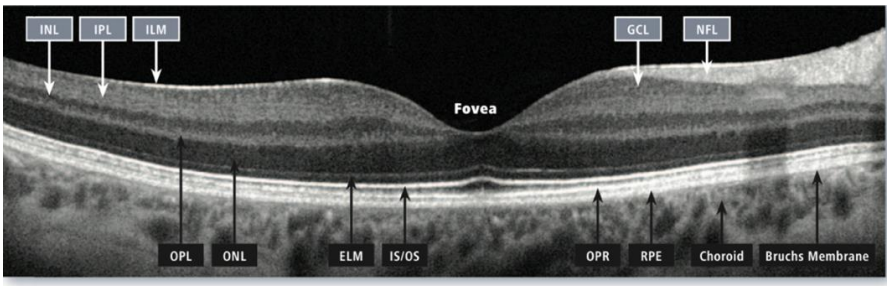

Figure 5. Retinal layers imaged by Optical Coherence Tomography (OCT) (Source: Desinee Drakulich).

1.2 Retinal Image Quality

1.2.1 Diffraction

Diffraction refers to various phenomena which occur when light, as a wave, interacts with an obstacle or an aperture and describes the bending and its consequent deviation from geometrical optics. In the particular case of the eye, diffraction occurs at the pupil.

In an imaging system, such as the human eye, the effects of the diffraction taking place at the pupil, can be calculated using the Fraunhofer (far-field) approximation, where the image plane (the retina) is far away from the aperture (pupil). For a circular aperture of radius *r*, the intensity is calculated by the following equation:

$$I(\theta) = I_o \left(\frac{2J_1\left[\frac{1.22\,\pi\, r\, sin(\theta)}{\lambda}\right]}{\frac{1.22\,\pi\, r\, sin(\theta)}{\lambda}} \right)^2$$

Equation 1

where θ the angle between the x and z axes and J_1 is the Bessel function of first order. Accordingly, the irradiance distribution is presented in figure 6:

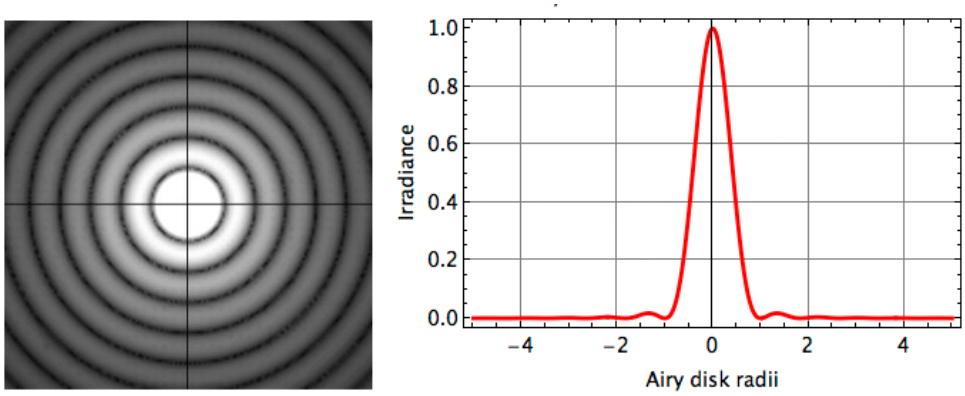

Figure 6 Irradiance profile for diffraction from a circular aperture

The equation show the dependence of diffraction on the size of the aperture and on the wavelength of the light. The size of the central disk is the minimum solution of *Equation 1* equals to: $\theta = \frac{1.22\lambda}{2r}$. From the above, for pupil diameters between 1-mm and 7-mm, it is clear that for the case of the eye, diffraction affects only the very central part of the PSF, limiting its effect no more than 3 minutes of arc.

1.2.2 Aberrations

A perfectly designed optical system would be limited only by diffraction. In the case of the human eye, this is far from happening. By rule, it is suffering from optical imperfections. As it was briefly described earlier, it is consisted of several parts and layers, that are always subject into small changes throughout life. These characteristics result to optical aberrations which depend on the different wavelength (monochromatic and polychromatic), are symmetrical and asymmetrical and as a result, can severely deteriorate image quality. The most optically significant monochromatic aberrations are *defocus, astigmatism, coma and spherical aberrations* whereas, the polychromatic aberrations can be either *longitudinal or transverse* (Artal, 2015).

Chromatic aberrations in the eye are caused by the fact that the index of refraction each eye's optical component is different for every wavelength. This is the main cause of the existence of two types of chromatic aberrations: Longitudinal Chromatic Aberrations (LCA) and Transverse Chromatic Aberrations (TCA). In LCA the difference in the refractive power causes shorter wavelength to focus earlier than longer wavelengths, whereas in the case of TCA, unequal refractive compensation at lens surfaces cause a lateral shift of the image (Figure 7). Moreover, assuming that the wavelength where LCA is zero at 560-nm for the average eye, the curve becomes steeper when moving towards the shorter region of the spectrum. Therefore, LCA is stronger for shorter wavelengths. LCA can severely affect the PSF, in the same way that defocus does, whereas TCA simply displace the image and have no effect on the PSF.

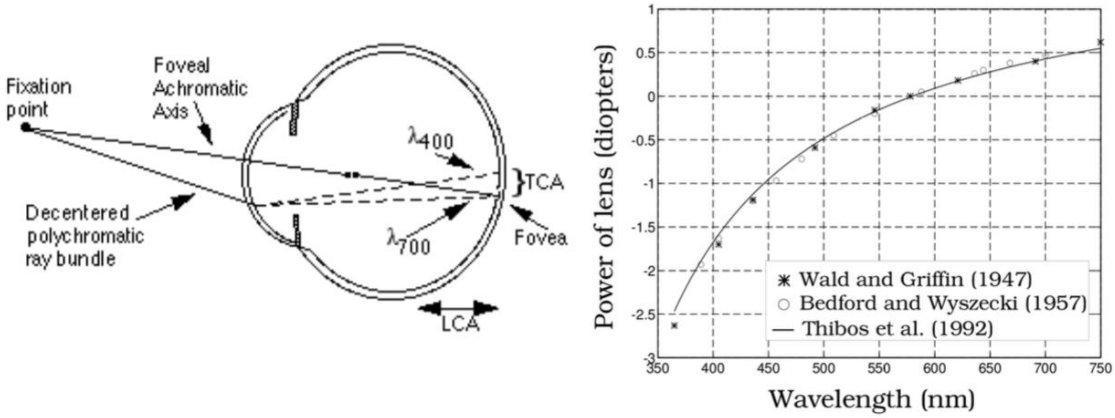

Figure 7: LCA and TCA in the human eye (left). Effect of LCA in diopters with respect to wavelength (Source: Bradley and Thibos)

Monochromatic aberrations are caused by the curvature of the optics, local deformations of the surfaces and describe any deviation from the paraxial optics approximation. The most common representation for monochromatic wavefront aberrations in physiological optics is the Zernike polynomial representation (Noll, 1976). Each term Z_n^m, also called mode of the polynomial, corresponds to a specific type of irregularity and it is accompanied by a coefficient c_n^m expressing the magnitude of the specific term. Its absolute value corresponds to the RMS

wavefront error. Eye's aberrations depend on pupil diameter, increasing significantly with it (see Figure 8). In order to achieve diffraction-limited imaging in the eye, the pupil needs to be smaller than 2mm.

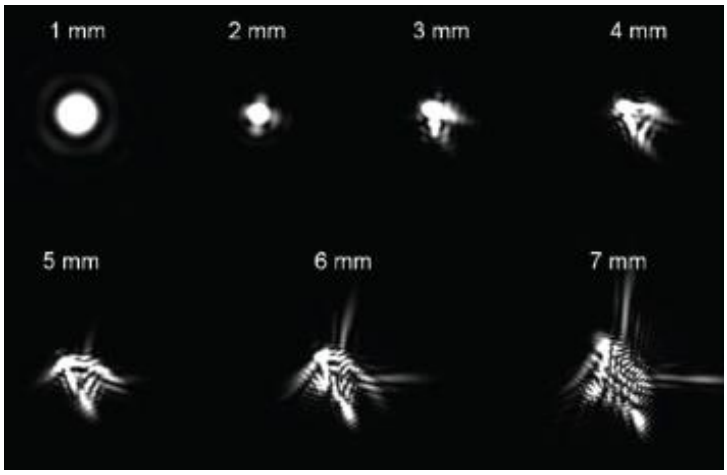

Figure 8. Characteristic Point Spread Functions (PSF's) for different pupil sizes (Source: Roorda).

Zernike modes are categorized in low-order, for radial order n < 3, and high-order, for radial order n ≥ 3. The lower the radial order, the more central the part of the PSF affected by it (Figure 9).

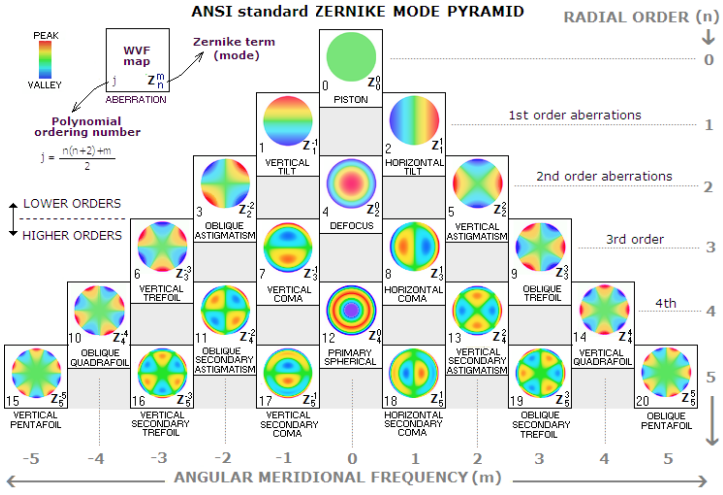

Figure 9. ANSI standard for Zernike modes (Source: Parra).

1.2.2 Straylight

The term “ocular straylight”, is used to describe the amount of light that has been scattered, due to optical imperfections, as it is propagated throughout the human eye. The effect of straylight is the deviation of light from the central part of the PSF, towards its skirts. In the literature, scattered light, intraocular straylight or disability glare, are almost synonyms and all of them refer either to the phenomenon itself or to its impact in VF (T J T P van den Berg, Franssen, & Coppens, 2010). Straylight affects VF differently than aberrations.

A useful observation that can help in the identification of the structures responsible for the scattering in the ocular media is the fact that the size of the scattering structure has a direct effect on the scattering angle. This dependence derives directly from the Maxwell's equations and it is generally called Mie solution, or Mie scattering, and it describes the scattering of the electromagnetic radiation from spherical particles. Depending on the particles size in comparison to the wavelength the scattering phenomenon can be describe by either the Rayleigh approximation, the Rayleigh-Gans-Debye approximation, or the Mie approximation.

In the Rayleigh approximation, or Rayleigh scattering, particles need to be sufficiently small, approximately a tenth of the wavelength (Van De Hulst, 2003). Scattering has a strong wavelength dependence $1/\lambda^4$ and is proportional to $1 + cos^2\theta$. That means that it is stronger for shorter wavelengths and it is higher at 0 and 180 degrees.

In the Rayleigh-Gans-Debye approximation, an additional restriction is applied; the refractive index of the scattering particle needs to be close to that of the surrounding, or more specifically, the difference between the refractive indexes multiplied by a dimension of the particle is smaller than the wavelength (Van De Hulst, 2003). This approach is generally valid for particles bigger than the Rayleigh approximation. The scattering angle is smaller and the dependence on wavelength weaker, depending on the size of the particle and the refractive index.

Mie scattering, though being the solution to Maxwell's equations is applicable to any scale, historically is defined as light scattering for particles at the order of the wavelength and bigger. There is no wavelength dependence and the scattering angle is lower.

From the qualitative description of the various scattering approximations, it is understood that different structures in the optics scatter at different angles, and therefore in order to properly identify the scatterers it is needed to carefully study the scattering spatial pattern and combine it with physiological data on the size of the structures.

Figure 10. The characteristic blue color of the sky is a result of Rayleigh scattering, as molecules of the atmosphere comparable, in size, to the wavelength of light emitted from the sun. Thus, blue wavelength is scattered more and fills the sky. On the other hand, the characteristic "white" halo ring that the human eye sees, is a result of light that has been scattered from molecules and formations relatively bigger than the visible wavelengths.

1.3 SCATTERING IN THE OCULAR MEDIA

Scattering occurs due to micro-scale optical anomalies of the optics at a spatial domain of approximately the same order as the wavelength. It occurs primarily at two sites in the eye; the cornea and the lens, with approximately equal contribution in young healthy eyes (van den Berg et al., 2010). In both cases, the physical cause are the local variations in refractive index, however, the actual structures responsible for these fluctuations in the refractive index are not fully determined.

As light propagates through the ocular media, it can be assumed that the total resulting straylight S is given by:

$$S(\theta)_{total} = S(\theta)_{cornea} + S(\theta)_{lens} + S(\theta)_{vitreous}$$

Equation 2

with the cornea, the lens and the vitreous humor. Another source of ocular straylight which is not included in the refractive elements of the eye, is the fundus. Its contribution may rise up to one third of the total amount of intraocular scattering though its contribution depends heavily on wavelength and is restricted to the more central part of the PSF (van den Berg et al., 2010).

The cornea owes it transparency mainly to the dense and very well organized packing of the collagen lamellae, which form the corneal stroma, that occupies the biggest volume of the cornea. Although it consists approximately 80% macro-molecules of collagen, it maintains a high level of transparency by a continuous pressure from the anterior chamber, and a continuous channeling and drainage of any aqueous humor transferring all the needed nutrients for its metabolic action (Qazi, Wong, Monson, Stringham, & Ambati, 2010). As a result, the gaps between collagen fibril that forms the lamellae, are relatively small,

compared to the visible wavelengths. The fibrils themselves, also have an average diameter of 10-20 nm, with no scattering interaction with the transmitted light. The very thin layers of the epithelium do not interact with visible light in physiological circumstances. In pathological instances, this degree of order in the stromal structure may be disrupted. In the case of corneal edema, the stromal consistency in water is increased, resulting to significantly big spaces filled with aqueous humor that increase the amount of scattered light (Elliott, Fonn, Flanagan, & Doughty, 1993)(Figure 11). Corneal traumas also disrupt the order of the stromal lamellae and trigger the metabolic actions of keratocytes and fibroblasts, leading to significant increases of straylight. Additionally, it has been reported that refractive surgery can lead to temporary increase of straylight due to damages on the epithelium which lead to corneal haze (Veraart, van den Berg, IJspeert, & Cardozo, 1992).

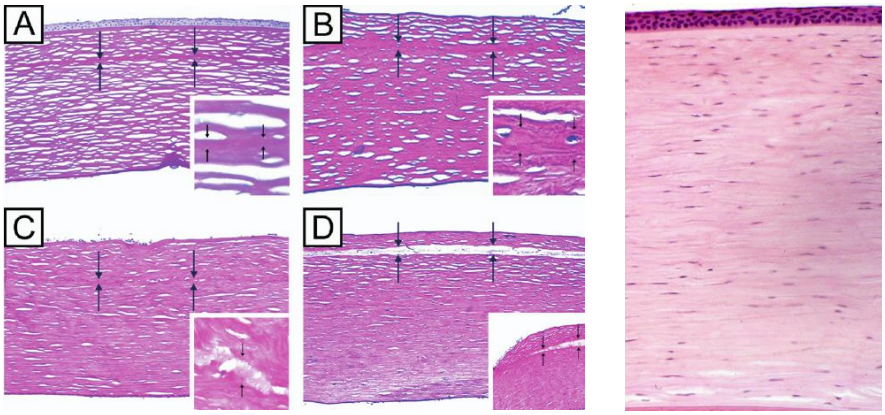

Figure 11. Examples of edematous corneal stroma (left, A.B.C and D) and physiological state (Source: Dawson et al. 2007).

The transparency of the crystalline lens depends on its a-vascularity, narrow inter-fiber spaces between fibers and the regular organization of its cells and proteins (Bassnett, Shi, & Vrensen, 2011). At the cellular size order of magnitude, the cellular organelles seem to provoke small amounts of scattering. These organelles are in relatively low concentration in the central epithelium and are mostly localized to the equator in the fibers, away from the central area where light passes through. Within the fiber cells, the *crystallines* (type of proteins that exist in the crystalline lens to a concentration up to 90%), exist with a size significantly smaller than the wavelength of light. Hence, they do not contribute significantly to lens scattering.

In the lens cortex transparency is attributed to the high spatial order of the fibers and the narrow spaces between them. In the lens nucleus, high spatial order of the crystallines is not essential since the refractive index is very similar between fiber membranes and cytoplasm resulting to almost no scattering (Costello et al., 2008; Michael, Van Marle, Vrensen, & Van Den Berg, 2003).

The sources of scattered light in the crystalline lens (Figure 12) have also been subject to scientific research through time. The problems arising are that in vivo measurements of scattered light originating exclusively from the crystalline lens, as for in vitro measurements, are not completely representative as the

structural and biological characteristics are altered ex vivo. Although microscopic findings from electron micrographs have identified as scattering sources cytoplasmic protein aggregates, result of both physiological metabolic action and abnormally high level of toxicity, fiber cells, multilamellar bodies (MLB), or refractive index differences between fiber cells and the gaps between them (Benedek, 1971; Kurt . Gilliland, Freel, Johnsen, Craig & Costello, 2004; Hemenger, 1988). In particular, in vitro scattering experiments with donor lenses, based on the Rayleigh-Gans-Debye approximation, suggested that the structures responsible for the forward scattering must be approximately 1.4 μm in diameter, excluding smaller particles randomly placed in the lens like proteins, and suggesting fiber cells and multilamellar bodies as the most possible candidates, with the later to show an increase in cataract patients (Costello et al., 2008; Gilliland, Freel, Lane, Fowler, & Costello, 2001). Lens scattering, contrary to corneal scattering, has a strong dependence on age (van den Berg et al., 2010), as a result of accumulating side effects of metabolic action and as previously mentioned, the size of the scatterers and as a result the intraocular scatter that they provoke, is strongly dependent on the wavelength of the propagating light (Ginis, Perez, Bueno, Pennos, & Artal, 2013).

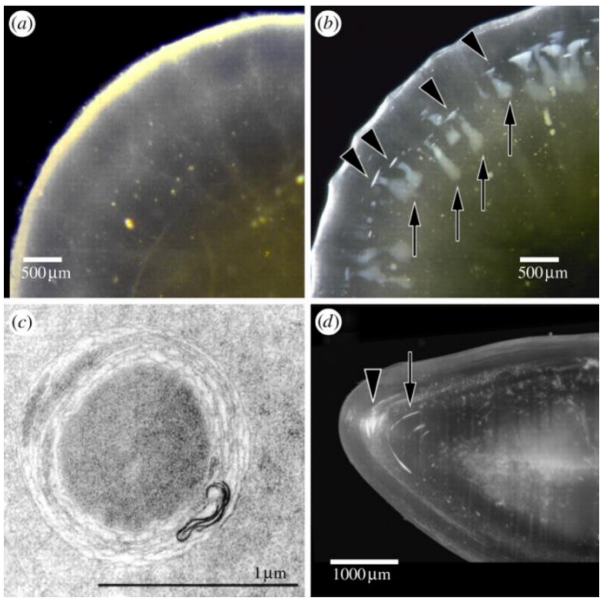

Figure 12. Dark-field micrographs of aged human donor lenses, illustrating (a) small, dot-like opacities and (b) radial and circular shades. (c) Multilamellar body, as frequently found in human lenses with early cortical opacities probably causing the star-like opacities seen in (a). A slice cut in the axial plane of the fixed donor lens (b) is shown in (d) (Source: Edited from R. Michael et al. 2011).

The pathological state of the crystalline lens, were opacities' concentration is increased to a degree that significant impairment of vision is provoked, is called cataract. A classification of the type of cataract depending on the location of the opacities, can be done. *Nuclear cataracts* are classified as those where the lens opacification is confined to the nucleus of the lens. *Cortical cataracts* are those where the superficial, cortical fibers of the lens are affected by protein aggregation resulting to light scattering. And, cataracts classified as *posterior subcapsular* are the cases where opacity of the lens capsule posterior pole is increased mainly

caused by lens migration from the lens equator to the posterior pole (R Michael & Bron, 2011).

Another contribution to the total amount of straylight is credited to the vitreous humor, the aqueous solution filing the eye globe. Floaters, the molecules dissolved in the vitreous in low concentrations, are present in all eyes and are known to produce scattered light. In normal eyes, this contribution is low. Changes in the consistency of the vitreous though, are reported to contribute significantly to an increase of straylight (Mura et al., 2011).

1.4 THE IMPACT OF STRAYLIGHT IN VISUAL FUNCTION

The effect of straylight is one of the most significant visual disturbances, affecting not only cataract patients, but the general population. This discomfort –or, in pathological situations, impairment- is becoming more disturbing when intense light sources appear in the visual field. The result, a veiling glare around these bright sources, has been reported to become more intense with age (De Waard, Ijspeert, Van den Berg, & De Jong, 1992) resulting to most of the cases to cataract extraction and implantation of an artificial intraocular lens (IOL). The effects of straylight in vision, can also be detected by the distortion on the intensity distribution of a light source, similarly to aberrations but affecting specific parts of the PSF.

An interesting observation (IJspeert, de Waard, van den Berg, & de Jong, 1990) of which areas of the PSF are affected by straylight, showed that mainly the peripheral zones (above 3 degrees) suffers the effect. Moreover, rotational symmetry of the PSF can be assumed and its spatial dependence can be expressed in respect to the angle (θ). Assuming as well that the total intensity of a point source is included in the described PSF, the PSF itself can be expressed as:

$$\int_0^{\frac{\pi}{2}} 2\pi\theta \; PSF \; d\theta = 1$$

Equation 3

The above equation, in a more simplistic sense, denotes that, due to spatial symmetry of the PSF, it can be expressed as a function of a single angle (θ). Additionally, it is assumed that only forward scattering occurs, with the angle θ being limited from 0 to $\pi/2$.

In early studies on the glare disability (Holladay, 1926; Stiles, 1929) the dependence of the PSF on the angle, was initially expressed as $1/\theta^2$. Later studies though (IJspeert et al., 1990; Ijspeert, Van Den Berg, & Spekreijse, 1993; van den

Berg, 1991; Vos, 1984), enriched the expression of the PSF with a number of empirical formulas.

The most simplified expression of the PSF as a function of angle was introduced by the Stiles-Holladay formula:

$$PSF(\theta) = \left[1 + \left(\frac{A}{70}\right)^4\right] \frac{10}{\theta^2}$$

Equation 4

where A expresses an age-dependent multiplication factor. Although simplified, the above formula was a good approximation for the description of the PSF between 3 and 30 degrees. It was falling short though, to describe the point's source energy distribution at narrower angles and at extreme outskirts (van den Berg & Spekreijse, 1997).

The exact contribution of different structures on straylight at these angular domains, was later identified (van den Berg & Spekreijse, 1997) and the pigmentation and age dependence was also included in a more complete expression:

$$PSF(\theta) = PSF\ (\theta)_{base} + \left(\frac{A}{70}\right) PSF(\theta)_{age} + p\ \cdot PSF(\theta)_{pigment}$$

Equation 5

Assuming that the corneal contribution is age-independent, the lens has no dependency on pigment and that the ocular wall and the fundus depend on both age and pigmentation, each term of the equation was fitted separately to experimental data (Ijspeert et al., 1993; van Den Berg & Ijspeert, 1995; Vos & Boogaard, 1963) resulting to the most complete expression of the straylight PSF, also referred in the literature as Glare function:

$$PSF_{CIE} = \left[1 - (0.08\ (A/70)^4\right] \left[\frac{9.2\ \cdot 10^6}{\left(1 + (\theta/0.0046)^2\right)^{1.5}} + \frac{1.5\ \cdot 10^5}{\left(1 + (\theta/0.045)^2\right)^{1.5}}\right] \cdot$$
$$\left[1 + 1.6(1/70)^4\right] \left\{\left[\frac{400}{1 + (\theta/0.1)^2} + 3 \cdot 10^{-8} \cdot \theta^2\right]\right.$$
$$\left. + p \left[\frac{1300}{\left[1 + (\theta/0.1)^2\right]^{1.5}} + \frac{0.8}{\left[1 + (\theta/0.1)^2\right]^{0.5}}\right]\right\} + 2.5 \cdot 10^{-3} \cdot p[sr^{-1}]$$

Equation 6

where θ is the angle in degrees, A the age and p the pigmentation coefficient, with values 0, 0.5 and 1 for black, brown and light-colored eyes, respectively.

For clinical applications, the PSF is not considered a well-understood and practical quantity, leading to a quantity called the *Straylight (S) parameter,* defined as:

$$S(\theta) = \theta^2 PSF(\theta)$$

Equation 7

Most often, the logarithm of the above parameter is used to express an individual's eye's straylight. An example of the age dependence of S is presented in figure 13, at an angle of 3 degrees:

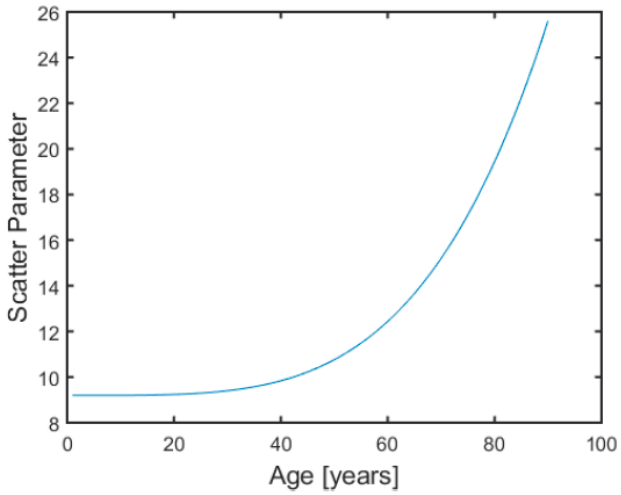

Figure 13. Scatter parameter for the CIE glare function with respect to age at ϑ=3°

1.7 CATARACT TREATMENT

Significant increase of the amount of scattered light deteriorates the contrast of the images formed at the retina, leading to a reduction of the Contrast Sensitivity (CS). In the case where retinal straylight becomes too intense, so that the visual acuity is also affected, a cataract extraction procedure may be performed. It is a surgical intervention where the natural crystalline lens is being removed, leaving the lens capsule in place, followed by the implantation of an IOL.

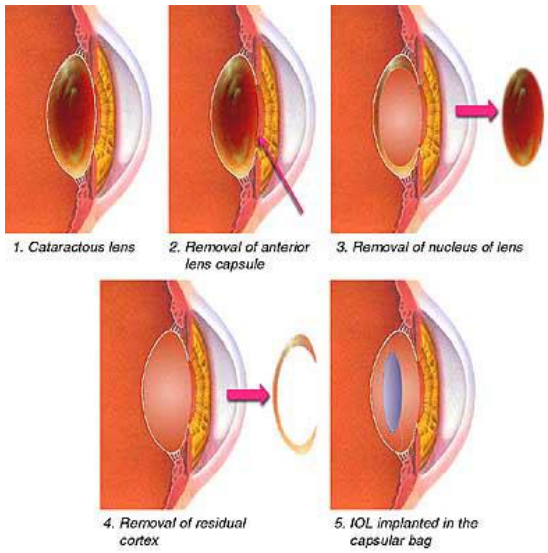

Figure 14. Crystalline lens extraction and IOL implantation procedure (Source: Perlman Care for Eye).

The surgical process of IOL implantation is a common procedure, at least in the advanced countries, with millions of surgeries taking place worldwide, yearly. This fact has led to a tremendous evolution of the technique, the last two decades, improving and adding more characteristics to each stage of it i.e. lens extraction technique, IOL insertion, IOL design and materials and positioning. The main categorization on the optical design of IOL's can be based on the dioptric power they induce, with the monofocal IOL's being dominant as they have been developed earlier, and the multifocal (bi- or tri-focal) ones becoming more popular recently.

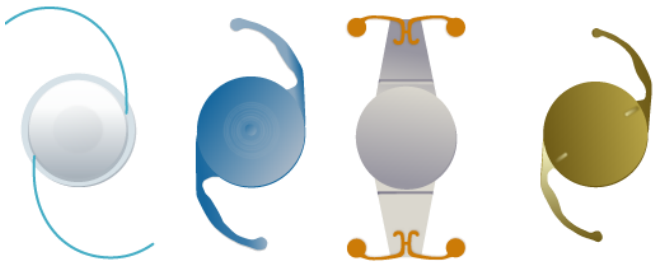

Figure 15. Examples of various designs of IOL's (Source: precision-eyecare.com).

A common discomfort after cataract surgery may be generated by after-cataract straylight originated by IOL-material failures (material/refractive index inhomogeneities) or by Posterior Capsular Opacification (PCO) where a hazy layer of migrated cells is formed between the capsule and the IOL.

1.8 Overview of established methods to quantify intraocular scattering

VA tests can only detect the presence of straylight when appears in high values. On the other hand, VF can be significantly limited due to scattered light, especially under specific conditions (such as night driving). Thus, it is essential to accurately quantify the amount ocular straylight or detect its effect on VF, not only for comfort and good visual performance but also for safety.

In this direction, two basic axes of detection are available in the clinic. One, relies on psychophysical tests that define the CS on various spatial frequencies, approximating, by this manner, the actual sensitivity on natural scenes. The latter, is incorporating specifically developed techniques and devices, that provide a metric of quantification of the total intraocular scattering.

1.8.1 Measuring contrast sensitivity

As defined by Pelli (Pelli & Bex, 2013), *the contrast of the target quantifies its relative difference in luminance from the background.* It can be specified as Weber contrast:

$$\frac{L_{max} - L_{min}}{L_{background}}$$

Equation 8

Michelson contrast:

$$\frac{L_{max} - L_{min}}{L_{max} + L_{min}}$$

Equation 9

or RMS contrast:

$$\frac{L_{\sigma}}{L_{\mu}}$$

Equation 10

where L_{max}, L_{min}, $L_{background}$, L_{μ} and L_{σ} are the maximum, minimum, background, mean, and standard deviation respectively. In addition, contrast threshold, is the contrast required from a viewer, to be able to see a target reliably. Sensitivity is the reciprocal of the contrast threshold.

The psychophysical methodology to measure contrast threshold could be generally categorized into objective and subjective (Ehrenstein & Ehrenstein, 1999; Li, Macdonald, Mahajan, Eds, & Optics, 2010). Objective tasks have a right answer though subjective tasks don't. In specific, during objective tasks, the observer has to make a decision upon the appearance of the stimulus (i.e. visible/invisible, left/right) which might be correct or not. On the other hand, in subjective tasks, the subject has to express his own visual experience, which is known only to the observer, so the experimenter cannot justify whether the report was right or wrong. Subjective tasks include rating, matching, and nulling (Pelli & Bex, 2013). Various external factors, including instructions, might force the subject to raise or lower his or her criterion, causing threshold to shift up or down. This unknown internal criterion of the observer typically differs among observers and may vary across populations and over time. Clinical and basic studies of visual sensitivity are usually not focused on these shifts, so they avoid the undesired variations of yes/no methods by using less-criterion dependent methods (Vaegan & Halliday, 1982). Finally, a general observation is that near threshold decisions take usually longer (Pelli & Bex, 2013).

Schade (Schade, 1956) made the first measurements of visual contrast sensitivity as a function of spatial frequency. This contrast sensitivity function (CSF) is typically built by measuring the contrast detection threshold at, at least five spatial frequencies, uniformly spaced on a log scale spanning typically from 1 to 16 c/deg, spatial frequency spectrum. The CSF is affected by optical and neural factors (Green & Campbell, 1965). Optically, the quality of the retinal image is determined by the Modulation Transfer Function (MTF), which depends strongly on pupil size, and can be measured physically (Artal & Navarro, 1994). Neurally, Campbell and Robson (Campbell & Robson, 1968) revealed the presence of multiple channels in vision, each selective to a different band of spatial frequencies. This greatly increased interest in measuring the CSF. Today, the set of thresholds as a function of spatial frequency is usually fit with a contrast sensitivity function (Watson, 2000). In order to establish the CSF of a standard human observer, a group of 10 laboratories collaborated to collect contrast thresholds for 16 observers on a standard set of 43 diagnostic stimuli (Carney et al., 1999). The resulting data were used to evaluate the goodness of fit of 5 (Watson, 2000) or 9 (Watson et al., 2005) competing CSF models. Several models provided approximately equally good fits to the data, with as few as four parameters. The peak spatial frequency of the CSF shifts to larger sizes during normal aging (Owsley, Sekuler, & Siemsen, 1983) and lower luminance levels (De Valois, Morgan, & Snodderly, 1974), and when eye diseases like age related macular degeneration are present (Mei & Leat, 2007). In many pathologies, contrast sensitivity is impaired at all spatial frequencies, but a range of different clinical conditions selectively affect different regions of the CSF. For example, uncorrected refraction reduces sensitivity at high spatial frequencies, without affecting sensitivity to low

spatial frequencies, as does amblyopia. And finally, as already discussed, glare reduces sensitivity to low spatial frequencies with a relatively smaller effect on acuity.

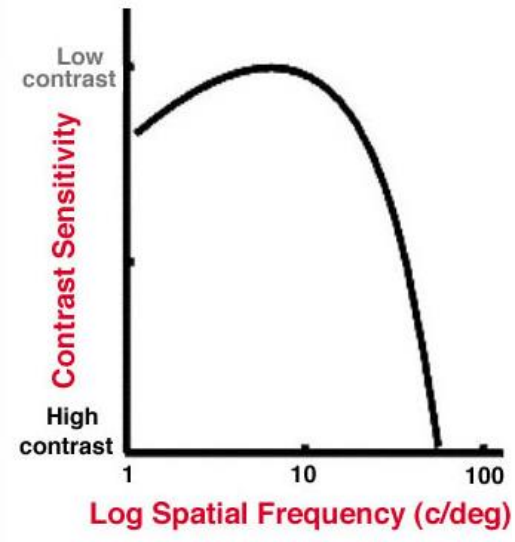

Figure 16. Photopic CSF (Source: webvision.med.utah.edu).

In order to estimate a contrast threshold, the observer is tested over many trials, at various contrasts. Each trial is at some contrast and is scored right or wrong. The proportion of correct responses at each contrast is recorded. The observer's probability of correct response as a function of contrast consist the psychometric function. Additionally, there are various tactics to select the adequate contrast of a stimulus, to test the sensitivity at a specific frequency. For example, during the method of constant stimuli, a predetermined set of contrasts in random order (Fechner, 1860/1966) is presented. This approach is easy to implement, but requires that the set of test contrasts be specified before the experiment begins. Additionally, this often lead the experimenter to test an insufficient range of contrasts, which might result problematic for special populations.

For this reason, many methods of measuring the CSF, based on printed charts where developed, with two of them being majorly used in the clinical practice. The first one, the Vision Contrast Test System (VCTS) chart, developed by Ginsburg (Ginsburg, 1984), consisted of rows of sine wave grating patches, tilted in either of three different directions. Many other types of printed chart tests where based on the same type of stimuli projection. The second, also regularly used, chart based, CSF test was the Pelli-Robson chart (Pelli, D. G., & Robson, 1988) .

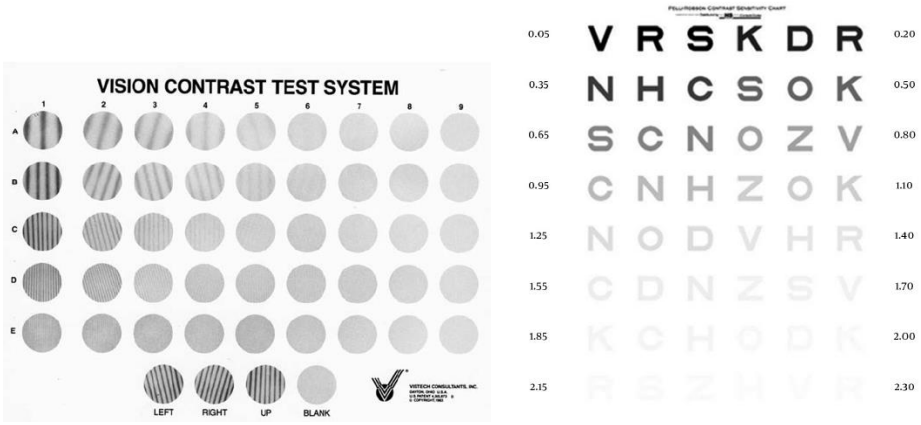

Figure 17. The VCTS (Left) and the Pelli-Robson (Right) chart (Source: Vistech, Precision-Vision.com)

The need to minimize the number of trials, and the total time needed for a complete examination, has led to the development of statistically efficient, computerized methods that make use of the preceding responses to stimuli, to predict the selected contrast level of the forthcoming ones. These methods reduce significantly the number of trials required for an accurate estimate of the threshold. More generally, adaptive staircase methods exploit existing knowledge of the likely parameters of the psychometric function for similar observers together with the results of previous trials on the observer that is being tested to fit the test level better to his visual performance and maximize the precision of the psychometric function that better describes his visual system. There are many alternative adaptive staircase methods, including 3 down 1 up (Wetherill & Levitt, 1965), APE (Watt & Andrews, 1981), QUEST (Watson & Pelli, 1983), PEST (Taylor & Creelman, 1967), ZEST (King-Smith, Grigsby, Vingrys, Benes, & Supowit, 1994).

Recently, new methods use prior knowledge of the CSF and the distribution of its parameters to select the spatial frequency and contrast of each trial to maximize the information gain (Hou et al., 2010; L. A. Lesmes, Lu, Baek, & Albright, 2010). These approaches provide significant gains in clinical data collection and have already demonstrated successful visual assessment in clinical populations with amblyopia (Hou et al., 2010), age-related macular degeneration and congenital cataracts (Kalia et al., 2012). In these populations, reliable estimates of the CSF are possible within 25 trials and an estimate of the area under the logCSF in as few as 15 trials (L. Lesmes, Lu, Baek, & Albright, 2010).

1.8.2 Direct measurement of Intraocular Straylight.

On a different approach, instead of the indirect estimation of the intraocular scattering through its effect on contrast sensitivity, there have been efforts to directly measure the amount of scattered light in the human eye. With these

methods, metrics are used to provide a degree of precision on contrast sensitivity. The biggest advantage of these methods is that some of them provide objectively measured metrics while others even manage to do it in a way that they require only the passive participation of the subject. Ultimately, the existence of these methods is credited to the need of accurate, fast and reliable measurements of the amount of intraocular scattering, with the least possible participation of the examined person, minimizing the human error factor.

Two psychophysical procedures were specifically designed for the quantification of intraocular light scattering: the direct compensation method and its altered version of compensation comparison (Franssen, Coppens, & van den Berg, 2006). Both methods are based on the principle the equivalent luminance caused by a flickering glare source will be matched by the subject by adjusting the luminance of a test object that is flickering in counter-phase. Alternatively, in the direct compensation method, a flickering annular glare source at an angle of about 7 degrees of visual angle, is similarly creating a flickering veiling glare spread upon a circular test field positioned at the center of the annulus with adjustable luminance flickering in counter-phase to the glare annulus. The task for the subject is to adjust the luminance of the test object in order not to perceive any flickering. Consecutively, the luminance required to null the flickering is equal to the glare, generated by the annulus that has been produced by scattering at 7 degrees and that has covered the test field. The accuracy of this type of measurements depended on the adjustment strategy that the subject was following, as well as the level of intuition the examiner was transmitting to the subjects. These factors could not be standardized or controlled thus, subjects had the ability to influence the test outcome.

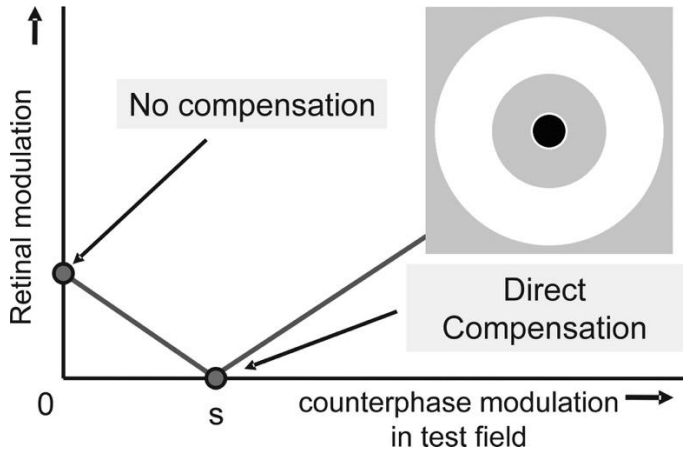

Figure 18. The direct compensation method. Retinal modulation in a foveal test field (inset: black field), resulting from scattered light from a constantly flickering annulus (white) is plotted against the amount of counterphase modulation in that test field. At point s, the flicker is extinguished, and the precise value of straylight found (Source: van den Berg et al.)

For these reasons a modified version of the same measurement was developed, called: the compensation comparison method. The methodology of testing was the following: the central test field was divided in two semi-disks and different amount of compensating light was presented to each half. The psychophysical procedure involved a series of two-alternative, forced-choice responses where the subject was forced to select the semi-disk from which he or she was perceiving the most intense flicker. The equivalent luminance was then estimated by means of fitting an appropriate psychometric function to the subjects' responses. Although, the compensation comparison method has been used in numerous studies, the basic limitation related to the psychophysical nature of the task was still present. The compensation comparison method is used in a commercially available device called C-Quant (Oculus Gmbh, Wetzlar Germany).

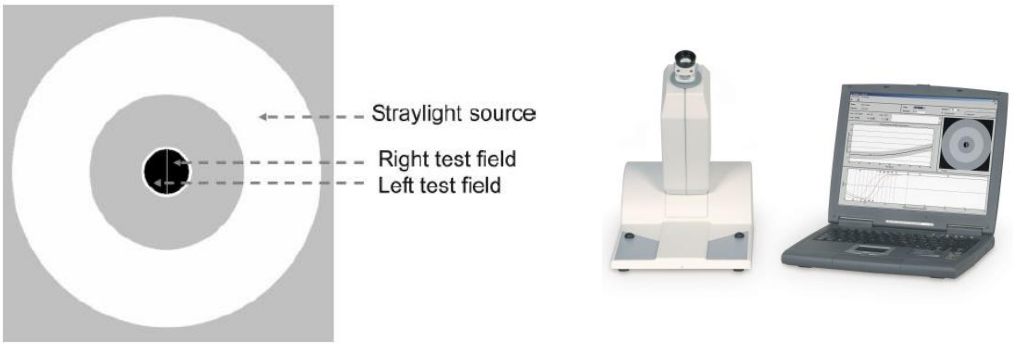

Figure 19. Stimulus layout (left) of the C-Quant device (right) (Source: Adapted from www.oculus.de).

Overcoming the limitations of a psychophysical method of measurement, a totally different approach for the measurement of ocular straylight was introduced by Artal et al. (Artal et al., 2011). According to this methodology, a scatter index is provided as a metric, calculated from the analysis of double pass images of a point source projected on the retina. A collimated infrared diode laser enters the eye with a fixed diameter of 2mm and is projected on the retina where was forming an illuminated area whom size was depended on the intensity of intraocular scattering, and other higher order aberrations (defocus or astigmatism were compensated). The double-pass images were recorded by a Charged Coupled Sensor-Device (CCD) camera.

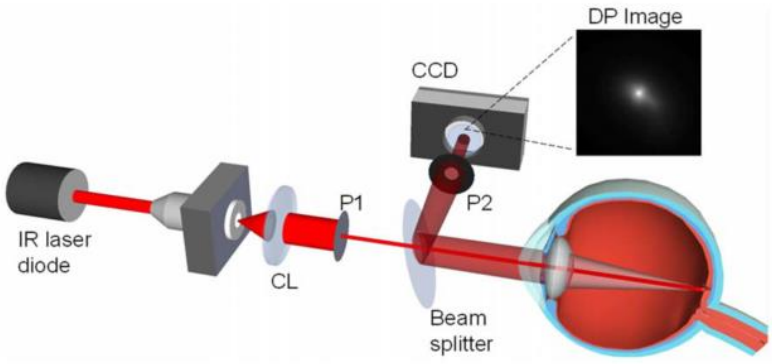

Figure 20. Schematic representation of the double pass setup applied for the acquisition of the OSI (Source: Artal et al, 2011).

The metric provided, called Objective Scatter Index, OSI was defined as the ratio between the integrated light in the periphery and in the surroundings of the central peak of the DP image. In specific, central area selected was a circle of a radius of 1 minute of arc, while the peripheral zone was a ring set between 12 and 20 minutes of arc. The before-mentioned method was applied for the development of a scatter measurement-specific device (HD Analyzer, Visiometrics SL, Barcelona, Spain).

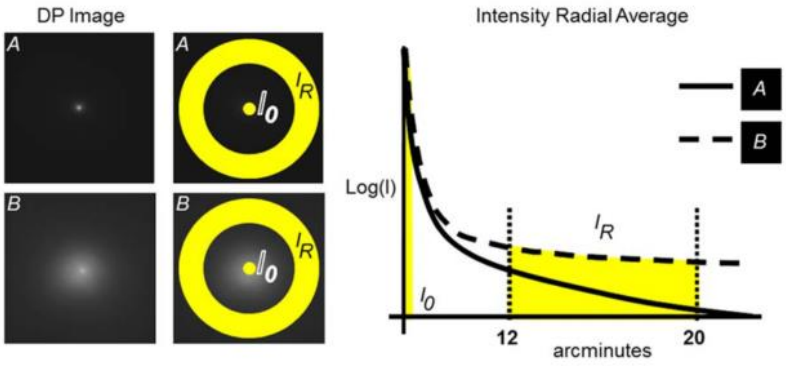

Figure 21. Example of the selection of the zone in the double-pass image used to define the objective scatter index (OSI). (A) solid line stands for less and (B) dashed for increased scatter (Source: Artal et. al 2011).

1.9 MOTIVATION OF THE THESIS

This thesis includes a series of studies performed on intraocular straylight; the consequence of optical irregularities in the human eye which can lead to a vision impairment through ageing or in pathological situations. As a result, the exact scope of the thesis was first of all to investigate and establish new methods for the precise evaluation of the scattering that stacks or elements made of various types of materials, generate. Such elements could potentially be the optical components of the human eye thus the fore-mentioned methods should be adapted properly to be applicable to measurements of intraocular scattering.

On the other hand, while myopia, hyperopia and astigmatism are far more comprehensible by the clinicians and the patients, defining the degree of the impairment that straylight and its exact effect, remains a "fine detail" on the description of functional vision. Thus, the other main content axis of the thesis was to match the precisely measured effects of straylight on the visual function, to universally used and defined metrics, like the Straylight parameter (S). And, finally, as surgical treatment of cataract (the main reason for increased intraocular straylight) is vastly applied in developed countries and as the need for –near to-perfect vision is increased, it is becoming more essential to come up with innovative methods and procedures to accurately measure the amount of intraocular straylight, and, how and to which extent and nature, it degrades the quality of vision (as for example in Figure 22).

Figure 22. The effect of Straylight on vision is demonstrated. The same scene is photographed with near to no straylight (left) and with the addittion of a significan amount of straylight (right).

2. SCATTER CHARACTERIZATION OF DIFFUSERS, MATERIALS AND BIOLOGICAL TISSUES

In this chapter, a novel optical method for the reconstruction of the PSF of an optical system is presented. With this technique, a basic barrier set by the limited dynamic range of the detectors that are being used in other methods, is exceeded. The details of the methodology that are being described, showcase other advantages of the method such as the relatively low cost of the needed equipment, the simplicity of the optical setup as well as the high level of precision on the reconstruction of the PSF even for angles up to 10 degrees.

The second part of the chapter is dedicated to the demonstration of the application of this novel method for -in vitro- characterization of ex-vivo corneas with different hydration states as well as different optical elements.

2.1 THE OPTICAL INTEGRATION METHOD

Let's assume a hypothetical optical system is free of aberrations but affected by imperfections that produce scattered light. Then, a point source, imaged by this system, will be focused on a plane, with the total intensity of the source being redistributed to a wider area, whom extend will depend exclusively on the system's scatter properties. The latter description, is the definition of the PSF. To reconstruct the PSF of this system, subsequently, the most simplistic and straight forward method would be placing a detector on the image plane of the optical system, and move it along one (since the PSF is symmetric) of its axes (as seen in figure 23) recording the intensity values at each position. The main problem that instantly arises, is that the dynamic range of this detector would fall short to record all the intensities in each position, as the difference in the intensity between the very central part of the PSF and its outskirts can be of several orders of magnitude.

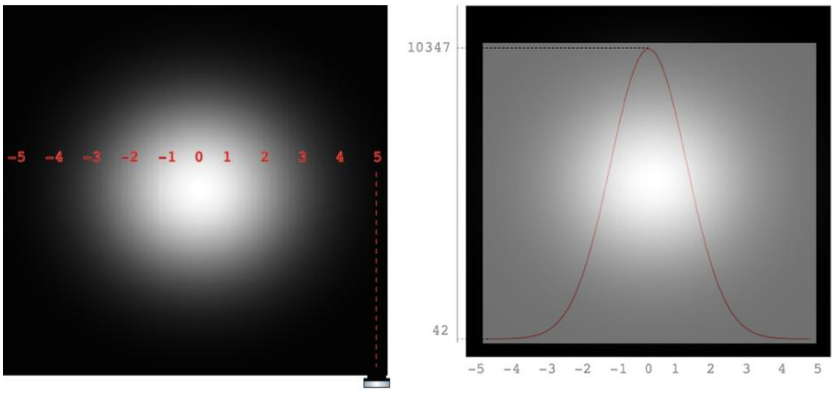

Figure 23: Left: A point source as imaged from an optical system suffering from scattering. Sampling positions from -5 to 5 are needed for a detector to record how the energy of the point source is being distributed. Right: The energy's distribution in two dimensions is depicted. Need to be noted the broad dynamic range that the detector has to be capable of detecting.

Instead of this approach, for the reconstruction of the PSF, the Optical Integration Method was proposed (Ginis, Pérez, Bueno, Artal, & Perez, 2012). The basic concept is the projection of extended sources of symmetrical shapes (uniform disks) on the object plane, and record the intensity at the center of these extended sources, imaged through the optics of the system. Assuming that the disk, before passing through the optical system has a uniform intensity, equal to I_o and that is covering an area of radius ϑ on the image plane, the intensity at the center of the disk, as recorded at the camera plane will be given by the following equation:

$$I_c(\vartheta) = I_o \int_0^{\vartheta} 2\pi\varphi \, PSF(\varphi) d\varphi$$

Equation 11

where $I_c(\vartheta)$ is the intensity at the center of the disk (which depends on the radius of the projected disk) and $PSF_{dp}(\varphi)$ is the PSF of the optical system. This value, will be equal to the surface integral of the PSF within a circle of radius ϑ, as seen in the figure below.

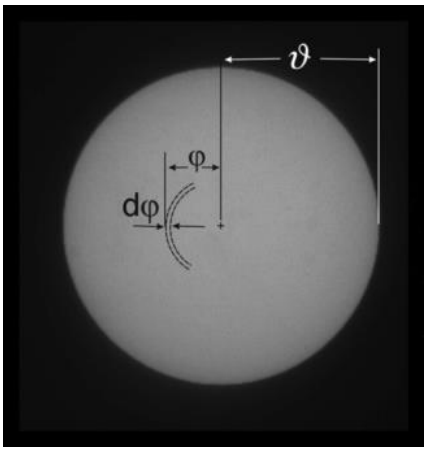

Figure 24. A uniform disk imaged through an optical system with a rotationally symmetric PSF that includes scatter (Source: Ginis et al. 2011)

Assuming that the integral of the PSF (either single pass or double pass) for $\vartheta = {}^{\pi}/_{2}$ is equal to unity, it can be shown that the central intensity of an infinite disk is equal to I_o. Qualitatively, this means that while for a small patch the central intensity is attenuated by light scattering this intensity is increased as peripheral annuli are added to the patch and scattered light from the annuli is complemented to the center of the patch. In an experimental situation where the analysis spans several degrees (i.e., about 10 degrees), it is a reasonable approximation to assume that effectively all the energy of the PSF is taken into account and therefore all measurements of I_c can be normalized in respect to the largest available disk. This assumption is supported by existing models of the PSF in the human eye (International Commission on Illumination., 1999; T. J. van den Berg, Hwan, & Delleman, 1993). Therefore, Equation 11 becomes simply:

$$I_c(\vartheta) = \int_0^{\vartheta} 2\pi\varphi \; PSF(\varphi) d\varphi$$

Equation 12

where $I_c(\vartheta)$ denotes the normalized intensity in respect to the central intensity of the largest disk and with the intensity's, I_c values, varying between 0 and 1. Because I_c is measured experimentally, the PSF can be calculated by taking its derivative, in respect to ϑ:

$$PSF(\vartheta) = \frac{1}{2\pi\vartheta} \frac{dI_c(\vartheta)}{d\vartheta}$$

Equation 13

2.2 EXPERIMENTAL SETUP AND PROCEDURE

2.2.1 Optical setup and hardware

For the application of the Optical Integration Method on an experimental setup, the required instrumentation should be adequate to produce extended uniform images of disks, imaged through a system that would not introduce, ideally, scatter and that should contain the material or optical element, subject to characterization.

The optical setup schematically depicted in figure 25 was developed.

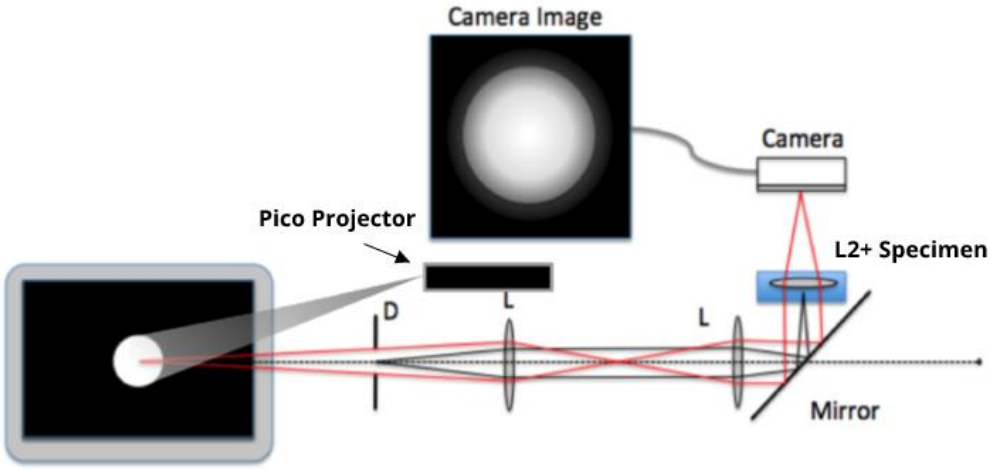

Figure 25: The experimental setup for the application of the Optical Integration Method.

A Digital Light Processing (DLP) pico-projector (PK 120, Optoma Ltd, Watford, UK) is employed to project extended disks with variying radious. These were directed towards a matte-brushed aluminum screen, tilted to a very small angle (less than 5 degrees), to avoid high intensity reflections which could saturate the sensor. The selected projection method was preferred to a conventional screen or digital monitor for two main reasons. First one was that by these means, more light would be available to the optical system and secondly, the pixel-size that could be achieved was significantly smaller compared to a conventional digital monitor. Moreover, a more compact character was given to the setup, a characteristic that was not necessary at the beginning of the design, but that was proved to be quite useful when the setup was used. For the imaging of the disks, a relatively simplistic approach was engineered. A tunable diaphragm (D) was implemented to control the amount of light entering the setup. A pair of Bi-Convex lenses of the same dioptric power were used to form a 1:1 telescope that conjugate the diaphragm plane on the plane where the imaging lens (L2) was placed along with the specimen subject to characterization. The specimen along with the L2 lens, were focusing

the light on the Complementary Metal Oxide Sensor (CMOS) camera (DCC1545M, Thorlabs Inc, NJ, USA).

2.2.2 Software

Appropriate software was developed in Visual Studio (Microsoft, Redmond WA, USA) Integrated Development Environment (IDE) to automatize and control the experimental process. Figure 26 presents the Graphical User Interface consisted of several parts, each one dedicated to manipulate a certain feature that the hardware provided.

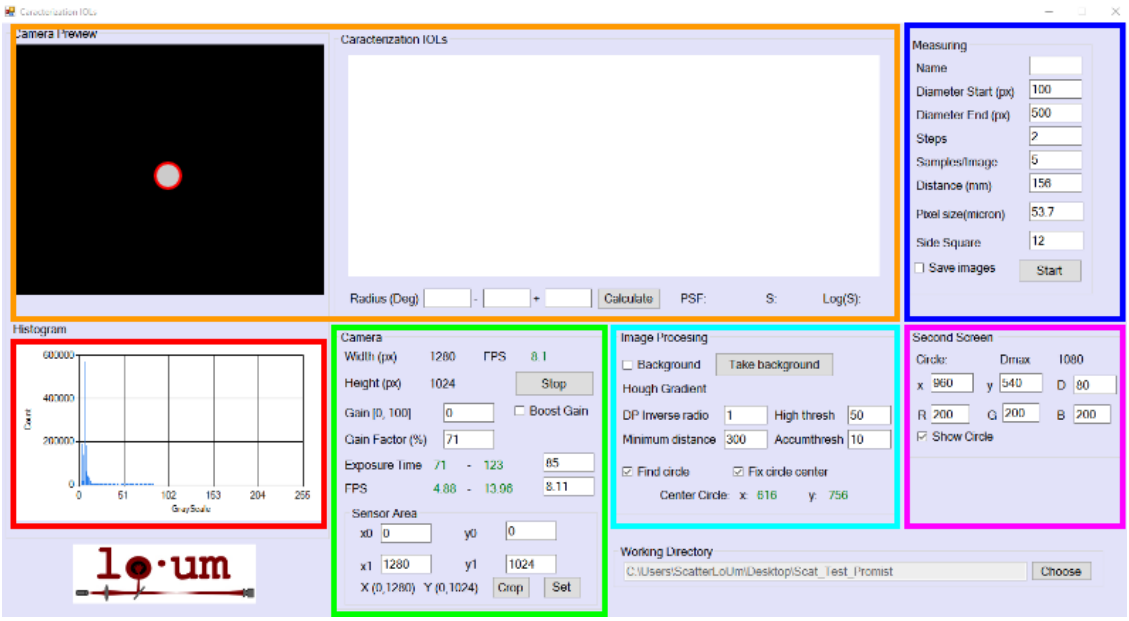

Figure 26: The GUI of the software with each of it's utility compartment highlighted with different color.

The main utility compartment of the software's Graphical User Interface (GUI), highlighted with orange in figure 26, is dedicated to a preview window of what the camera is recording, an additional window where the intensity recorded at the center of the uniform disks (mentioned previously, at the equations as I_c) is plotted in respect to the size of the disk (in degrees) and finally a text box where a range of angles is selected in order to calculate the straylight parameter for the given angular range. By using Equation 13, its $\frac{dI_c(\vartheta)}{d\vartheta}$ component is practically the slope of the curve (see Figure 27) of the normalized intensity plotted with respect to the angle. As a result, the PSF can be also calculated and then by using Equation 7, the straylight parameter S and its logarithm (logS).

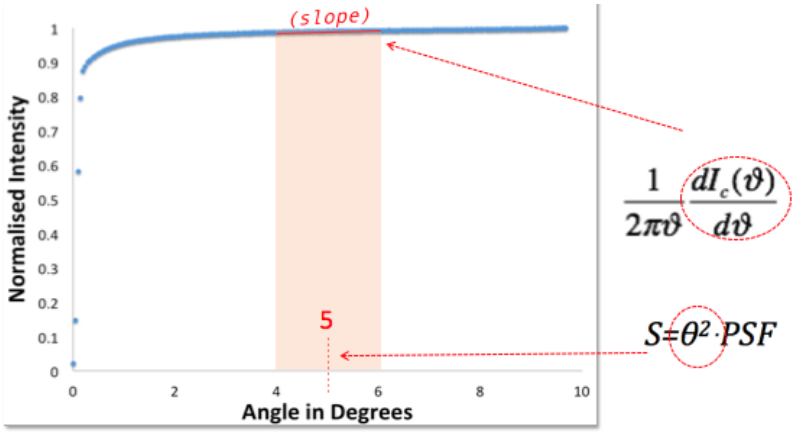

Figure 27: The normalized intensity as measured for a specimen with a relatively low S and the angular range that is being used for the calculations of the PSF and the S.

The camera control compartment (highlighted in green) was created to control basic characteristics, as exposure time, gain and frame rate while it also provided the option to partition the effective area of the sensor and use only a fraction of it, in cases where relatively small amount of light could be detected and the levels of noise were needed to be minimum.

To specify where the region of interest (ROI) would be for each measurement, a specific detection of elliptical shapes was implemented. The detection contrast threshold of the circular shape (in this specific application) could be defined along with the whether the detection of the center would be dynamic or static. It is to be reminded that the recorded intensity of each disk was recorded. All the previous parameters, along with the size of the ROI in pixels, are enclosed in the section of the software marked with cyan.

The position of the disk that is projected can be also modified, along with the color of the disk, controlling the three separate color channels of the projector (red, green and blue), allowing measurements in different wavelengths. These properties are included in the magenta-highlighted part of the GUI.

Finally, in the upper right part, highlighted with blue color, is the part that defines the measurement's characteristics. The range of the projected disk sizes is control along with the interval steps that will be done. Additionally, the number of samples per measurement, for each disk, can also be controlled.

2.3 RESULTS

2.3.1 Characterization of Diffusers

To check the validity of the method, a series of commercially available diffusers, that have been previously reported to approximately reproduce the effects of cataracts (Ginis, Sahin, Pennos, & Artal, 2014), were evaluated. The used were the "Black Pro Mist" series by Tiffen (Tiffen S.L. Hauppauge, NY, USA), with their grades of density being the ¼, the ½, the 1 and 2. For all the measurements, 5 samples for each disk size where recorded, with their average value being recorded in each series of measurement. Three series of measurements where obtained for each diffuser, with the scatter of the optical setup itself, being subtracted from the final results. Figure 28 shows the normalized intensities as a function of the projected disk size, for each diffuser.

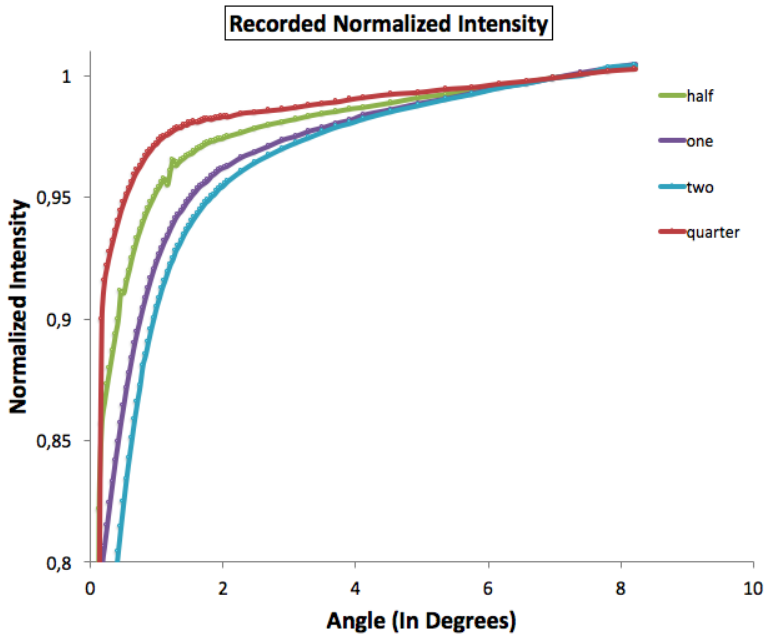

Figure 28: Recorded normalized intensities for each Tiffen Black Pro Mist diffuser.

The straylight parameter and its logarithm was calculated with the method described in the 2.3.2 subsection, for the angular range from 5 to 5.5 degrees. The results are collected in the table below:

Diffuser Number	Calculated S	Calculated Log(S)
1/4	4.93 ± 0.01	0.69
1/2	9.10 ± 0.03	0.96
1	14.58 ± 0.05	1.16
2	16.38 ± 0.03	1.21

Table 1: Calculated S and Log(S) values for each measured Tiffen Black Pro Mist Diffuser at 5.25 degrees

The straylight parameter, measured with the presented methodology, was in accordance with the density grading provided by the manufacturer (the higher the number of the grading, the denser the effect). The results were also in accordance with other studies (Ginis et al., 2014; van den Berg et al., 2011) not only relatively, but also in absolute numbers.

The upper results confirm that the described theoretical and experimental methodology is capable of accurate measurements of the produced scattered light by an optical element in single-pass.

2.3.2 Characterization of Intraocular Lenses

A plethora of intraocular lenses (IOL's) are currently commercially available. They vary in optical design (mono-, multi-focal), their materials and the manufacturing method. Thus, the measurement of the wide-angle PSF associated to various intraocular lenses is another application for the experimental optical integration setup. In this section, it is reported whether different functional design has an impact on their associated PSF, particularly on the straylight they introduce.

The IOL's materials, either hydrophilic or hydrophobic, interact with water and water solutions (absorb water to different percentages, depending on the polymer or co-polymer used). Therefore, in order to achieve more precise measurements, the lens was needed to be immersed into an aqueous solution. For this reason, a custom container was designed and 3D-printed, allowing the lens being immersed into an aqueous-saline solution during the process of characterization.

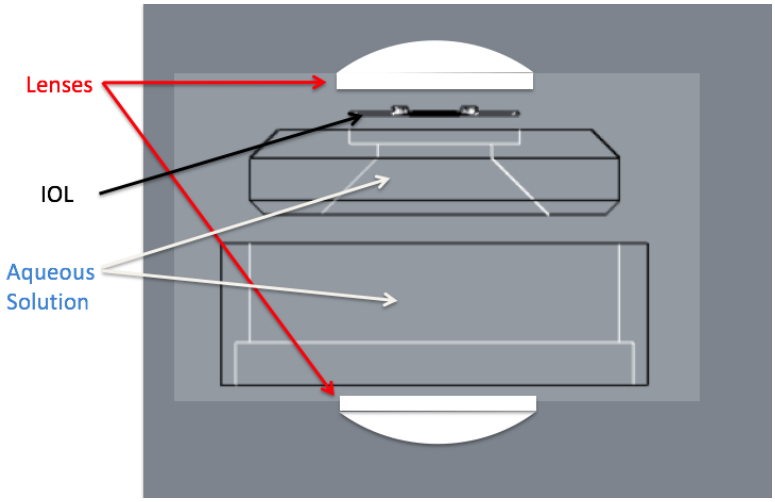

Figure 29: Side view of the engineered IOL container needed for the measurements.

PSF's where optically measured from 2 different diffractive, multifocal IOL's and 1 mono-focal IOL.

For each lens, four different measurements were performed, covering a field from 0 to 9.7 degrees (radius), separated in 200 partitions. For each partition, 10 recordings where accumulated to produce one mean record. The gain, exposure time and frame-rate of the camera were also pre-defined and constant for every measurement. The PSF was obtained by calculating the slope of the curves on specific angular ranges. Finally, an additional characteristic that was evaluated was the possible effect of the wavelength that is propagated through the lenses, on the amount of scattered energy and its angular distribution.

Regarding the effect of wavelength, no significant dependence was recorded, between the color of the propagated light and the amount of produced straylight and its spatial distribution (Figure 30).

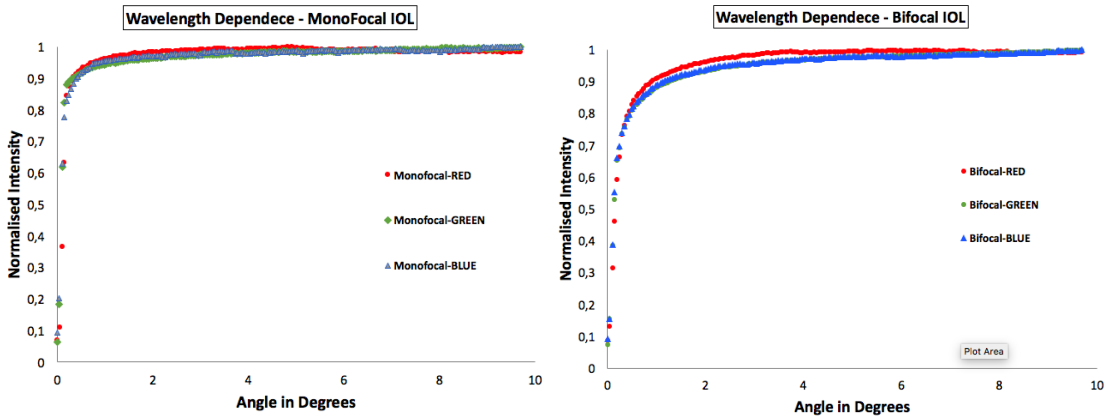

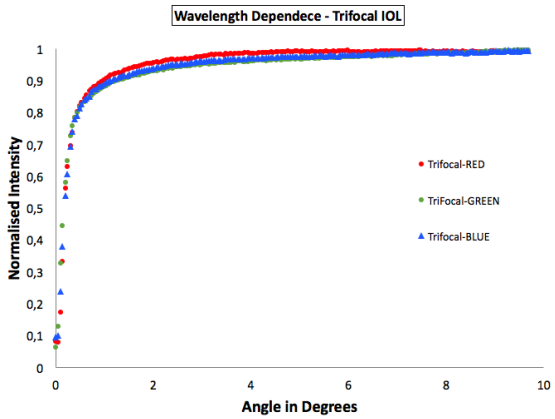

Figure 30 Wavelength dependence on straylight for the three different types of IOL's that were evaluated.

As no significant effect of the wavelength was measured, the straylight parameter was measured for all three types of IOL's, with white light, with the same methodology described previously. The results are shown in the Figure 31 and table 2:

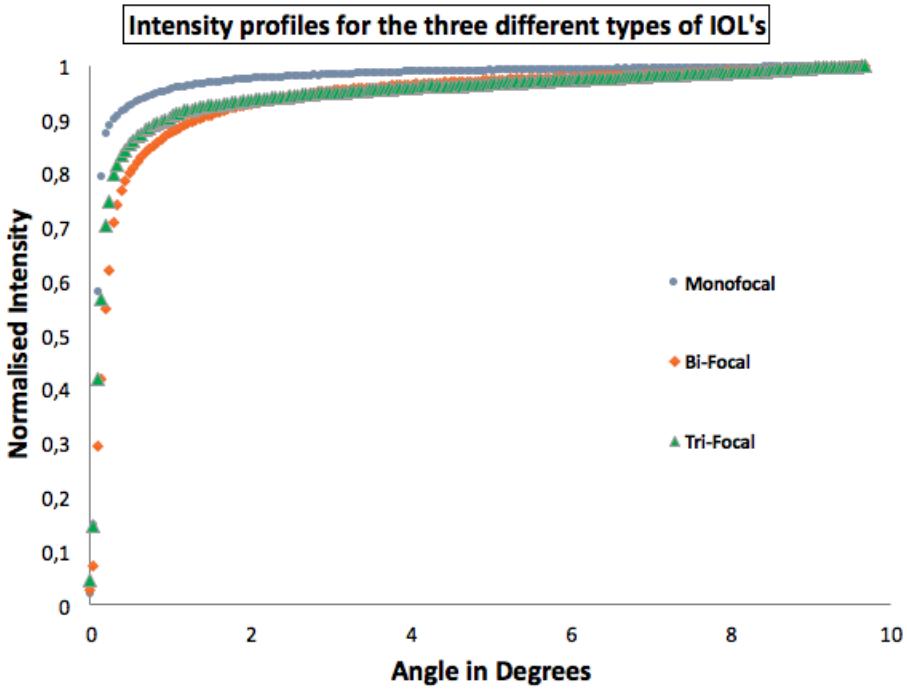

Figure 31 Intensity profiles for the three different types of IOL's that were characterized

IOL Type	Calculated S at 3 degrees	Calculated S at 5 degrees
Monofocal	3.28 ± 0.01	3.13 ± 0.03
Bi-Focal	9.27 ± 0.01	9.05 ± 0.01
Tri-Focal	8.59 ± 0.01	9.72 ± 0.01

Table 2 The calculated values of the straylight parameter, as measured in two different angles, at 3 and 5 degrees.

Significant differences were observed in the measured values of the straylight parameter, characterizing these different types of IOL's. Although characterization of the materials is not possible due to lack of precise documentation of their syntheses, it can be assumed that this is not the source of the recorded differences, as the composition differences that could arise, could not affect visible light wavelengths. This assumption is also supported by the fact that no significant differences of the straylight parameter were measured, employing different wavelengths. The characteristics that can provoke increased straylight are the structures that are relatively bigger that the visible wavelengths are those that grant the characteristic of multifocality to the IOL. Moreover, the last manufacturing stage of the monofocal IOL's, is the immersion into an abrasive bath, in order to polish both surfaces of the lens and remove any minor, surface imperfections. This process cannot be performed in multifocal IOL's as it can damage the diffractive patterns in the case of diffractive IOL's. The lack of polishing may result to imperfect surfaces and, consecutively, to increased scatter. The absolute differences between mono- and multi-focal IOL's are small, and possibly without detectable effect on the visual function, but, on the other hand, it is a proof that the measurement method is able to pick up slight differences of the measured scattering which can be a result of such a fine detail in the manufacturing process of the lens

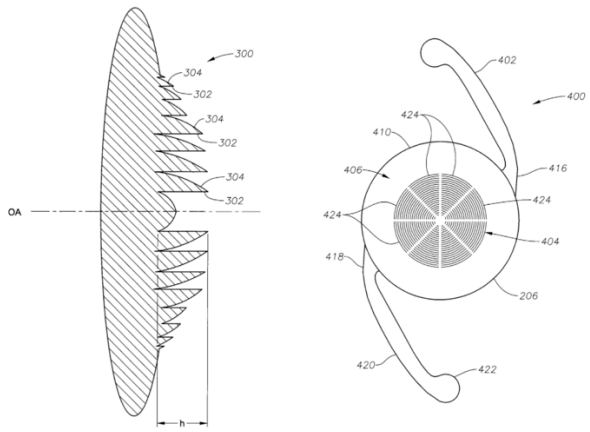

Figure 32: An example of a diffractive IOL. The diffraction "zones" formed by the depicted elongated structures can affect the amount of generated straylight (Source: Novartis).

2.3.3 In vitro measurement of straylight as a function of corneal swelling

An additional application of the optical setup for the measurement of straylight, was the quantification of scattered light resulting from structurally disrupted corneal stroma.

For this objective, fresh corneal crafts were extracted from porcine ocular globes which were enucleated just after death and immediately transported to the laboratory. The samples were neither fixed nor stained. All corneas appeared clear and transparent during the craft preparation. The corneal samples were harvested with the use of a trephine, extracting only their central 8-mm. Additionally, they were previously de-epithelialized with the use of a mechanical brush and after extraction they were immersed into Dextran (Sigma-Aldrich, St. Louis, MO, USA) aqueous solutions of different concentrations (20, 10 and 5% w/v). Dextran, a polysaccharide that is commercially available in various mean molecular weights, when dissolved in water is forming solutions that can be used to control the hydration levels of corneas in vitro (Kling, Ginis, & Marcos, 2012; Kontadakis et al., 2013).

The purpose of theses series of measurements was to quantify the effect of excess hydration of the corneal stroma, on the transparency of the cornea. By this means, a correlation of corneal edema with increased intraocular scattering could be investigated. Although previous studies proved that edematous corneas can contribute to the increase of scattered light (Elliott et al., 1993; Hsueh et al., 2009), with this methodology, in vitro measurements are possible. Additionally, using different concentrations of dextran solution, would create different swelling pressure into the aqueous solutions and would bring the corneal crafts to different degrees of hydration. To quantify the severity of the in vitro edematous state of each corneal specimen, a high-precision scale was used to measure the weight of each craft before and after the immersion in the dextran solution. The thickness of the button-crafts was also evaluated as a means of swelling quantification, using a digital Vernier caliper as a pachymeter (Mitutoyo Corp., Kanagawa, Japan).

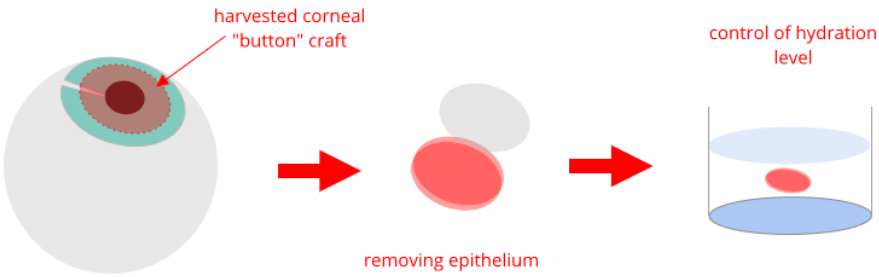

Figure 33: Schematic of the corneal craft preparation and manipulation

Two corneal crafts were forming each group, which was immersed into each different concentration solution. The treatment procedure involved 2-hour immersion, weighting and pachymetry registering before and after immersion and finally, optical characterization only after hydration treatment.

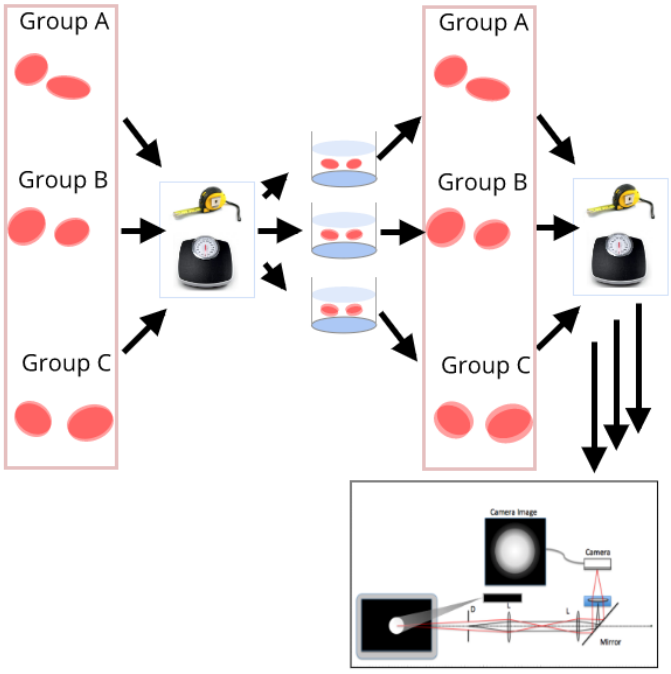

Figure 34: A schematic of the protocol that was followed during the experimental procedure for the optical characterization of corneal craft; immediately after de-epithelialization, the corneal crafts where separated and their mass and pachymetry were recorded. Consecutively, immersed into a bath to buffer their hydration, for a specific timeframe before their physical properties were re-measured and optically characterized.

As expected, the group that was immersed in the less dense (5% w/v) dextran solution underwent a more severe swelling. On the other hand, the crafts that were reserved in the 20% aqueous-dextran solution showed the least gain in pachymetry and mass. Unarguably, the changes recorded in mass and thickness are attributed to the absorption of water from the corneal specimens. Another noticeable effect of the swelling procedure was the loss of transparency and blurriness, which could be also verified even visually. This emulsion-like characteristic is potentially the outcome of the disrupted order of stromal collagen lamellae, where large water-containing areas, with different refractive index, interfere among the lamellar capes, augmenting the amount of scattered light.

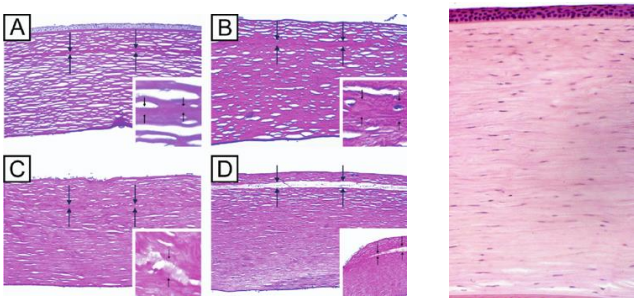

Figure 35:,Edematous corneas demonstrate higher values of straylight due to the areas of different refractive index, filled with water, between collagen lamellae.

Figure 36 shows the mean values for each group, preserved in different dextran concentration-solution. The swelling is expressed as the relative percentage difference of their weight and thickness consecutively:

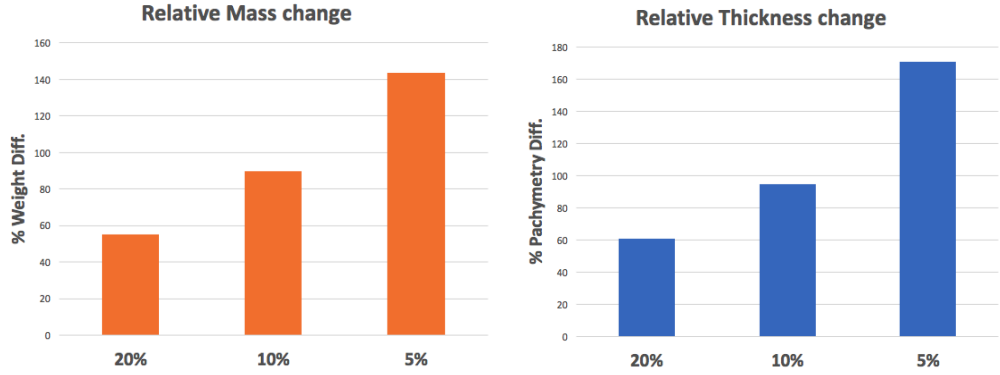

Figure 36: The relative change in mass and thickness depending for each group of corneal crafts.

The loss of transparency, although visibly identified was also quantified by measuring the straylight that each craft produced. Given the fact that the initial thickness of each cornea was not the same for each globe (depending majorly on the age of the animal that they have been extracted), the absolute S parameter could not be representative for each specimen group. For instance, as straylight is proportional to the thickness, crafts that were initially thick, could result to higher levels of scattered light, despite being less swollen and more tightly packed, compared to ones that were initially thinner but underwent a swelling process while immersed into the dextran solutions. As a result, the means of comparison of transparency was the ratio of the Straylight parameter, representative of each craft, to its thickness, $\frac{S}{thickness}$. The results of these measurements are summarized in Figure 37.

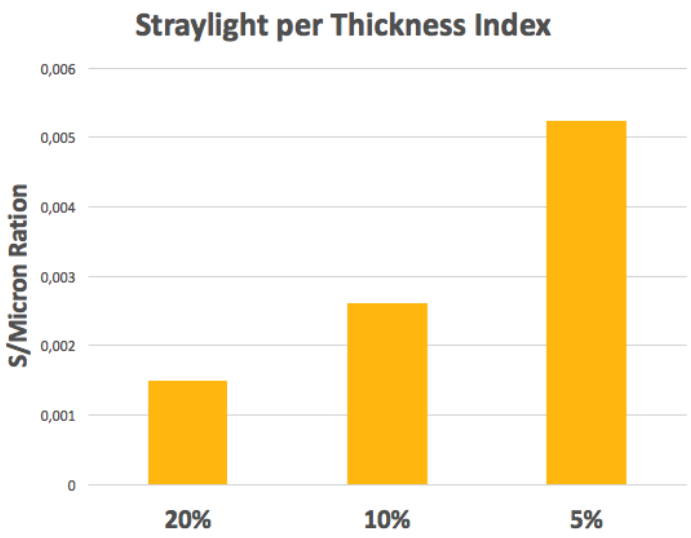

Figure 37: Straylight parameter to microns of thickness for the three different groups of corneal crafts.

We confirmed that the loss of organization of the collagen fibers throughout caused by the increased concentration of water, reduced the corneal transparency.

3. THE OPTICAL INTEGRATION METHOD FOR IN-VIVO MEASUREMENTS OF INTRAOCULAR SCATTERING

In the previous chapter a method for the quantification of intraocular scattering was described. Its novelty lied on the methodology of detecting the effect of straylight in wide angles, with precision and free of the impact of aberrations.

In this chapter, it is presented how this method is applied for the measurement of intraocular straylight in the human eye in vivo. Given this possibility, it also discussed whether there is a detectable effect of the wavelength that is being used for this type of measurements and, in this case, which wavelength should be ideally used for the measurements of scattering in human eyes.

3.1 THE DOUBLE-PASS MODALITY OF THE OPTICAL INTEGRATION METHOD

The adaptation of the optical integration method for measurements of human intraocular straylight provides precise, optically obtained estimations of the amount of scattered light. The illumination (i.e. the projection of the uniform disks) and consecutively the image acquisition have to follow the same, almost route, meaning that the projected, uniform disks, will pass once, while they enter the optical system of the human eye, with the optical elements and twice, when the intensity of the center of these disks will be needed to be recorder by the detection arm.

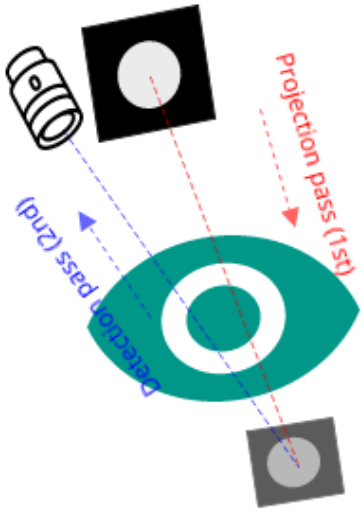

Figure 38: The two passes through the eye's optics that the imaged object needs to cross before being detected by the camera's sensor.

This double pass design, although used in many applications for imaging, is emerging the need of an additional analysis of the experimental data, as this double

passage would not be representative of the actual amount of straylight that a person perceives, as during visual function, the effects of straylight are the ones that are imaged on the retina, having gone across the eye's optics only once. Hence, the calculation of the PSF, using equation 13, would refer to the double-pass PSF (PSF_{dp}):

$$PSF_{dp}(\vartheta) = \frac{1}{2\pi\vartheta}\frac{dI_c(\vartheta)}{d\vartheta}$$

Equation 14

To calculate the actual PSF of the eye and assuming that rotational symmetry applies on the recorded PSF, the PSF_{dp} can be considered as the autocorrelation of the PSF itself (Ginis et al., 2012; Santamaría, Artal, & Bescós, 1987) and derives from the following equation:

$$PSF = \mathbb{F}^{-1}\left[\sqrt{\left|\mathbb{F}(PSF_{dp})\right|}\right]$$

Equation 15

where $\mathbb{F}$ and $\mathbb{F}^{-1}$ stand for two-dimensional Fourier and inverse Fourier transforms respectively.

3.1.1 The Experimental setup and procedure

The experimental setup for the double-pass setup is summarized in figure 39.

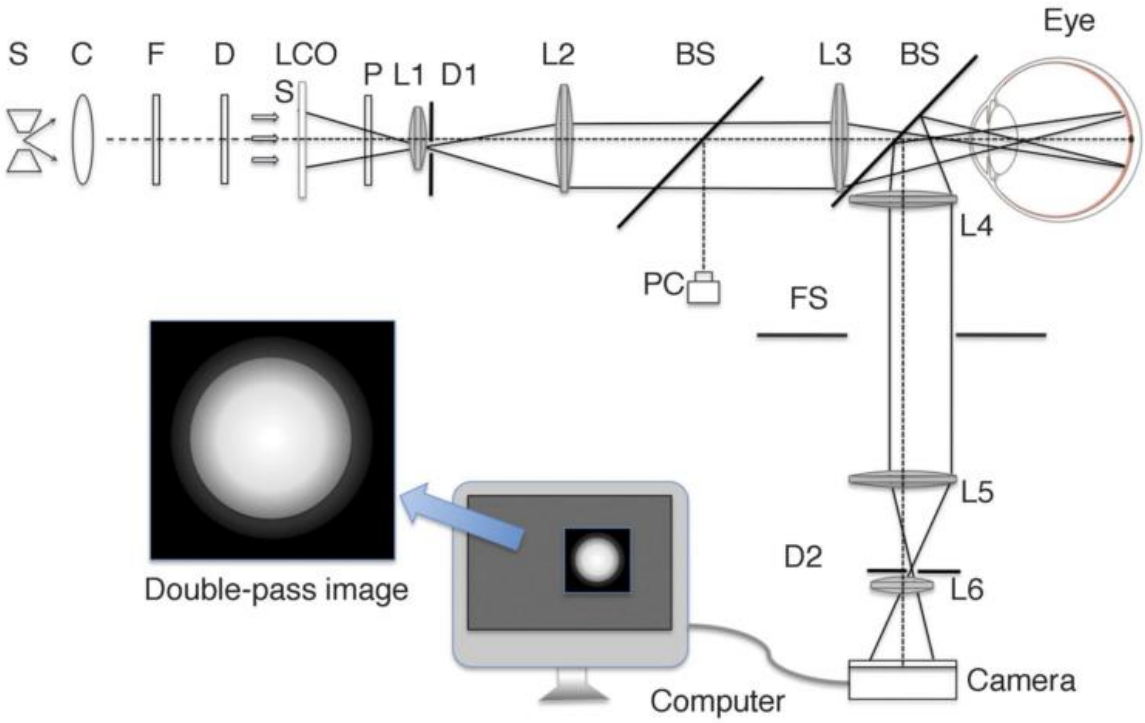

Figure 39:Schematic representation of the experimental setup. S, light source; C, collimating lens; F, green filters; D, diffuser; LCOS, liquid crystal spatial light modulator; P, linear polarizer; L1–L6, lenses; D1 and D2, diaphragms; BS, beam splitters; PC, pupil camera; FS, field stop.

A liquid crystal spatial light modulator (LC-2002, Holoeye, Germany) modulating only intensity (and not the phase), is used to reproduce each disk, that is back-illuminated by a Xenon lamp. Appropriate optical filters were used to select only a band of green light of 530 nm (30 nm FWHM). The light distribution is made uniform at the plane of the liquid crystal modulator by means of collimating optics (C) and diffusers (D). On the first pass, the light passes lenses L1, L2, and L3 and enters the eye and the image of the disk is formed on the retina. Diaphragm D1 is conjugated with the pupil plane of the eye (by lenses L2 and L3) and therefore controlling the part of the pupil that is used for the object projection. In the second pass, the image of the disk at the retina is imaged onto an electron multiplying CCD camera (EMCCD Luca, Andor, UK) through beam splitter BS and lenses L4, L5, and L6. Diaphragm D2 is conjugated with the pupil plane by lenses L4 and L5 and controls the part of the pupil used for imaging the retina.

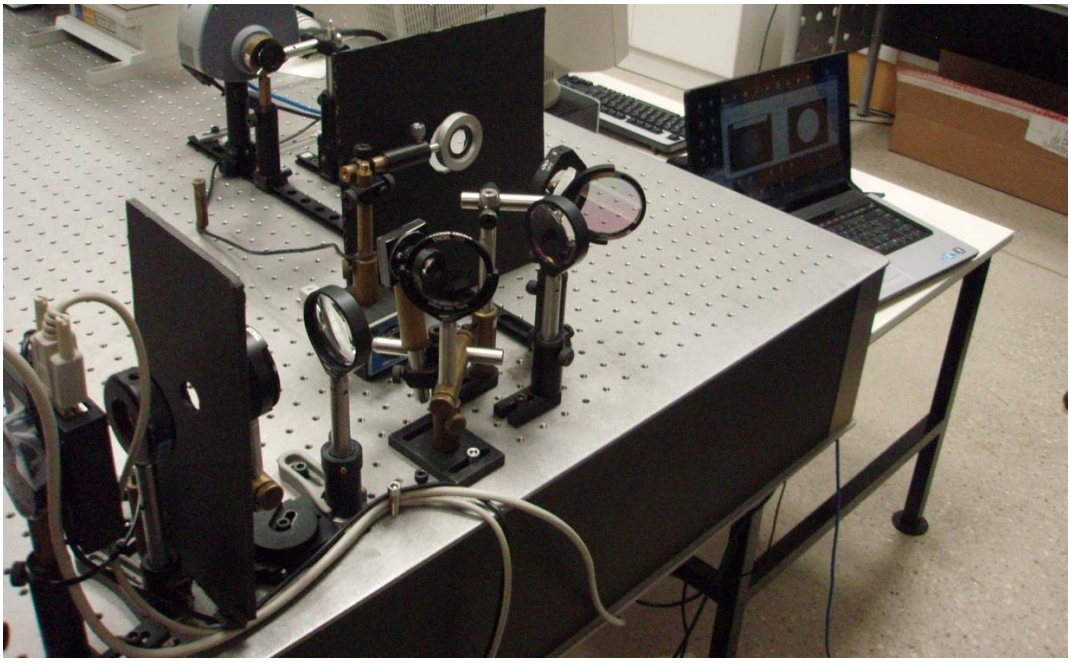

Figure 40: A photograph of the actual experimental setup.

Another feature included in this setup is that, diaphragms D1 and D2 are displaced transversely to each other so that a different part of the pupil is used for illumination/projection (first pass) and recording (second pass). The two sub-apertures have diameters of 2 mm and their centers are separated by 4 mm. As a result, a minimum of 6-mm pupil is required for image acquisition for this particular experimental configuration. When the two sub-apertures are spatially separated at the pupil plane, backscattering from the cornea and the lens is removed from the recorded retinal images. Without this strategy, light from the anterior segment reflections would degrade all the recorded images, invaliding the procedure.

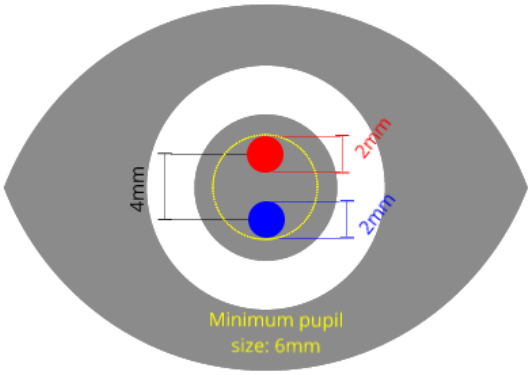

Figure 41: Schematic describing the configuration of the entrance and exit pupil modality.

The dimensions of the disks on the spatial light modulator were computer controlled and synchronized with image acquisition. In each recorded double-pass

image, the intensity at the center of each disk was computed by averaging the central 3 by 3 pixels. The approach for the calculation of the double-pass PSF was the same as with the single pass approach. The intensity at the center of each disk was normalized in respect to the intensity of the largest available disk, creating then an experimental data set for Ic. Similarly, the derivative of this intensity with respect to the disk radius was numerically estimated by fitting a linear function to two regions of angles (0.5–2 and 2.5–8 degrees) and applying Equation 14. The particular values of the computed double-pass PSF at 1.25 and 5.25 degrees were used as metrics to quantify the amount of the recorded straylight.

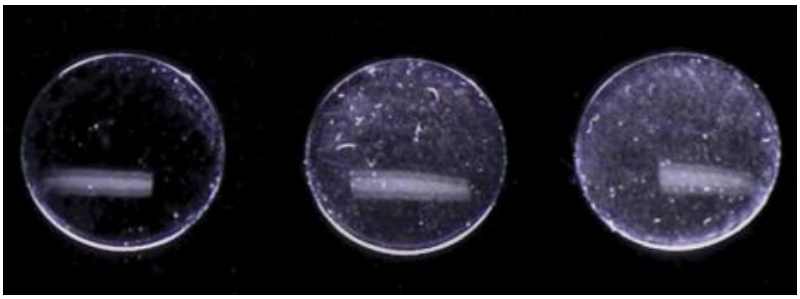

Figure 42:Dark field photography of the rigid contact lenses used to increase light scattering.

Measurements were done to evaluate an artificial eye and the effect of the Black Pro Mist 2 diffuser on the straylight of the same artificial eye (H. Ginis et al., 2012). Additionally, some custom made, rigid, gas-permeable contact lenses were employed as diffusers for measurements in human subjects. These contact lenses (see figure 42) provided by Menicon (Menicon Co. Ltd, Tokyo, Japan) contained glass microspheres in different concentrations, varying in diameter from 1 to 20 μm, with no refractive power and have been used as scattering inducers in previous study (Bueno, De Brouwere, Ginis, Sgouros, & Artal, 2007).

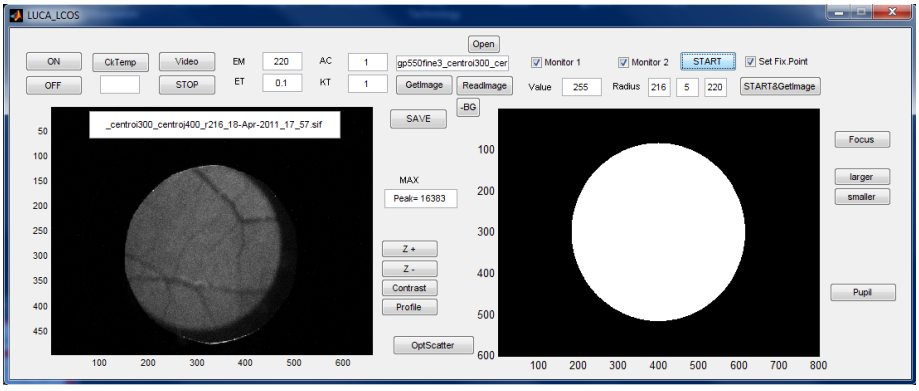

Figure 43: The GUI of the software built for the synchronous projection and the recording of the projected disks. On the left side, a frame, as recorded from the fundus is displayed while on the right side, the mask created on the spatial light modulator is drawn. Controls for the temperature of the fundus camera have been also added, along with its capture properties (Exposure time, Gain, and frame accumulation per capture). Fields for the filename, the minimum and the maximum radius of the projected disk have also been added.

3.1.2 Preliminary measurements – Proof of concept

The results are presented in figure 44, where both measurements on the artificial eye with and without the Black Pro Mist 2, the measurements on human subjects (GP, GP with the custom contact lens CL3 and JB) and measurements of the custom contact lenses CL3 and CL5 are included. The values of the double-pass PSFs at 5.25 degrees are represented.

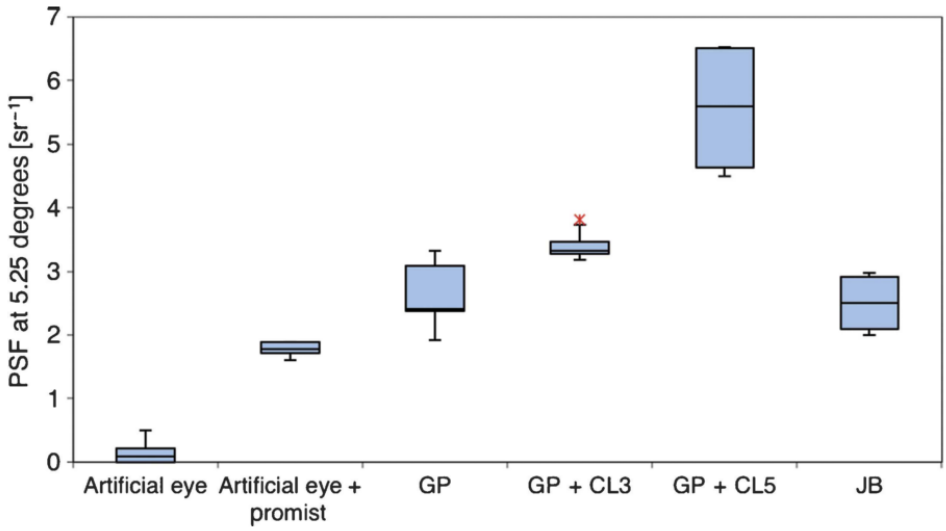

Figure 44: Double-pass PSF calculated at 5.25 degrees for the artificial eye and the human eyes under different additional scattering conditions.

3.2 WAVELENGTH DEPENDENCE OF THE INTRAOCULAR STRAYLIGHT

In this section, the results of measurements of the ocular straylight on healthy subjects, with various wavelengths, are presented.

The same setup previously described was used. As the projection of the uniform disks, and the record of the intensity at their centers, is now consuming more time, compared to the single-pass version of the setup (described in chapter 2), a series of 50 uniform disks was chosen to be projected covering an angular range from 0.18 to 7.3 degrees. Accordingly, for each captured image, synchronized to the projection, a central area of 5 by 5 pixels was used to provide an average value that would represent the recorded central intensity (Ic). Finally, similarly to the previous procedure, some initial, trial frames were recorded in order to make sure that the central disk 5 by 5 area was not coinciding with a blood vessel. In case

that this was happening, the fixating target was slightly displaced to accordingly move the ROI on the retina.

Nine Caucasian subjects (age range, 25–51 years; mean, 34 years) with no known ocular or systematic pathology were enrolled in the measurements. To ensure that the needed 6 mm of pupil diameter was ensured, two drops of tropicamide 1% (15 minutes apart) were instilled to each tested eye for pupil dilation. A pupil camera (Hercules Classic Webcam; Guillemot Corporation, La Gacilly Cedex, France) was used to control that the subjects' pupil was on the appropriate focal plane. The head was stabilized by means of a bite bar. The subjects fixated on a target at a nasal direction, and was properly adjusted to avoid large retinal blood vessels at (or near) the center of the projected disks during initial trial images. For each wavelength, the sequence of the 50 disks was recorded in a randomized order. The subjects were given time to blink between consecutive images. Finally, the measured irradiance at the corneal plane was below 25 μW/cm² for all wavelengths, for safety purposes.

An additional classification of the participating subjects was attempted based on the qualitative criterion of the iris color. Hence, two major groups where created classifying the subjects' eyes to dark and light-pigmented. he iris is forming part of the a, Tuchin, & Bakutkin, 2005) same anatomical layer with the choroid and can be a visible index of the degree of melanin pigmentation (Koblova, Bashkatov, Genin.

The PSF (retrieved from the PSF_{dp}) and the S (Straylight parameter) were used to quantify the ocular straylight. In this experiment, in order to avoid noise associated with numerical differentiation, a function (Equation 16) was fitted to the experimental data and the derivative was extracted analytically.

$$PSF_{dp} = \frac{a}{(\theta + \theta_o)^n}$$

Equation 16

where θ_o and n are arbitrary constants and α is a normalization coefficient (which depends on θ_o and n) so that the radial integral of the PSF is equal to unity. This function is also giving the possibility to approximate different values of the PSF at its most peripheral parts while θ_o can be adjusted to match different widths of the central part of the PSF. Finally, the 0.5 and 6 degrees were selected for the calculation of the S parameter, expressing scattering at narrow and wide angle respectively.

Figure 45 shows the fitted PSF's for one subject from each pigmentation group, for various wavelengths.

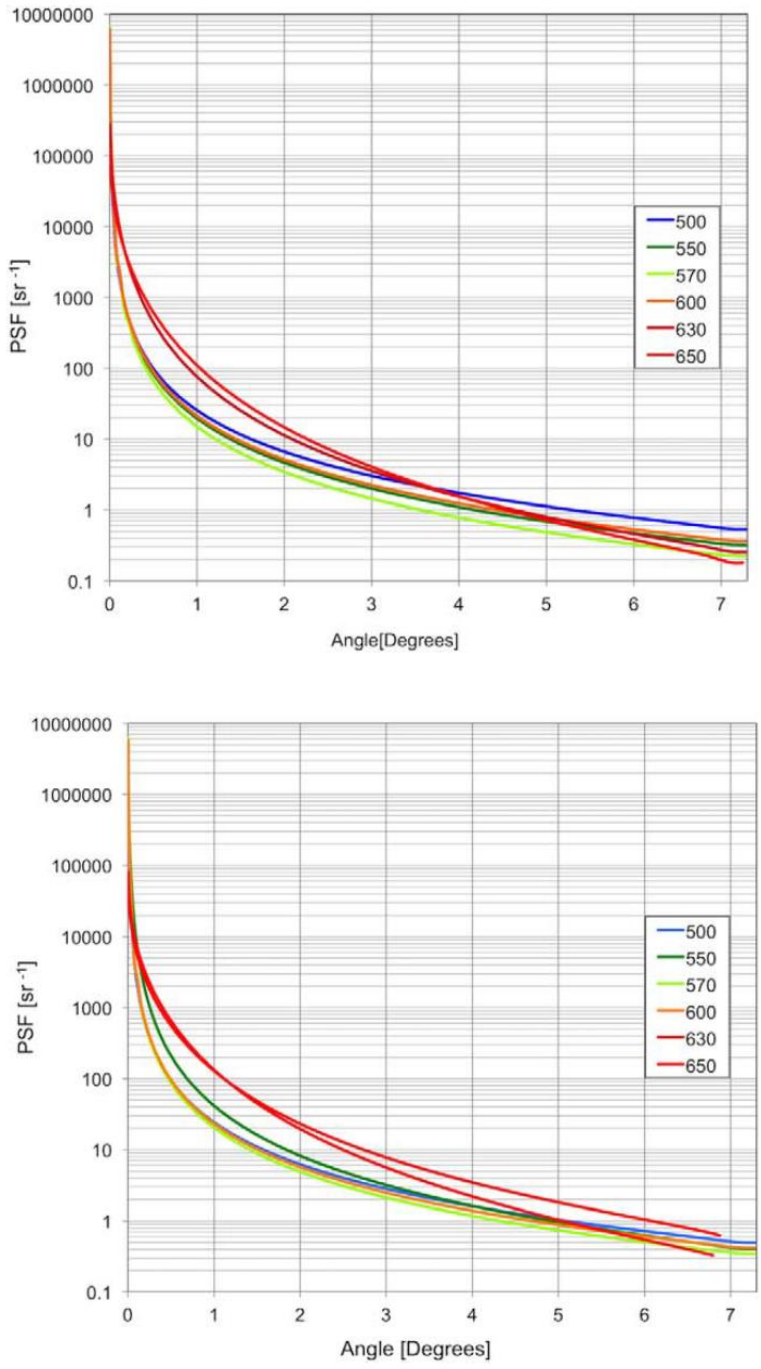

Figure 45: Reconstructed wide-angle PSFs for two eyes and different wavelengths. Upper: HG (dark pigmentation, age 43); Lower: PA (light pigmentation, age 51).

Interestingly, the PSFs for each subject are very similar for shorter wavelengths between 500 and 600 nm. However, for 630 and 650 nm, the PSFs significantly increased (approximately by a factor of 5) especially for angles up to 4 degrees.

This characteristic dependence of straylight on the wavelength is more clearly illustrated in Figure 46 where the - across subjects- average straylight parameter, S, is plotted for different wavelengths. Small-angle scattering has a stronger wavelength dependence being measurable by a significant increase for

wavelengths longer than 600 nm. The dependence was similar both in eyes with dark and light pigmentation. Thus, at wider angles (six degrees in this experimental procedure), the straylight parameter did not exhibit a noticeable increase at longer wavelengths neither for dark nor light pigmented eyes. However, for eyes with light pigmentation, a minimum in the straylight parameter between 550 and 600 nm was observed.

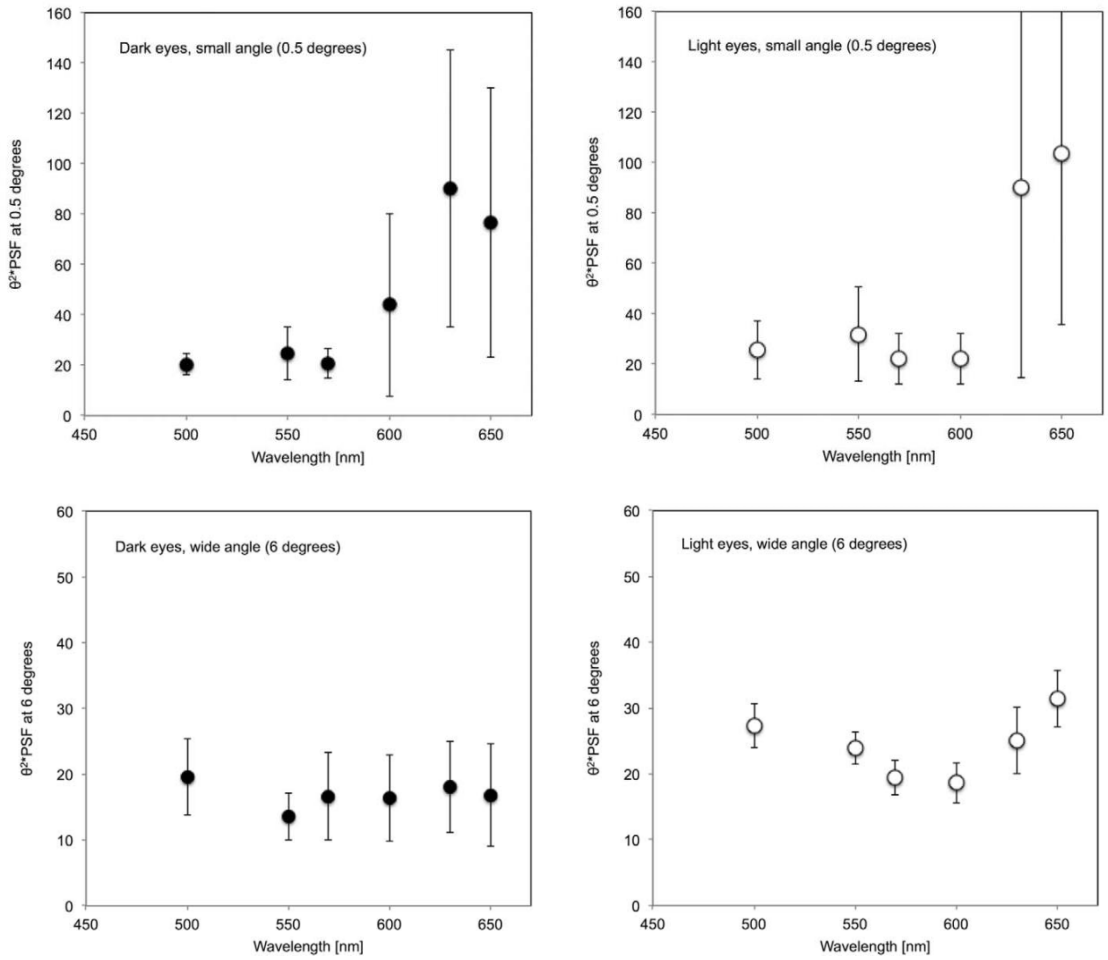

Figure 46: Straylight parameter as a function of wavelength calculated for small angles (top) and wide angles (bottom) and for two groups of eyes, those with dark pigmentation (left) and those with lighter pigmentation (right).

This also occurred when the straylight parameter was averaged for all subjects involved in the study (Figure 47).

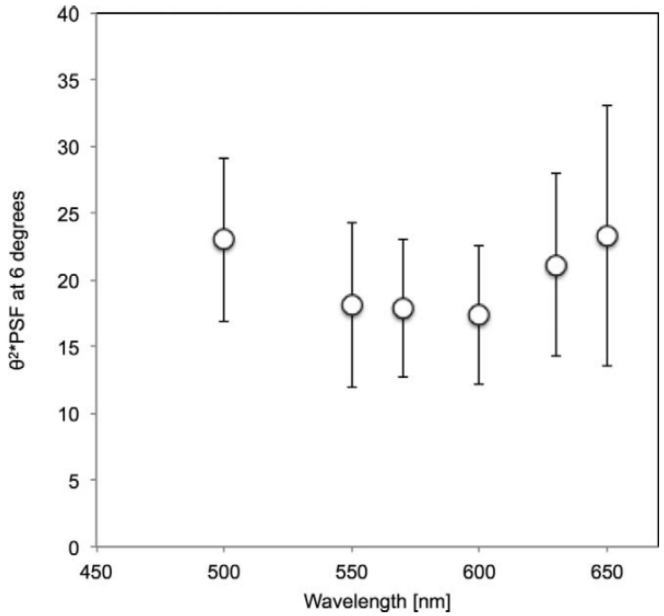

Figure 47: Straylight parameter at 6 degrees as a function of wavelength averaged for all subjects.

An additional finding is resulted if the S measurements for "long" and "short" wavelengths (averages from 630, 650nm and 500, 550, 570 nm, respectively) are plotted separately, comparing them in respect to the angle where they were recorded.

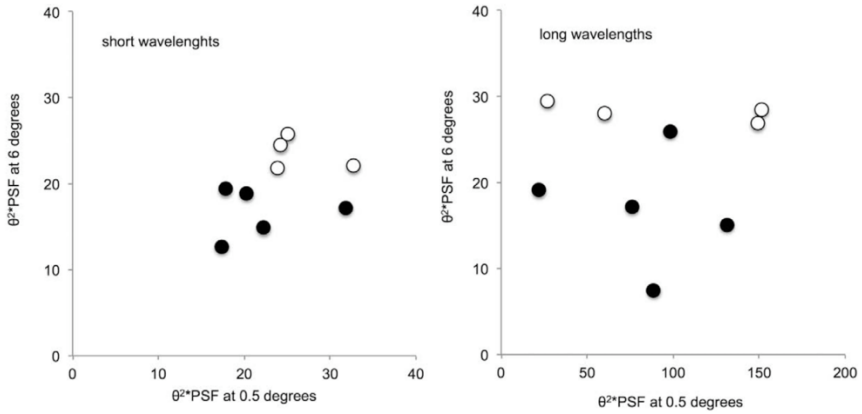

Figure 48: Correlation between the straylight parameter at 68 and 0.58 for (left) short wavelengths (average of 500, 550, and 570 nm) and (right) long wavelengths (average of 500, 550, and 570 nm) and (right) ''long'' wavelengths (average of 630 and 650 nm). Black and white symbols correspond to eyes with dark and light pigmentation respectively

For shorter wavelengths, the correlation seems to be clearer, while, on the other hand, the results do not present any correlation, denoting that longer wavelengths are interacting differently with the optical elements and tissue layers of the human eye.

In an effort to define the angular domain of the wavelength dependence of straylight, a Red/Green ratio, plotted in respect to the angle throws more light. In specific, PSF values for red (630 and 650nm) and green (550 and 570nm)

$$\frac{PSF_{Red}}{PSF_{Green}} = \frac{PSF_{630} + PSF_{650}}{PSF_{550} + PSF_{570}}$$

Equation 17

wavelengths were used to calculate a ratio and plot its values for the whole measured angular range. The results that are shown in Figure 49, demonstrate that angles further than 4 degrees show less dependence on the wavelength.

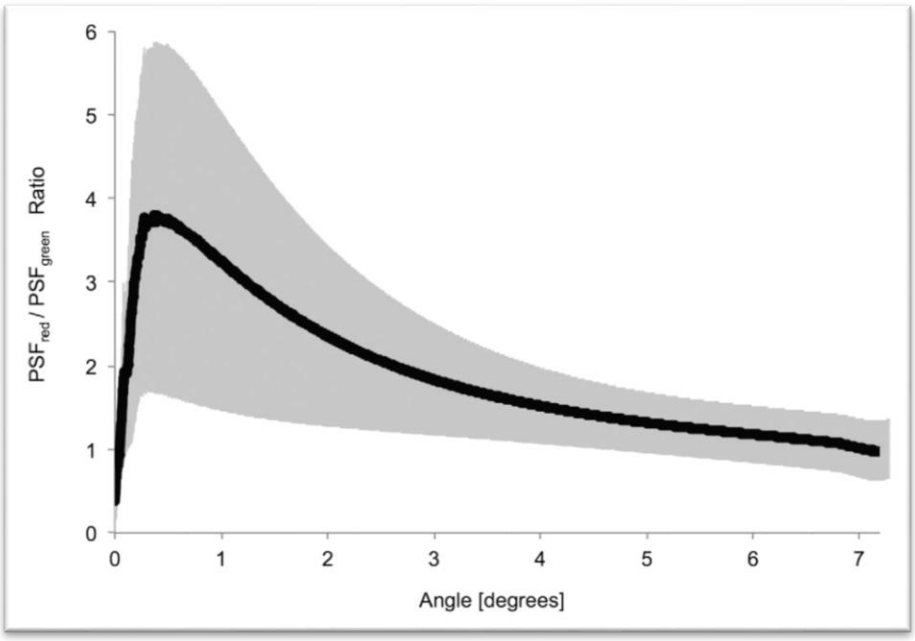

Figure 49: Ratio of the PSF at ''red'' wavelengths to the PSF at ''green'' wavelengths. Gray area corresponds to 2 standard deviations (across subjects).

Finally, to attribute this effect of wavelength on straylight, taking into account spectral absorbance and reflectance properties of the fundus, density of Oxyhemoglobin, a protein responsible for the distribution of oxygen along the human vital organs, and the standard deviation of the PSF reported in previous studies (T. Berendschot, 2003; F C Delori & Pflibsen, 1989; Hodgkinson, Molteno, Greer, & Molteno, 1994) and examining the results for the measured Straylight parameter at 0.5 degrees from all the subjects, it is clear that longer wavelengths are subject to additional interactions with the fundus (i.e. diffusion or reflection) thus, the recorded straylight values are "polluted" by light that it is not only deviated because of scattering. The following figure (Figure 50) is depicting this, later statement.

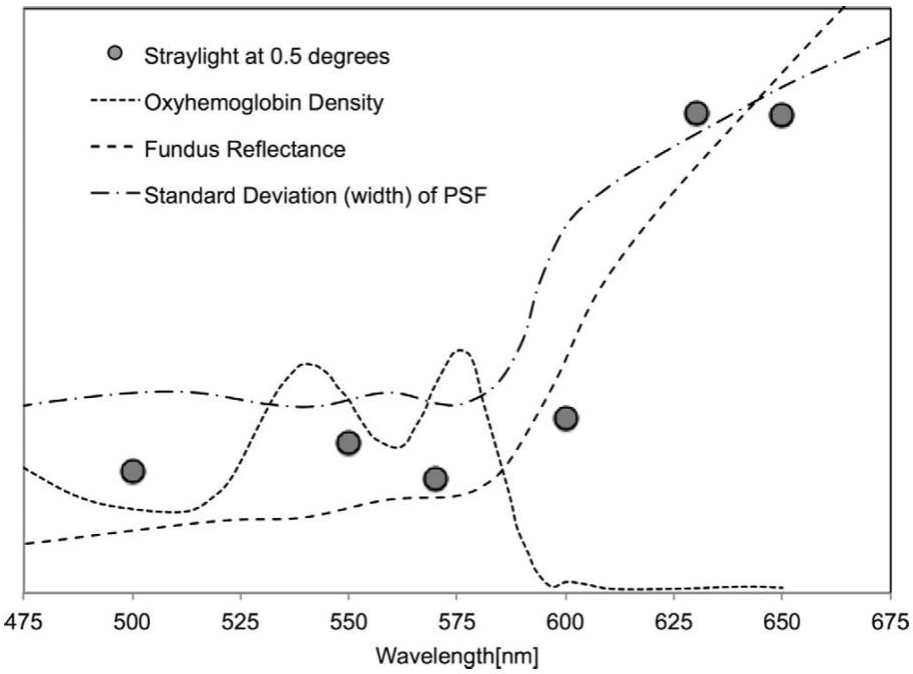

Figure 50: Straylight parameter at 0.5 degrees (average of all subjects) and other spectral properties of the fundus.

4. A PROTOTYPE CLINICAL DEVICE FOR THE OPTICAL MEASUREMENTS OF INTRAOCULAR STRAYLIGHT

Having evaluated the efficiency and the advantages that the optical integration method may bring to the measuring of intraocular straylight, and by knowing, in parallel which wavelength would be more suitable for this type of measurements, addressed to the general population, it was also concluded that to obtain more reliable results, quantifying the amount of scattered light in the human eye, these measurements have to be applied on the wider-angle of the PSF.

Keeping the previous results in mind, an effort to include all these characteristics into a device, which in the same time would perform these measurements comfortably (for the subject) and that could be relatively compact and low cost, has been attempted. This chapter includes all the details and characteristics of a prototype for measuring intraocular straylight in a clinical setting.

4.1 CHARACTERISTICS, DESIGN AND MODE OF OPERATION

Fitting the complete optical integration optical setup into a significantly more compact design for an easy to use clinical device, required several compromises. In addition, additional characteristics, such as speed of measurement and low cost, were required.

The first compromise was the need of the reconstruction of the whole PSF for a broad angular range. Only a part between 3 and 8 degrees was selected to be acquired. Having studied which portion of the PSF is better to be used for the estimation of intraocular straylight, evaluating an area where straylight dominates the angular distribution would provide more accurate measurements. Additionally, limiting the angular range would made the duration of the measurement significantly faster.

The second basic characteristic of the device, was the wavelength and spatial distribution of the illumination source. The effect of wavelength on this type of measurements has highlighted the interaction with deeper layer of the fundus, that longer wavelengths have. For this reason, they were excluded, forcing a selection of shorter wavelengths. The lowest values of straylight recorded in all subjects (independently to their level of pigmentation) between 550 and 600 nm led to the selection of a source of illumination falling to this spectral area, demonstrating a full width half maximum (FWHM) at 528 (± 10 nm). As a result, instead of a broadband source, a simplest and more cost effective custom-built LED (LTCP7P-KXKZ-25, Osram AG, Munich, Germany) array was employed as illumination source.

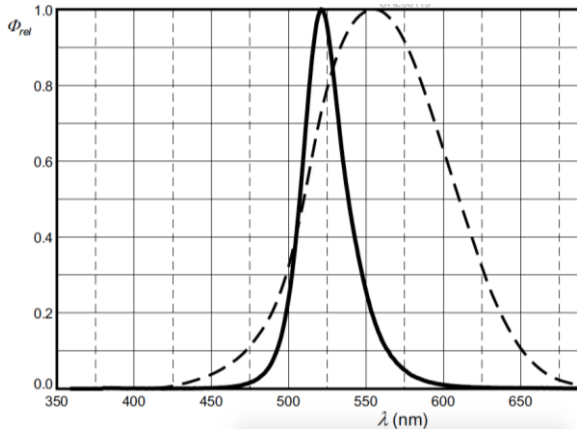

Figure 51: Relative spectral emission of the selected LED's for the illumination source (continuous line) (plot taken from www.osram.com) .

An additional difference of the operation of this device, was the actual design of the illumination source. Instead of projecting various disks of different sizes (as in the procedure of the optical integration), the LED-array was built to form two different zones: a central disk (spanning from 0 to 3 degrees) consisted of a single LED and a peripheral annulus, consisted of seven LEDs that would lay on an area from 3 to 8 degrees on the retina. Both the disk and the annulus were spatially homogenized by light shaping diffusers.

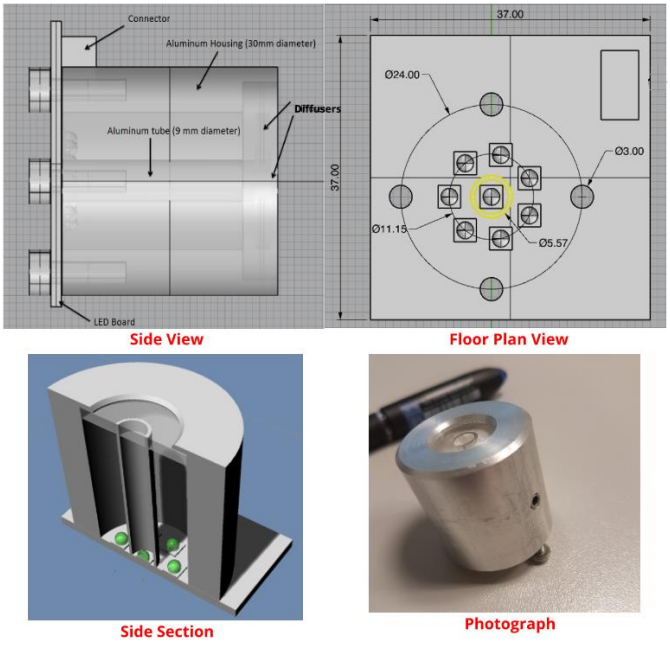

Figure 52: Conceptual schematics (Upper row and lower left) and actual photograph (low right) of the illumination source.

The operating mode of the illuminating LEDs also involved an intrinsic characteristic. In both zones, the LEDs were square-wave, temporally modulated at two distinct frequencies (483 Hz and 769 Hz for the peripheral and central areas respectively) by specially built microcontrollers. The generated signal, that would eventually be sensed with a silicon photomultiplier device (Excelitas, Waltham, MA, USA), would be further analyzed and its Fourier transform reveals the intensities reflected by the two different illumination zones.

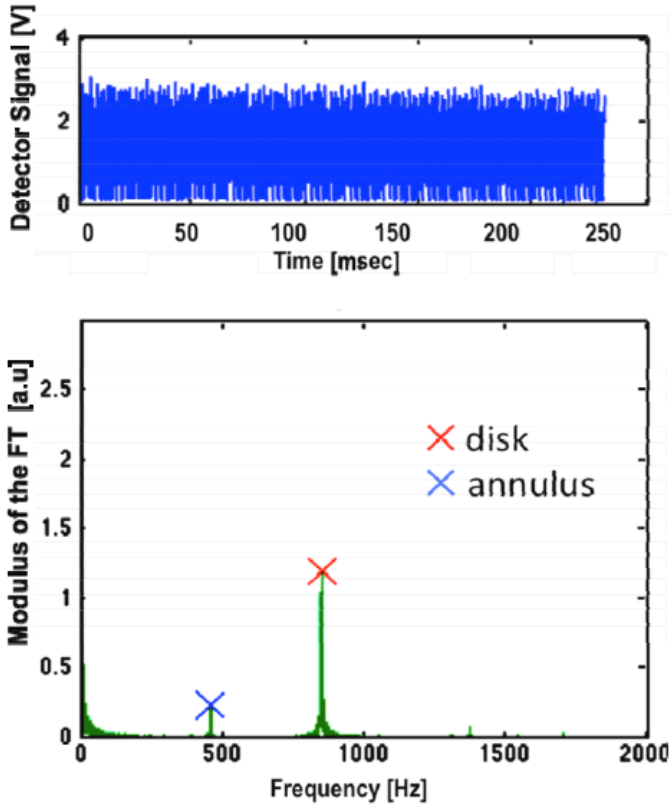

Figure 53: The Fourier transform of the detected signal, of total duration of 250ms, revealing the intensity picked up by the detector, coming from the two distinct illumination zones.

For the needs of a measurement, it was experimentally concluded that no more that 250 ms were needed. This was enough to project several times the central disk and the peripheral annulus on the retina to extract a mean intensity value for a reliable measurement. By projecting only 2 zones, instead of tens of disks and achieving it simultaneously, by temporal modulation, allowed the total time for a measurement to be reduced to a fraction of a second. Additionally, the need of pupil dilation was eliminated, since the reaction time for the pupil to be contracted is marginally above the duration of the measurement.

To image the illumination source on the retina and retrieve their intensity redistribution due to scattering, a set of lenses and diaphragms was incorporated. The challenging task was to minimize the space which was achieved by folding the optical paths appropriately. The unfolded, and simplified schematic of the design is presented in Figure 54. During the first pass, the light passes lenses L1, L2, and L3 and enters the eye and the image of the two illumination zones, is formed on the retina. Diaphragm D1 is conjugated with the pupil plane of the eye (by lenses L2 and L3) and therefore controlling the part of the pupil that is used for the object projection. The second pass that the light from retina follows towards the detector, is the same, with the only difference being that the second diaphragm, D2, is slightly displaced in respect to the first, D1, using a lower part of the pupil for its exit.

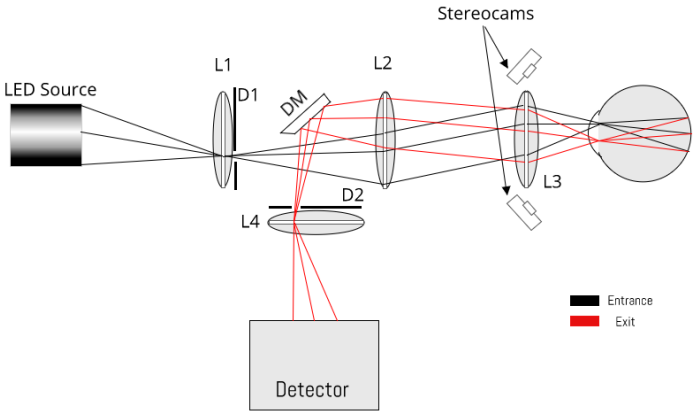

Figure 54: A simple schematic of the optical design of the device.

Three additional mirrors made possible the folding, giving a geometrically more practical shape as represented in Figure 55.

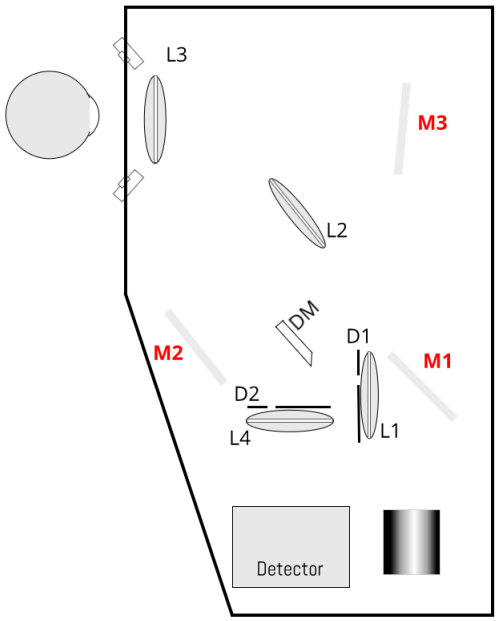

Figure 55: The folded version of the optical design.

The diaphragm displacement is also applied in this design. Thus, in this given modality, the geometrical shape of the diaphragms used is rectangular with dimensions of 2 x 7 millimeters and the space between them being another 2 millimeters. This pupil arrangement requires a total of 6 mm of pupil diameter for a proper measurement. Using this modality for entering and exiting the pupil, a very precise centration and positioning of the plane where the actual pupil will be during the measurement, is crucial. For this objective, a pair, instead of a single, pupil cameras were used. An alignment process was also developed for the special

purposes of this stereo-camera centration. Although the position of the cameras was symmetrical to the ideal centration of the eye, the viewing angles from each was not the same. As a result, the pupil was imaged with a distorted (ellipsoid) shape instead of circular. The images were post-processed to counter-stretch them and restore the circular shape of the imaged pupil. In order to compare the images from each camera, a composite video resulting from both images was displayed, in live mode, where the frames grabbed from the two cameras were being patched as so the upper half of the live video was coming from one and the lower from the other camera. Ideal centration would result to a circular pupil shape, consisted by the two halves acquired from each camera.

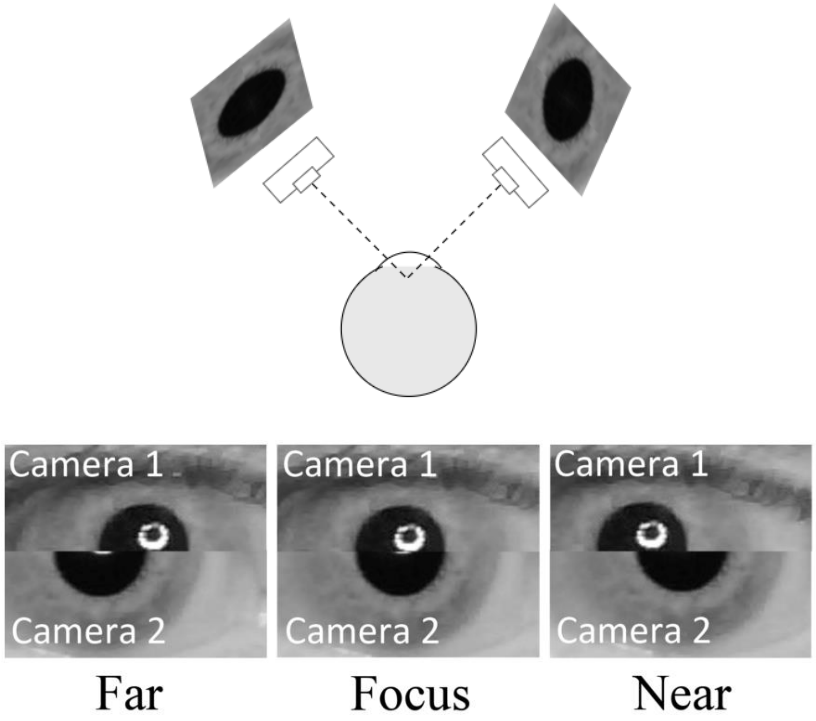

Figure 56: (Upper figure) A schematic representation of the positions of the stereo-cams and the "distorted" pupil shape that were recording due to the angle. (Lower figure) An example on how the pupil would appear in not placed in the correct plane.

The initial alignment of the camera was also essential in order to establish a correctly centered and focused pupil plane. An appropriately design target was printed for this purpose. On it, the exit and entrance pupils appeared on a 1:1 geometrical schematic representation. This target was initially placed in front of the last lens, were the pupil would approximately be positioned. Then, the illuminating source was turned on, on a continuous emitting mode and the plane where the correctly focused rectangular-shaped beam appeared, matching the shape and dimensions of the printed target, was were the ideal pupil plane should be. The next step would require the recording of a frame from each stereo-cam. Each of the frames would contain the distorted shape of the printed –on the target- pupil, as it would appear when the pupil would be correctly focused. Finally,

appropriate stretching and reconstruction of the two images would result to the required perfectly circular shape of the printed pupil.

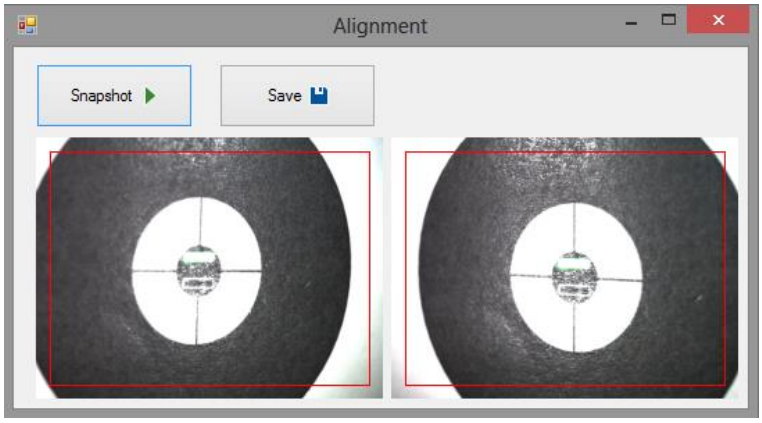

Figure 57: The alignment procedure as it was done through the GUI of the custom- developed software

The system was designed to detect light received only from the central part of the disk. A signal detected that carries the flickering frequency of the annular part of the source, is a result of light scattering that deflects light from the annulus to the center of the disk. Small refractive errors or aberrations are theoretically neglected. The dimensions of the PSF associated to aberrations are much smaller than the spatial separation between the edges of the annulus and the measurement zone. As for the signal detection and manipulation, the temporal resolution of the two regions is marking the origin of the intensities detected. The amplitude of the signals, after Fourier transform, are used for the calculation of the straylight parameter. If I_d and I_α are the recorded intensities from the disk and the annulus respectively, then it can be assumed that the contribution of the annulus to the center of the image would be:

$$I_\alpha = I_o \int_{\theta_1}^{\theta_2} 2\pi\ \theta\ PSF(\theta) d\theta$$

Equation 18

while the contribution of the disk to the center would be:

$$I_d = I_o \int_{0}^{\theta_1} 2\pi\ \theta\ PSF(\theta) d\theta$$

Equation 19

where θ_1 is the radial size of the disk and θ_2 the outer angular size of the annulus. Accordingly, the double-pass PSF at the middle of the angular range of the annulus (which is selected as the representing angle for which the straylight parameter would result), can be calculated as follows:

$$PSF_{dp} = \frac{1}{2\pi\theta_s} \frac{1}{\theta_1 - \theta_2} \frac{I_\alpha}{I_\alpha + I_d}$$

Equation 20

Finally, the double-pass straylight parameter would be:

$$S_{dp} = \theta^2 PSF_{dp}$$

Equation 21

and assuming that the intraocular straylight is the half of the value estimated in double-pass, the representative S parameter would be:

$$S = \frac{S_{dp}}{2}$$

Equation 22

It is interesting to observe that in Equation 20 the absolute intensity of the annulus and the disk are eliminated. The calculation is performed only based on the relative contributions and source geometry. Similarly, parameters as fundus reflectance or detector gain are eliminated from the calculations. The experimental values for the amplitudes of the fundamental frequencies associated to the disk and the annulus resulting from the Fourier transform can be directly used in Equation 20. This approach greatly increases the dynamic range. Even the value PSF at an angle of 5.5 degrees is expected to be more than six orders of magnitude lower than the PSF value at the peak, the recorded signals are within the same order of magnitude (Figure 53). The equations above provide the theoretical basis for the calculation of PSF values and the straylight parameter. However, in the instrument the measurement is not performed at an infinitesimally small area in the center of the disk/annulus. Moreover, the finite differences implied in Equation 20 is an approximation of the derivative required for the exact calculation. Since these approximations are not necessary in a computer-based instrument for the actual measurements a lookup table linking the values of I_α and I_d with S was generated. This numerical calculation involves the 2-dimensional convolution of PSFs with varying amount of straylight (S) and numerical integration over the angular range of the measurement area to derive I_α and I_d. During calibration, baseline values for I_α and I_d were recorded and the system intrinsic straylight was calculated by taking measurements of an artificial eye (a glass lens) that was assumed to have no straylight. These background signals and straylight were subtracted from the values obtained from human eyes.

4.2 PROOF OF CONCEPTUAL DESIGN AND VALIDATION OF THE DEVICE

To test the sensitivity and accuracy of the device, diffusers from the Black Pro Mist series were used to induce straylight mimicking cataracts. Ten eyes of ten subjects with no known pathology were measured with four different grades of these filters simulating mild to moderate cataract. The filters were introduced as close as possible to the eye. The results from these measurements are presented in Figure 58.

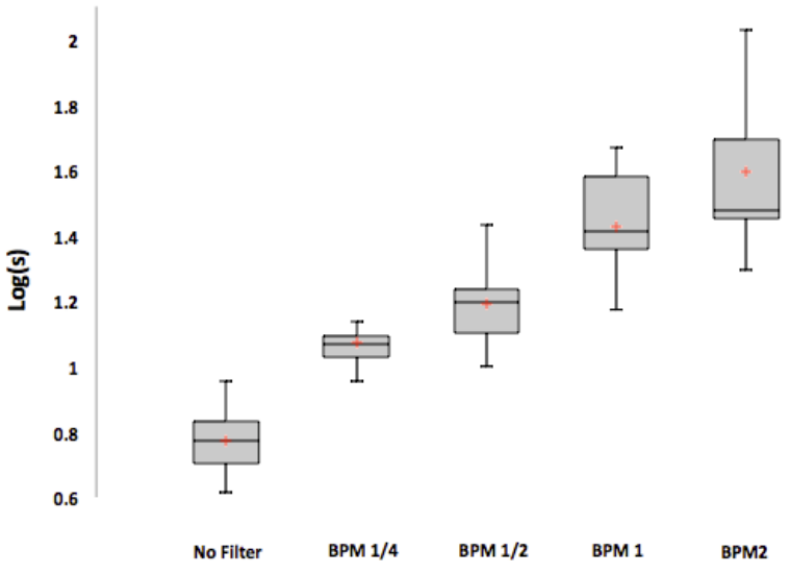

Figure 58: Straylight induced by the filters (expressed as the logarithm of the straylight parameter). BPM1/4, BPM1/2, BPM1 and BPM2 refer to different diffusing filters that were introduced in front of the eyes that are manufactured to introduce progressively more straylight.

It was confirmed from the above, that the prototype device could quantify correctly the amount of intraocular scattering, for young and healthy subjects. Additionally, the increase of straylight that the diffusers provoke was also quantified correctly and according to the density of the diffusers that the manufacturer provided.

4.3A CLINICAL APPLICATION OF THE DEVICE: MEASUREMENT OF STRAYLIGHT IN CATARACT PATIENTS

As a next step, and after having validated the device we explored whether it could also potentially be a used in clinical applications. Its primary objective, in a clinical setup, would be to objectively determination of the level of transparency of the ocular media, by quantifying the intraocular scattering. For this reason, the prototype device was deployed in the Ophthalmology Service of the University Hospital (Hospital Virgen de la Arrixaca, Murcia). The objective was the measurement of straylight in patients suffering from cataract and compare the results with other methods of quantification of the severity of the cataract.

In this study, 44 patients with cataract (mean age: 62.9 ± 5.08 years; range: 55 to 72 years) and 9 young healthy volunteers (mean age: 34.6 ± 6.75 years; range: 28 to 45 years) were recruited. Although measurements were performed in both eyes, only one eye of the patients and healthy volunteers was used for the screening and comparison. After standard clinical examination, patients with no pathology other than mild to severe nuclear cataract were informed about the objectives and methods of the current study. Those who consented underwent three consecutive measurements with the prototype. The average value of these three measurements was used for analysis.

Additionally, a subjective grade for each eye was obtained after classification according to the LOCS III method, based on slit-lamp photographs acquired during clinical examination. The value reported was representative for the nuclear opalescence only and was done by an experienced (in this classification process) clinical investigator. Finally, straylight for each eye was measured psychophysically by using the compensation comparison method (C-Quant straylight meter; Oculus Optikgeräte GmbH, Wetzlar, Germany).

After the psychophysical measurements, the patients received 1% tropicamide and 10% phenylephrine eye drops for mydriasis and the optical measurements were repeated.

A first conclusion derived from this clinical study was that drug-induced pupil dilation was not necessary for the measurements. The results from the measurement process before and after pupil dilation demonstrated a good correlation, as shown in the following graph:

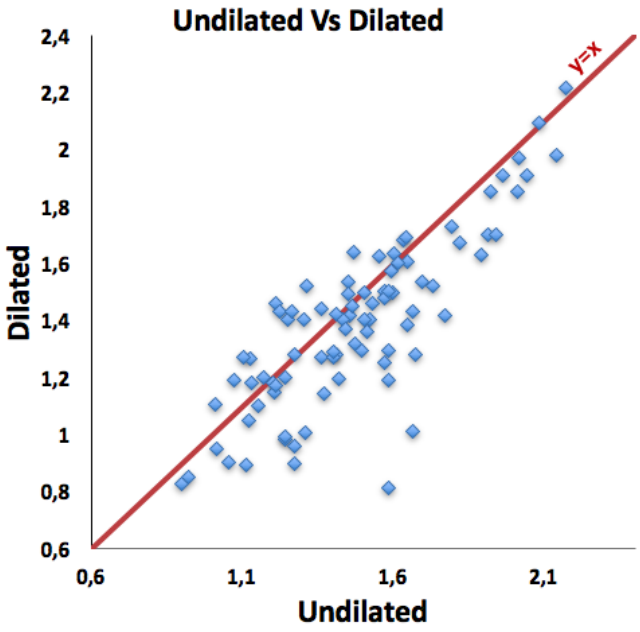

Figure 59: Scatter plot demonstrating the correlation between measurements acquired before and after dilation.

The Pearson correlation coefficient between the two groups of measurements was R=0.868, denoting strong correlation between measurements of dilated and non-dilated eyes. This is adding an important characteristic to the type of the measurement required, as it can be achieved with the least invasive method, not being limited to pathological instances where drug-induced pupil dilation cannot be performed. It needs to be mentioned, that as seen in Figure 59, for some subjects, the straylight was measured significantly different before and after pupil dilation. This disagreement between measurements is attributed to the size of the pupil (correlated also with age) where, possibly, light reflected directly from the iris, is perceived as scattered. From this observation, it was made very comprehensive that adequately large pupil was essential for a correct measurement.

The measurements resulted from the prototype device and the compensation comparison method device were also in accordance:

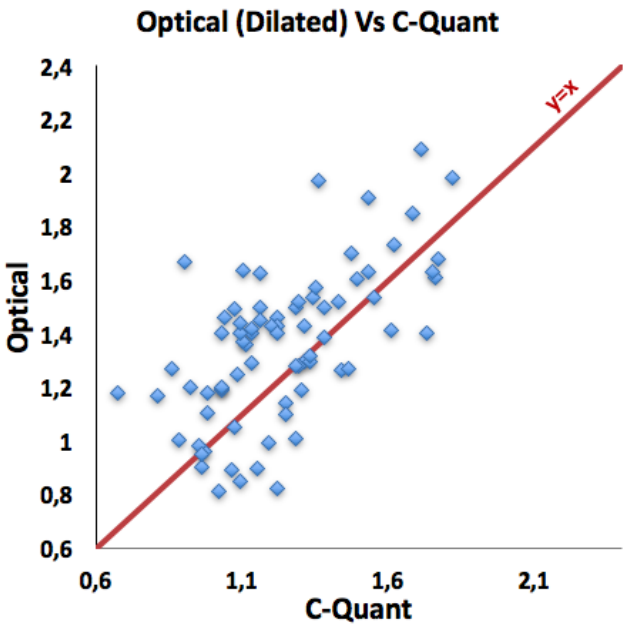

Figure 60: Scatter plot comparing the results from the optical prototype device (in dilated eyes) and the C-Quant.

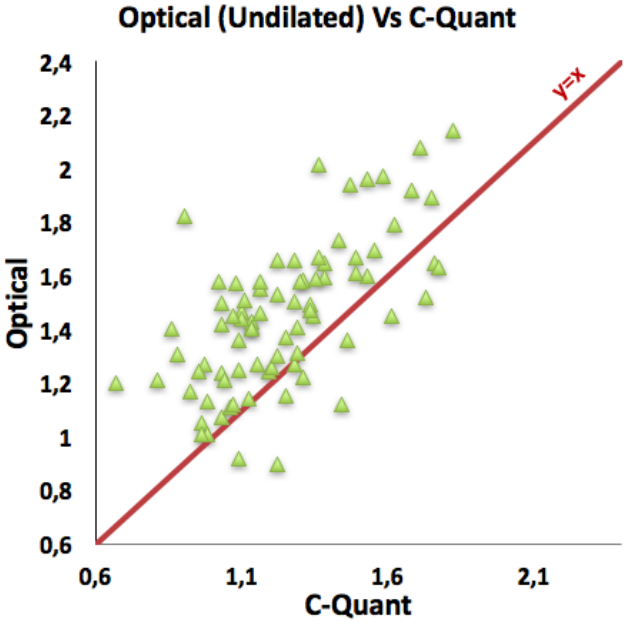

Figure 61: Scatter plot comparing the results from the optical prototype device (in undilated eyes) and the C-Quant.

Pearson correlation coefficient, R, for dilated eyes measured optically, and the C-Quant device, was 0.652 thus for undilated 0.623. This good correlation between the two devices, that has been recorded, is further backing up its validity since the C-Quant straylight meter has been an already established device for the measurement of intraocular scattering.

Pearson correlation (R) coefficient between different methods of measurement	**Optical (Dilated)**	**Optical (Undilated)**	**C-Quant**
Optical (Dilated)	**N/A**	**0.868**	**0.652**
Optical (Undilated)	**0.868**	**N/A**	**0.623**
C-Quant	**0.652**	**0.623**	**N/A**

Table 3: Pearson Correlation Coefficients between different types of intraocular scattering measurement.

Finally, the measurements from subjects with dilated pupils, were compared with the LOCSIII grading method. Similarly, the results were in agreement, as subjects that were highly graded in the LOCSIII scale appeared to generate high values of straylight parameter, too:

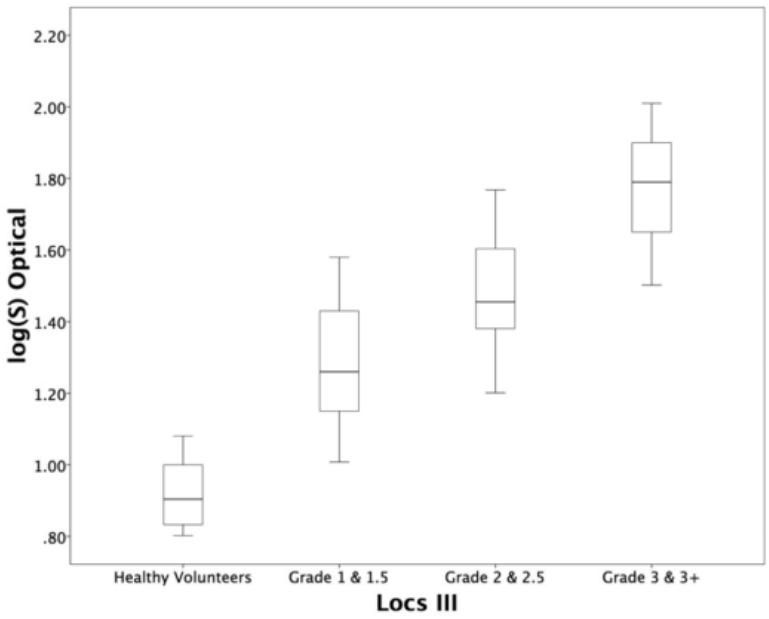

Figure 62: Straylight values for different (LOCS III) groups.

It can be concluded that the compact device for the measurement of intraocular scattering, using the optical integration method, was successfully used in a clinical setting. Moreover, it was demonstrated that the improvements that carried, contrary to the experimental optical double-pass setup, have given it characteristics as ease and convenience of use, short examination time and relatively low cost, making its application on measurements in a clinical environment, possible. Its final re-design of the optical path, made also possible its

size reduction, making possible to be manufactured with a size comparable to other ophthalmo-diagnostic devices (as seen in Figure 63 where the actual prototype is demonstrated).

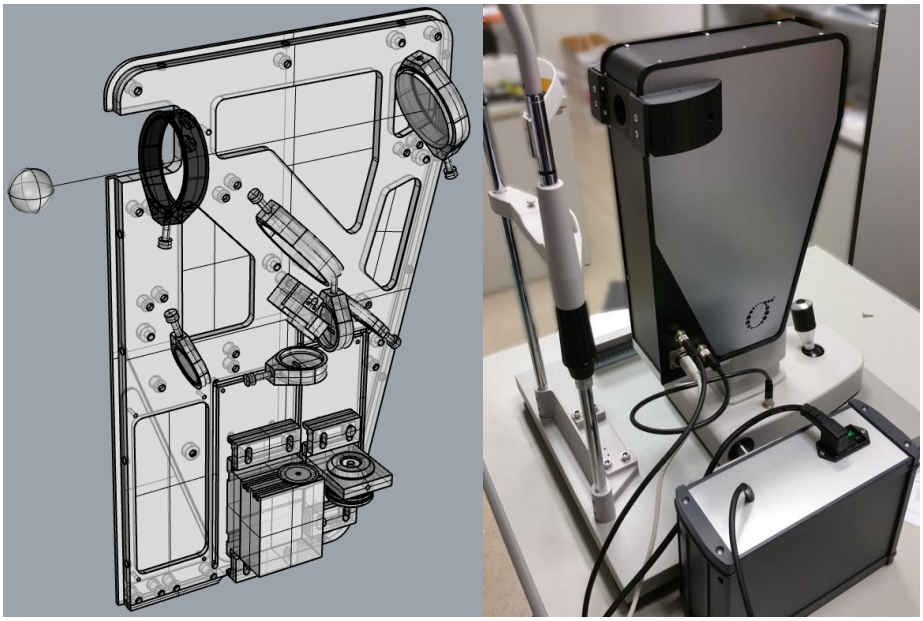

Figure 63: A conceptual design of the device (left) and its final appearance after the manufacturing process.

5. NEW PSYCHOPHYSICAL METHOD FOR INTRAOCULAR SCATTERING MEASUREMENTS: THE DIFFERENTIAL CONTRAST SENSITIVITY TEST

In this chapter, an effort to relate contrast sensitivity (CS) with the straylight parameter is presented (Elliott, Hurst, & Weatherill, 1990; Howes, Caelli, & Mitchell, 1982; Ross, Bron, & Clarke, 1984; Sabour-Pickett et al., 2013). Additionally, such an effort could result to a preliminary screening of intraocular scattering and to an effective method of measuring intraocular scattering, when and where appropriate instrumentation or equipment is not accessible.

5.1 MEASURING CONTRAST SENSITIVITY DIFFERENTIALLY

Usually, most of the applied methods for measuring CS are usually condensed and are limited in the detailed description of the CS at a broad range of spatial frequencies, in order to be more convenient and useful both for the clinicians and the patients. Most measurements are done with the use of pre-printed charts, though quite recently, computerized methods were also developed. One of them, called "the q-CSF (q standing for quick) is particularly proven to be effective and fast (L. A. Lesmes et al., 2010) as it encloses some novel characteristics that cannot be applied in other conventional methods of CS measurements.

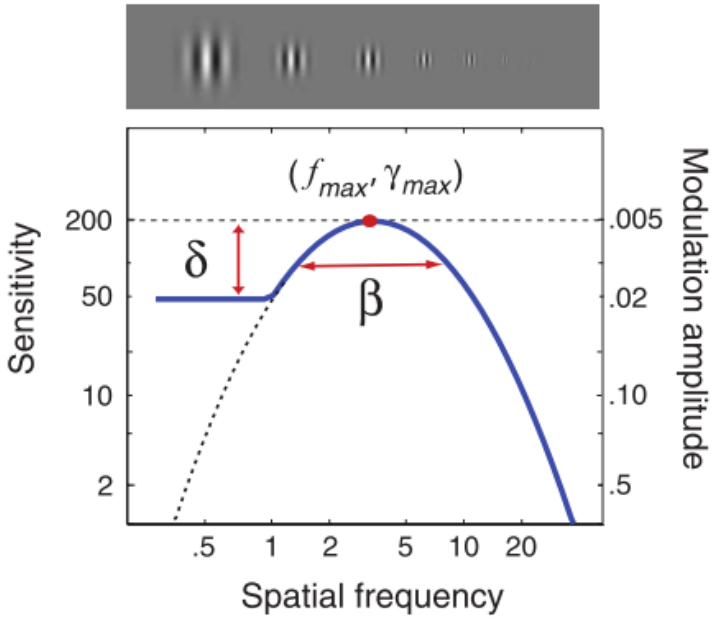

Figure 64: The spatial contrast sensitivity function, can be described by four parameters: (1) the peak gain, γ_{max}; (2) the peak frequency, f_{max}; (3) the bandwidth β; and (4) the truncation (plateau) on the low-frequency side, δ.

The strategy that q-CSF methods applies, is to estimate some parameters, that define the CSF, by fitting the psychometrics function with an adaptive method

of predicting the stimulus that will be presented, to a two-alternative forced choice (2AFC) method. The four parameters that are predicted, and define the CSF, are the Peak Gain, the Peak Frequency, the bandwidth (its FWHM) and a truncation point for the low spatial frequencies (Figure 64). The stimulus that the subject has to judge his decisions on, are sinusoidal gratings, projected on computer monitors, windowed through a Gabor patch which was constant across all frequencies. The two alternative choices given at the subject, were to select, upon inclination of the gratings, left or right, depending on the angle of them (±45 degrees from vertical).

We used a modified version of the q-CSF method, implementing a glare source for differential tests. A uniform fluorescent lamp was used as a glare source. It was concentrically placed to the area where the sinusoidal stimuli of the q-CSF test were projected (test area), while the rest of the monitor was covered with a black carton, to avoid any luminance irrelevant to the test being detected by the subject. Special care was also taken so as light from the glare-lamp wouldn't illuminate the test area and invoke changes of the mean luminance of the projected stimuli. The angle that the glare source was positioned as well as the spatial frequencies of the test depended on the distance that the subject would be positioned, away from the screen. For the measurements performed in this study, the subject was positioned 1 meter away from the computer screen, resulting the retinal area covered by the glare source to have a thickness of 1.60 degrees, starting at 3,18 degrees, radially. The test area, for this distance was spanning on a total of 7.36 degrees of visual field (Figure 65).

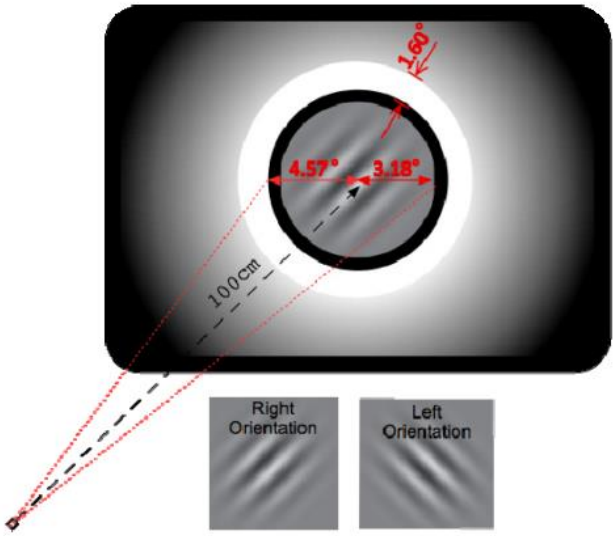

Figure 65: Schematic representation of the test screen used for the differential q-CSF measurements.

The mean luminance of the test area was 40 cd/m² whereas the luminance of the glare annulus was 8030 cd/m². Although it may appear exaggerated, the luminance of the glare source was essential to be orders of magnitude larger the stimulus'. It is reminded that the intensity of scattered light, at these wide angles, is several orders of magnitude that this of the central part of its PSF, a problem

that initially led to the Optical Integration Method solution. Additionally, the straylight has to be noticeably enough, in order to degrade the contrast of the projected stimuli.

Being differential, the method would require 2 series of measurements. The first should be without the presence of glare, though, the second with its effect present. By this manner, a relative difference would be detected, and as described later, an estimation of the straylight parameter could potentially be possible.

For the effect of straylight, estimated by the relative difference of the CS, as a range of spatial frequencies was evaluated, the metric chosen for comparison was the area below the plotted CSF in logarithmic scale (logCSF), referred in the text as AULCSF (Area Under Log CSF) (Figure 66).

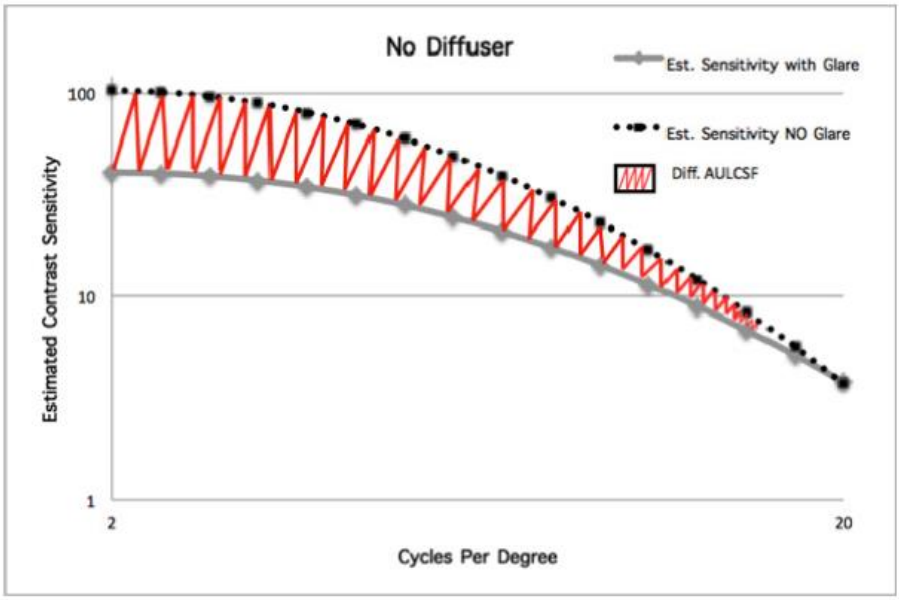

Figure 66: Difference of the area Under the Logarithmic values of CSF (Diff. AULCSF) from the measurement with the glare source on and off.

The second metric that was extracted and used as a means of comparison, was the amount of straylight described by the straylight parameter, S. For its estimation, the CS at only one spatial frequency was used (set at 2 c/deg) with (CSon) and without (CSoff) the presence of glare. This specific spatial frequency was selected for three reasons: The first was that the peak sensitivity of the human visual system is around this frequency area (Robson, 1966). Secondly, the part of the CSF that is mostly affected by the presence of glare sources is the low-spatial frequency part (Abrahamsson & Sjöstrand, 1986). Thus, it would be a suitable area for differential measurements even for subjects with very mild ocular opacities. And, finally, the q-CSF method demonstrated higher accuracy for low-frequency CS, as preliminary verified.

The method of calculating the S value is described in detail below. Following the formalism of Paulsson et al (Paulsson & Sjostrand, 1980), and assuming that the effects of adaptation and pupil size can be neglected, as all measurements were performed at photopic conditions and no measurable changes

in pupil size was detected, the relationship between the CS for each glare condition can be written in terms of luminance parameters as:

$$\frac{CS_{on}}{CS_{off}} = \frac{L}{L + I_g}$$

Equation 23

where I_g is the intensity from the glare source superimposed over the central area where the sinusoidal patterns are displayed, and L is the mean luminance of the grating stimulus. Moreover, assuming that the glare source has a uniform intensity equal to E and α_{min} and α_{max} its minimum and maximum angular radius respectively (where $\alpha_{min} = 4.57$ degrees and $\alpha_{max} = 6.17$), the intensity I_g at the center of the ring lamp is given by the equation:

$$I_g = E \int_{a_{min}}^{\alpha_{max}} 2\,\pi\,\alpha\,PSF(a)da$$

Equation 24

where α is the visual angle and the PSF is the Point Spread Function of the eye. For further simplification, the PSF expression from the Stiles-Holladay equation was adopted ($PSF = \frac{S}{a^2}$, α units in degrees). By introducing this expression into the integral of the Equation 24 and developing it, the intensity provided by the glare source becomes directly proportional to S:

$$I_g = 2\pi \mathrm{E} \mathrm{S} Ln\left[\frac{\alpha_{\max}}{\alpha_{\min}}\right]$$

Equation 25

Finally, S can be calculated replacing Ig from the Equation 25 in Equation 23:

$$\mathrm{S} = \frac{1}{2\pi}\frac{\mathrm{L}}{\mathrm{E}}\left(Ln\left[\frac{\alpha_{\max}}{\alpha_{\min}}\right]\right)^{-1}\left(\frac{\mathrm{CS}_{\mathrm{off}}}{\mathrm{CS}_{\mathrm{on}}} - 1\right)$$

Equation 26

This expression provides a direct procedure to determine S from the contrast thresholds measures with and without glare.

5.2 PROOF OF CONCEPT AND PRELIMINARY MEASUREMENTS ON SUBJECTS

For the effectiveness and evaluation of the method, measurements on subjects were performed and compared with the results from measurements with two additional devices, the compact prototype of the optical integration method and the C-Quant.

The CSF was estimated for a range of spatial frequencies between 2 and 20 cycles per degree (c/deg). Seven normal subjects aged 31 ± 4 years old, all nearly emmetropes and without any known ocular pathologies, participated as volunteers in the study. Measurements were done monocularly, on the dominant eye of each participant. Additionally, the Black Pro Mist diffusers were again used in this experimental procedure. The grades that were selected were the ¼ and 1. For every subject, 2 measurements of 100 trials, for each glare condition (on and off) was performed. The same procedure was followed for the subjects with the diffusers added separately. Both metrics, DiffAULCSF and estimated S parameter, were used as a means of comparison to the other two devices. Additionally, prior to comparison, a relative repeatability evaluation was performed (Vaz, Falkmer, Passmore, Parsons, & Andreou, 2013).

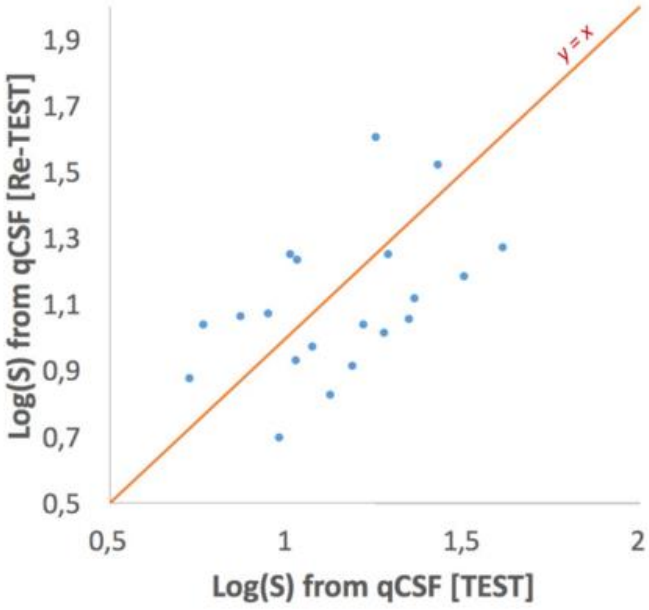

Figure 67: The test-retest comparison for the evaluation of the relative reliability of the Differential q-CSF method on the estimation of the straylight parameter S.

The repeatability of the CSF method for calculating the intraocular straylight parameter was evaluated by calculating the Pearson's correlation coefficient for the

test-retest (relative reliability) results (Figure 67). In particular, the Pearson's correlation coefficient was 0.592.

The average values of intraocular scattering for the 3 situations as measured with the differential q-CSF method, C-Quant and the Compact Optical Integration device (Sigma) are presented in Figure 68 along with the AULCSF metric:

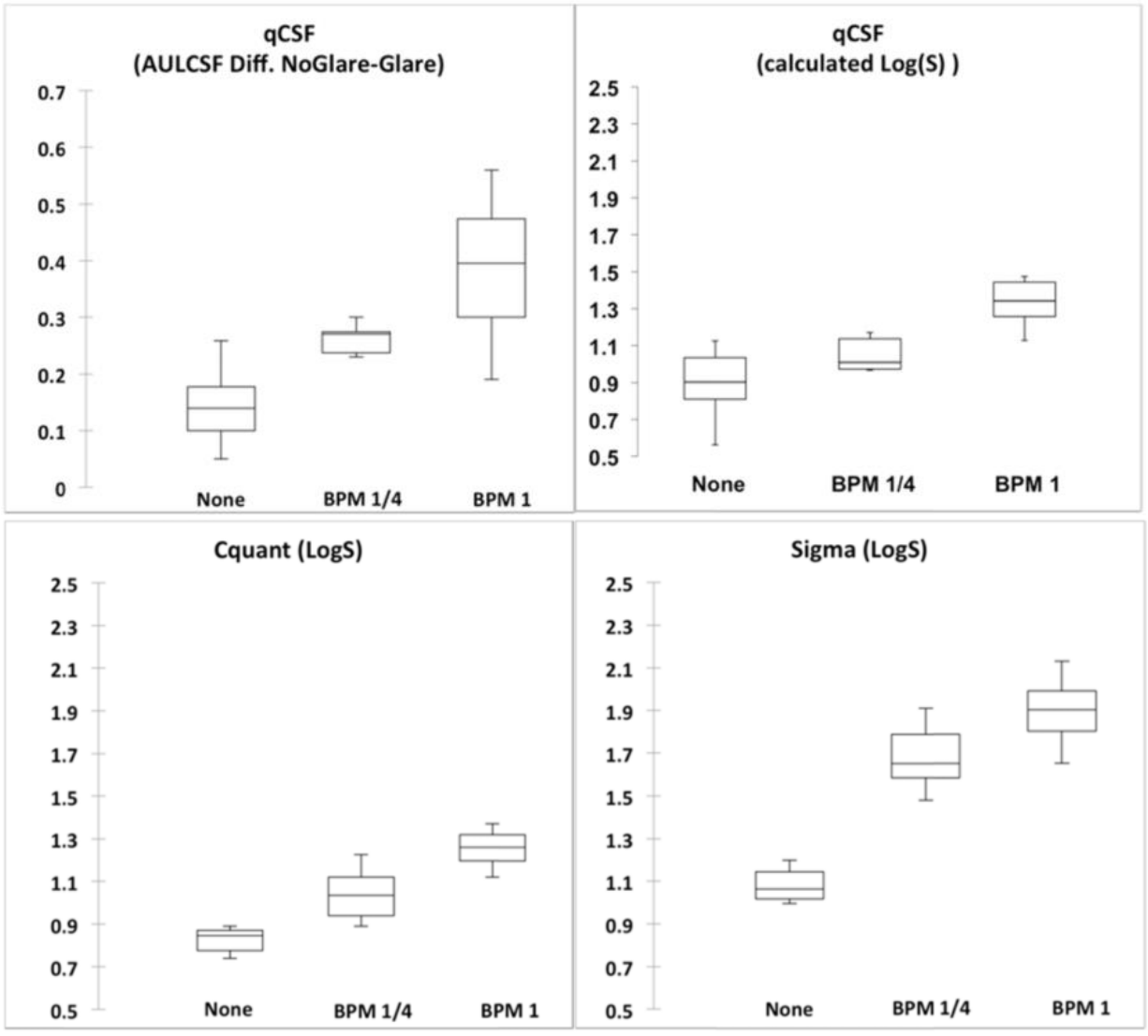

Figure 68: The median (central line inside each box), minimum and maximum values (whiskers) and the Q1 and Q4 quartiles (lower and higher borders of each box, respectively) of the Diff. AULCSF (upper left box) and the intraocular scatter, as measured by the three different methods.

The Pearson correlation coefficient was calculated to compare the results recorded by the differential CSF method with the ones retrieved from the C-Quant and the optical integration devices. The results are presented in Figure 69 and Table 4.

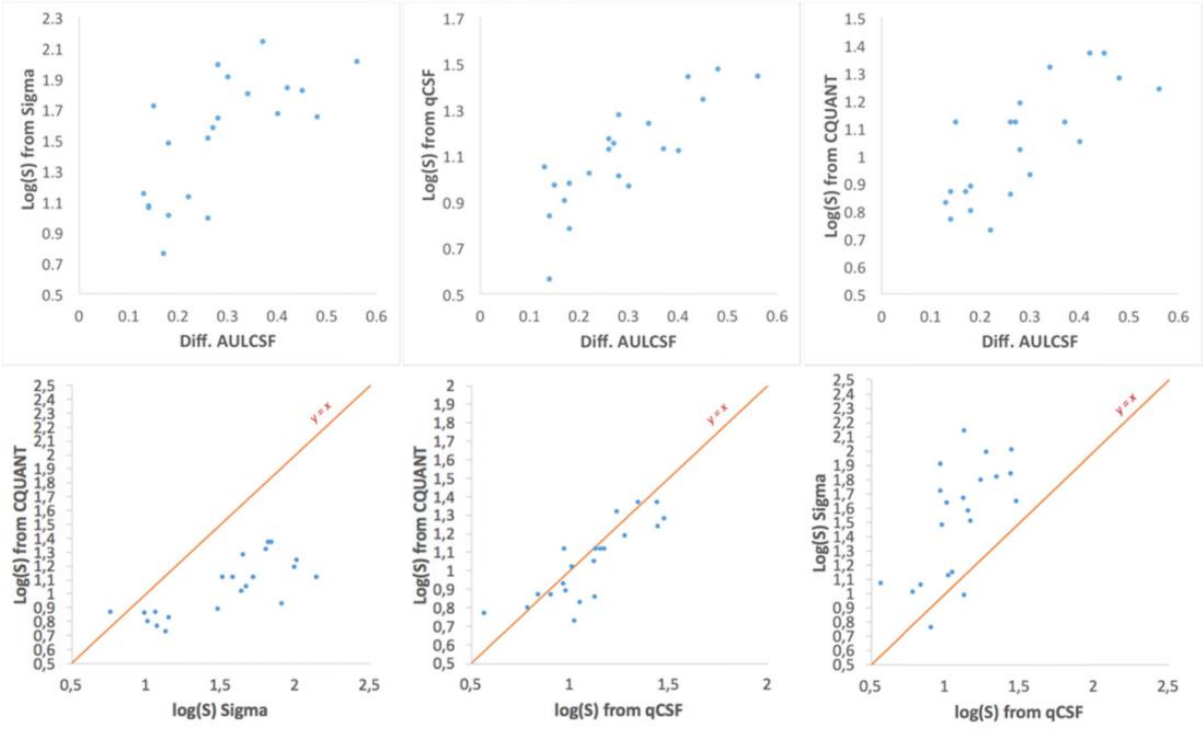

Figure 69: Scatter plots depicting the inter-agreement between all the different metrics acquired from the measurements. Each data point denotes a different subject in all of the three different scatter conditions.

Methods	Diff. AULCSF	C-Quant	Sigma	S from q-CSF
Diff. AULCSF	1	0.766	0.693	0.834
C-Quant	0.766	1	0.771	0.833
Sigma	0.693	0.771	1	0.638
S from q-CSF	0.834	0.833	0.638	1

Table 4: Pearson Correlation Coefficients among different methods (Diff.AULCSF, q-CSF Estimated S, C-Quant and Sigma).

This is a simple method based on a commonly used clinical test, and is proven to be able to estimate the amount of straylight in patients, with the appropriate modifications and calculations. The performance of this method was compared with another two devices dedicated to measure intraocular scattering, showing a reasonably good correlation. The repeatability together with the ease of use for both the clinician and the subject are proofs that the differential CSF method can potentially be applied to detect changes in the scattering properties and transparency of the eye. Finally, it can potentially be an option for a quick, cost-effective screening of cataract or other age related pathologies associated with elevated intraocular scattering.

6. COST EFFECTIVE AND PORTABLE DIFFERENTIAL-CONTRAST SENSITIVITY SCREENING DEVICE BASED ON SMARTPHONE OR TABLETS

Despite the existence of the previously documented methods for the estimation of intraocular scattering, there are instances where these devices and techniques are not always accessible. Although tests using printed charts could potentially fill this gap, the complexity of these methods may sometimes lead to wrong visual evaluations. Additionally, they fall short in providing a metric that would estimate the amount of intraocular scatter light, as they are limited in estimations on the CS on specific spatial frequencies.

On the other hand, CS tests that have been adjusted to be used along with electronic devices or dedicated software/hardware equipment, have also the disadvantage of being costly and of limited access.

As electronic devices of everyday use, like smartphones and tablets, are being equipped with higher specification processors, bigger and of higher resolution screens, this may turn into portable and powerful screening devices, for such tests, along with specifically developed equipment.

Towards this direction, we developed a method that uses a tablet (iPad, Apple Inc., California, U.S.A.) combined with an inexpensive external glare source. Similarly to the Differential q-CSF method, we showed how a tablet along with a simple annulus LED-glare can be used to quantify the amount of intraocular scattering of a subject by providing an estimation of the straylight parameter S after a relatively short psychophysical trial (depicted in a simplistic draw in Figure 70).

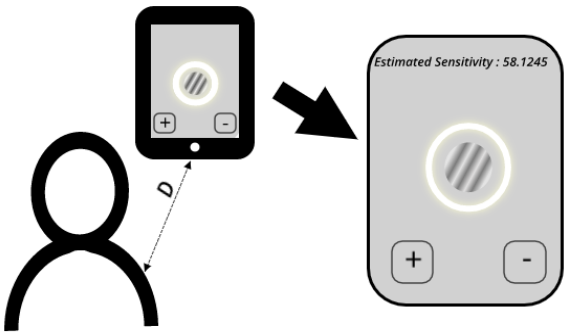

Figure 70: A schematic representation of how the measurements where achieved.

6.1 ENHANCED GRAYSCALE DEPTH. THE BIN-BIT-STEALING METHOD

The precision of the straylight estimation depends on the number of available contrast levels for the stimulus generation, which is limited by the dynamic range of the display. In the case where the glare cannot interfere with the contrast of the test area the dynamic range of a portable device's display would fall short on presenting all the adequate gray levels. Conventionally, a gray-graded stimulus is produced by addressing the same value to the red (R), green (G) and blue (B) channels in each pixel of the monitor panel. Most of the displays, including the iPad's, are limited to the representation of 8-bit depth (256) gray levels for each channel.

An advantage that the iPad (and other portable devices) has is the significantly higher pixel density (264 per inch), compared to the average 100 that computer monitors have. In order to extend this dynamic range, the bin-bit-stealing technique was developed. This is an extended, depth-wise, version of the bit-stealing technique (Tyler, 1997). The bit-stealing technique increases the dynamic range up to 10.8 bits through imperceptibles color variations calculated from the luminance differences among the RGB channels. An additional extension of dynamic range was achieved binning pixels where bit-stealing technique is applied to each pixel. This procedure, is defined as bin-bit-stealing and it takes advantage of the high pixel density of the tablet used, which by binning four pixels in rectangular sequence, can extend the dynamic gray-scale range to 12.8 bits (Figure 71).

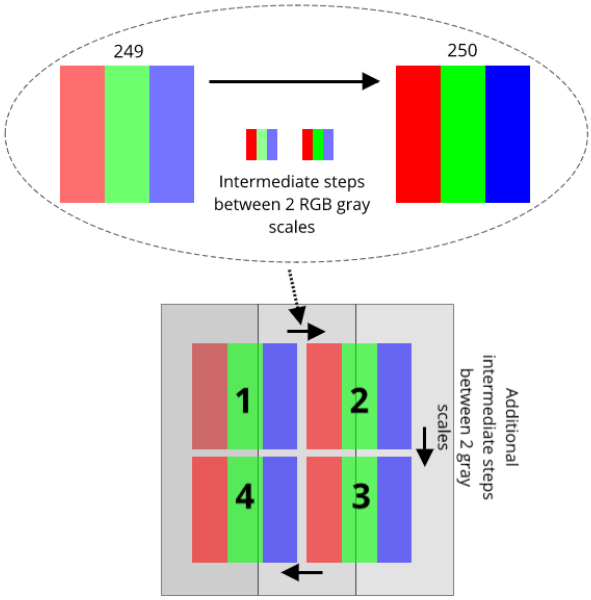

Figure 71: A schematic, demonstrating the increase in gray-depth that the bit-stealing technique is demonstrated (upper half). Going a step further, the proposed bit-bin-stealing technique, is offering even more grey level to be demonstrated, by creating pixel groups, each consisted of four, and managing them as one, offering four additional intermediate grades on top of bit-stealing.

Prior to every stimulus presentation, a color correction for the luminance of the three-color channels was applied. For this procedure, the luminance of each step between 0 and 255, for each color, was measured using a luminance meter (LS-100, Konica-Minolta Inc., Marunouchi, Chiyoda, Tokyo, Japan). The real intensities for each RGB gray level were re-adjusted according the lookup table created to link the nominal with the theoretical luminance.

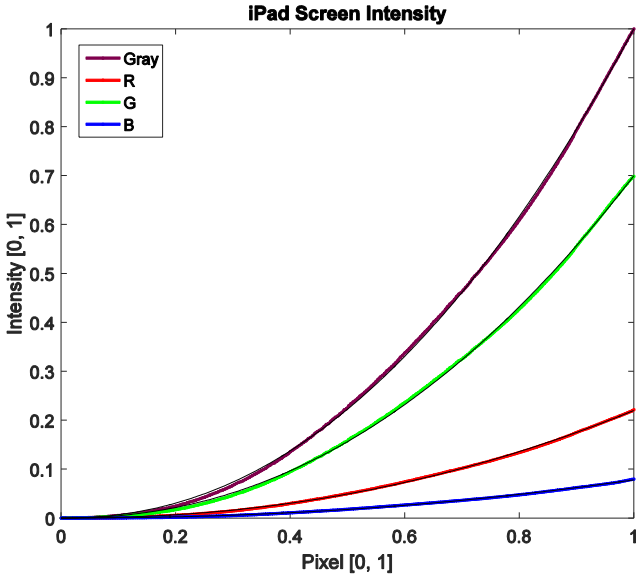

Figure 72: Correlation between the separate RGB pixel intensities (normalized) and the final gray-level generated intensity (normalized), measured to apply a luminance correction upon RGB pixel nominal intensities.

For the evaluation of the method, the actual contrast that the screen can reproduce in comparison to the calculated, was measured. A silicon-amplified photodetector (PDA36A, Hamamatsu Photonics KK Co., Sunayama-cho, Japan) along with a Data Acquisition Card (DAQ) (NI USB 6210, National Instruments, Austin, TX, USA) where employed to measure the actual luminance of each gray-scale grading. The normalized measured intensity was then compared to the theoretical/nominal one. A lookup table was generated to re-adjust to provide real measurements of CS. The total number of contrast values that can be actually reproduced by the screen where 161 for the conventional RGB gray depth, 548 for the bit-stealing method and 1161 for the bin-bit-stealing method.

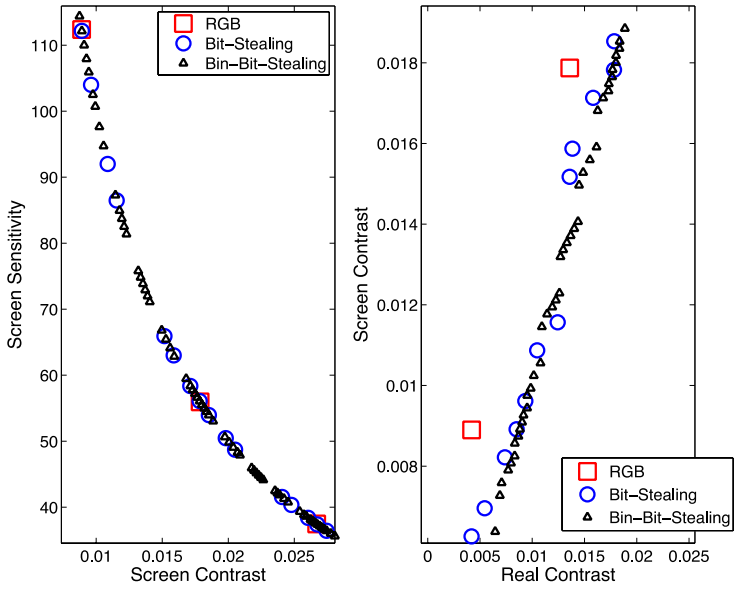

Figure 73: Nominal and real contrast levels reproduced by the screen using the three different methods, RGB, bit-stealing and bit-bin-stealing.

Figure 73 shows that the bin-bit-stealing method is significantly increasing the number of contrast levels that can be projected by the screen. This is an essential characteristic for a CS measuring method where the contrast changes that are to be detected are extremely small.

After calibration, it was remaining to be proven that it can be applied to the Differential (Diff.) q-CSF method to measure the intraocular scattering. The measuring methodology was to project constant sinusoidal gratings, enclosed by a Gabor patch, of a specific spatial frequency of 2 c/deg. The stimulus appearing on the screen (c), subtends 1.5 degrees of retinal area for a distance of 45 cm from the subject. Accordingly, the LED glare annulus covered an area between 2.86 (a) and 3.3 (b) degrees. For the estimation of the Straylight parameter, the same formalism of the Differential q-CSF method (described in equations 23, 24, 25) were used:

$$S = \frac{1}{2\pi}\frac{L}{E}\left(\ln\left(\frac{a}{b}\right)^{-1}\left(\frac{C_{on}}{C_{off}} - 1\right)\right)$$

Equation 27

where a and b are the outer and inner limits (in degrees of visual angle) of the glare source, E the total intensity of the glare source and the contrast thresholds, C_{on} and C_{off} the measured contrast sensitivity measured with the glare source turned off and on, respectively (Figure 74).

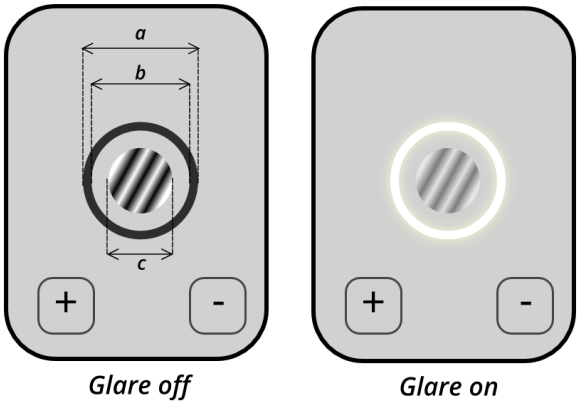

Figure 74: A schematic representation of the test screen where the size of the test area is depicted (c), the outter (a) and inner (b) limit of the glare source as well as the effect of the loss of contrast when the glare source is on (right part of the figure).

The impact of the enhanced projection of the stimulus (i.e., more available C_{off} and C_{on} values) on the relative error of the estimated straylight is quantified by calculating the error propagation:

$$\frac{\Delta S}{S} = \frac{1}{S}\sqrt{\left(\frac{\partial S}{\partial C_{on}}\Delta C_{on}\right)^2 + \left(\frac{\partial S}{\partial C_{off}}\Delta C_{off}\right)^2}$$

Equation 28

where ΔC_{off} and ΔC_{on} are the step size in the contrast tuning when the glare is switched off and on, respectively. Finally, using Equation 27, Equation 28 becomes:

$$\frac{\Delta S}{S} = \left(1 - \frac{C_{off}}{C_{on}}\right)\sqrt{\frac{\Delta C_{on}^2}{C_{on}^2} + \frac{\Delta C_{off}^2}{C_{off}^2}}$$

Equation 29

Figure 75 presents the relative error for each discretization technique. This was estimated by replacing all available C_{off} and C_{on} values in equation 29. The associated errors to straylight less than $5\,\frac{deg^2}{sr}$ were discarded. The dashed rectangle in each plot depicts the regions with usual and practical contrast values according to the luminance conditions. Although the reduction of the relative error by the increment of available contrast levels is depicted in Figure 75, an additional descriptor based on the maximum relative error in each interest region was also calculated. The descriptor values are 0.64, 0.21 and 0.06 for the standard RGB, *bit-stealing* and *bin-bit-stealing* techniques, respectively.

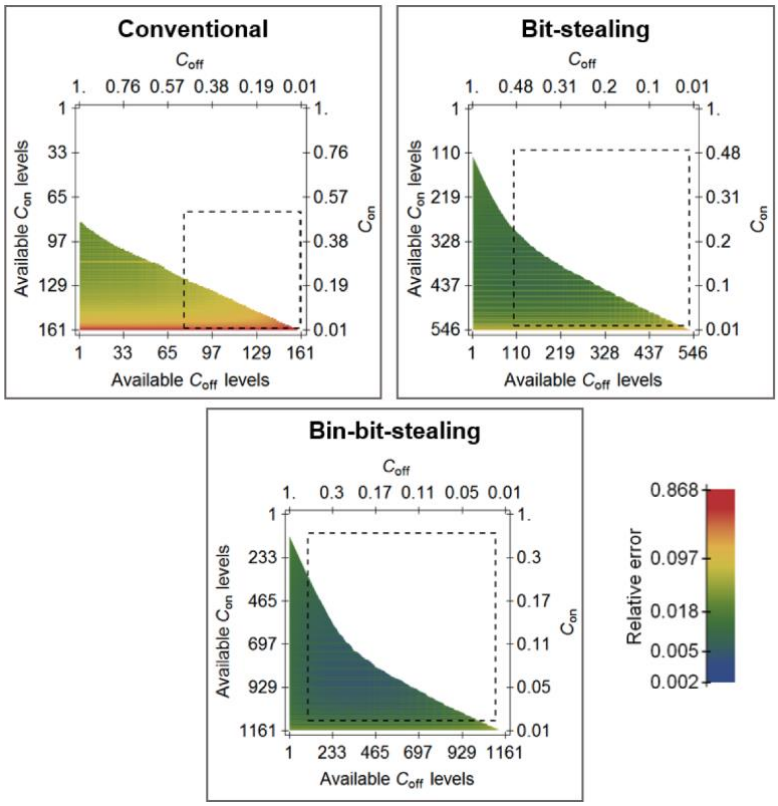

Figure 75: Relative error of straylight estimations for the three intensity discretization methods.

The above calculations showed that the *bin-bit-stealing* method reduced almost ten times the relative error of straylight estimation in comparison to the conventional intensity discretization.

6.2 ESTIMATION OF STRAYLIGHT PARAMETER USING THE PORTABLE DEVICE

To verify the procedure, 9 young (30±4 years old) subjects, without any ocular pathology participated in the study to determine the amount of intraocular straylight for each of their eyes. A pair of contrast thresholds (with and without glare) was additionally estimated using two diffusers, the Black Pro Mist 2 (BPM2) and the Black Pro Mist 3 (BPM3).

Initially, the relative repeatability of the method also evaluated. The Pearson correlation coefficient, for the results of two consecutive measurements for every eye and the added diffusers, was 0.90:

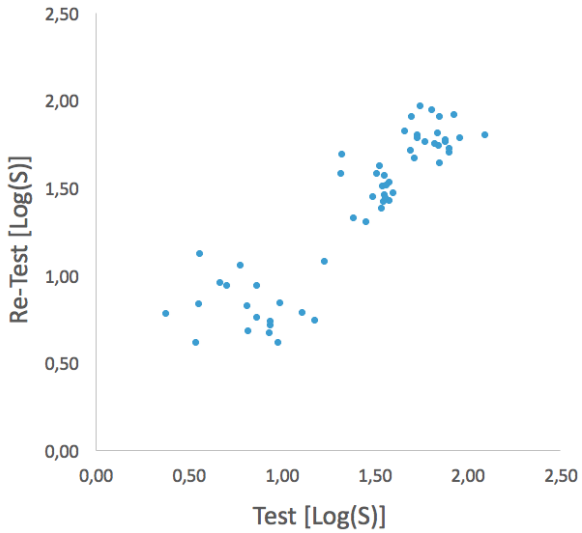

Figure 76: Scatter plot for results from 2 consecutive measurements (test - re-test) with the portable Diff.CS device.

Figure 77 shows the average results:

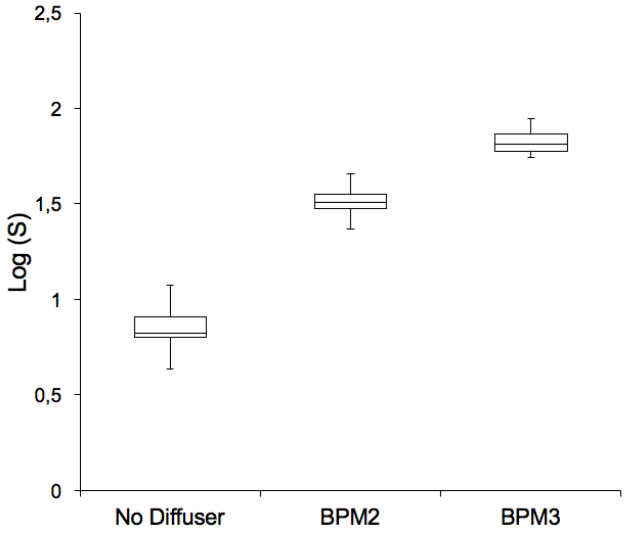

Figure 77: The range of the logarithm of the straylight parameter S for the subjects' eyes and its increase as an effect of the addition of two different diffusers, estimated by the portable Diff.CS device.

The estimated S values were within the ranges that previous measurements with other devices have demonstrated. The same conclusion applied for the increased scatter induced by the diffusers.

The method of enhancing the contrast grading using a pixel-dense monitor is useful to evaluate the level of intraocular scatter and its through-time changes in an easy manner. The fact that the needed equipment is of significant low cost and that can be accessible to a larger population that could probably consist part

of undeveloped or developing countries could contribute to the early detection of cataract or other ocular anomalies that affect scatter.

7. COMPACT DOUBLE-PASS INSTRUMENT TO MEASURE THE MACULAR PIGMENT OPTICAL DENSITY

In this chapter, we present a modification of the optical integration device used before to measure scatter applied for the quantification of the Macular Pigment Optical Density (MPOD).

The central area of the retina contains the Macular Pigment (MP) (Richard A. Bone, Landrum, & Tarsis, 1985), where high concentrations of certain carotenoids (lutein and zeaxanthin) are identified. Although its precise role is not yet completely understood, the MP is thought to protect the retina from high-energy, short-wavelength light (Beatty, Boulton, Henson, Koh, & Murray, 1999) and shield it from free radicals generated from oxidative stress (Edge, McGarvey, & Truscott, 1997; Krinsky, 1989). This may have an important role on the prevention of macular degeneration diseases (Loane, Kelliher, Beatty, & Nolan, 2008; D M Snodderly, 1995). Several studies have also indicated that the MP is related to improved visual performance (Davison et al., 2011; Loughman, Akkali, et al., 2010; Loughman, Davison, Nolan, Akkali, & Beatty, 2010). Studies on the spatial distribution of the MP have shown a highly localized concentration of lutein (L) and zeaxanthin (Z) on the very central part of the retina spanning around the fovea and an abrupt extinction in a few millimeters eccentrically (D Max Snodderly, Auran, & Delori, 1984). Additionally, the absorbance spectrum of the MP is also extensively studied, peaking approximately at 460nm (Brown and Wald 1963)(Figure 78).

Figure 78: Section of the fovea of a rhesus monkey viewed at white (top), blue (middle), and green (bottom) light. The macular pigment appears dark in the middle image because of its high absorption at blue. (Image adapted by Snodderly).

There are several methods and devices to measure the MP optical density (MPOD) in vivo, classified in two main categories: The subjective/psychophysical and the objective. Among the various psychophysical methods, the heterochromatic flicker photometry (R. A. Bone & Sparrock, 1971; Loughman, Scanlon, Nolan, O'Dwyer, & Beatty, 2012; Van Der Veen et al., 2009) (HFP) technique appears to be the most common for the measurement of MPOD. On the other hand, the techniques for the objective quantification of MPOD, make use of the reflectance of the fundus in specific wavelengths (T. T. J. M. Berendschot & van

Norren, 2004; Kilbride, Alexander, Fishman, & Fishman, 1989; van de Kraats, Berendschot, Valen, & van Norren, 2006) or in other cases the fundus autofluoresence where the attenuation of the intrinsic fluorescence of lipofuscin located at the RPE is measured and compared at different retinal sites (François C. Delori, 2004; Wüstemeyer, Jahn, Nestler, Barth, & Wolf, 2002).

Both type of instruments presents some drawbacks arise. For instance, in most of the psychophysical techniques there is always the possibility that some subjects won't be able to complete the test. In the case of the objective techniques, the equipment for the measurements are usually complex and costly and making them less accessible.

In order to find a new alternative, we developed a compact instrument for the objective measurement of the MPOD. It was conceptually designed and built to carry out measurements in a way that is suitable for clinical use and cost efficient. It is based on fundus reflectometry where 2 different regions (centrally and peripherally) are illuminated by two different wavelength LED sources and the measurement is achieved in fractions of a second.

7.1 INSTRUMENT SPECIFICATIONS AND OPTICAL SETUP

The instrument uses 2 different consisted of two LED sources, one emitting green (528 ± 10 nm) and the second, blue (465± 15 nm) light. Each source was comprised of two parts, a central circular and a peripheral annulus with light-shaping diffusers beeing used to spatially homogenize each part.

A dichroic mirror allowed the two sources two overlap on the same path. Different combination of lenses and mirrors where used so that the central disk would cover an area of 1.4 degrees on the retina while the peripheral annulus laid on an area between 1.4 and 4.5 degrees. A fixation light is making the light source visible to the subject, which is asked to fixate on the central part of the overlapping sources. The entrance and exit of the light were spatially separated using a relay - telescope lens system conjugating a diaphragm in front of the source to the pupil plane of the eye so that light enters from this part of the pupil only. As a result, the light reaching the detector is light returning from the fundus and not reflected at other planes (e.g. at the cornea).

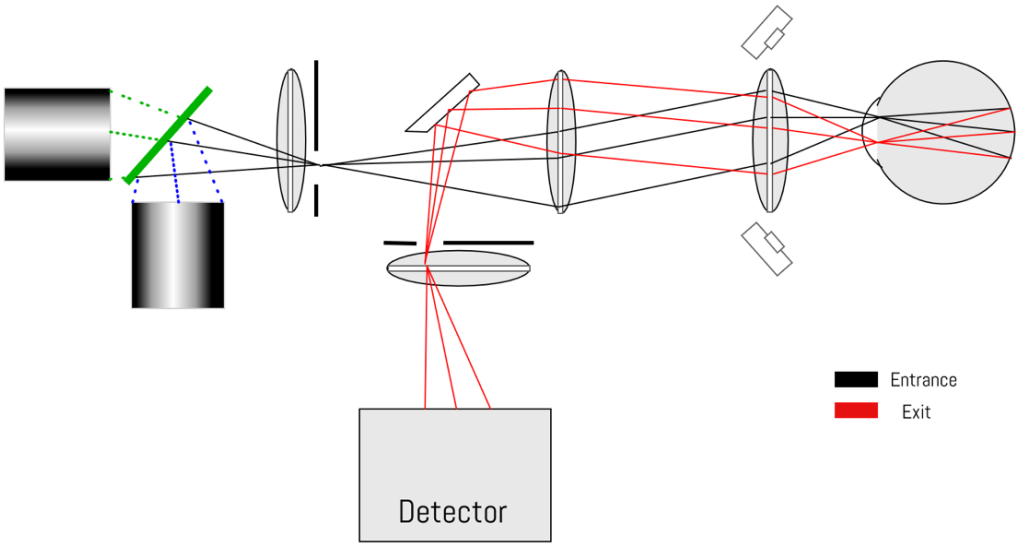

Figure 79: Schematic representation of the optical setup of the instrument for the optical measurement of the MPOD.

The duration of the measurement was 0.3 seconds, time enough to ensure that involuntary pupil contraction caused by the intense light, would occur after the measurement. The four different illuminance areas, projected on the retina, were temporarily modulated with different frequencies as represented in Figiure 80 (central blue, peripheral blue, central green and peripheral green frequency).

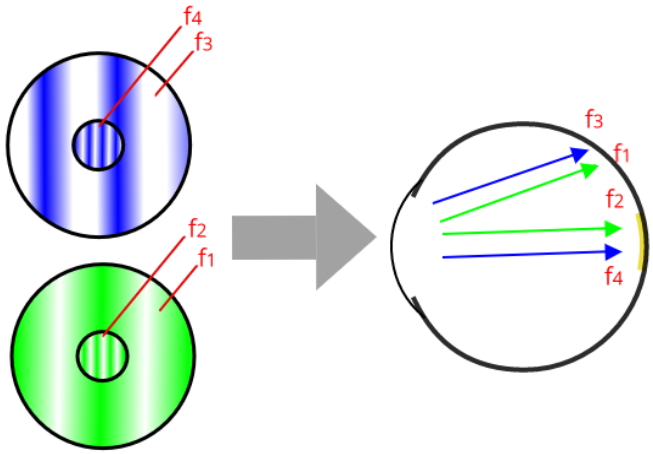

Figure 80: The four discrete illumination zones (central and peripheral) were illuminated by the two sources subsequently but temporarily resolved.

For the initial calibration of the device, a yellow band pass filter (DI8, Noir LaserShields, South Lyon, MI, USA), with similar absorbance spectrum to the macular pigment, was used (Figure 81).

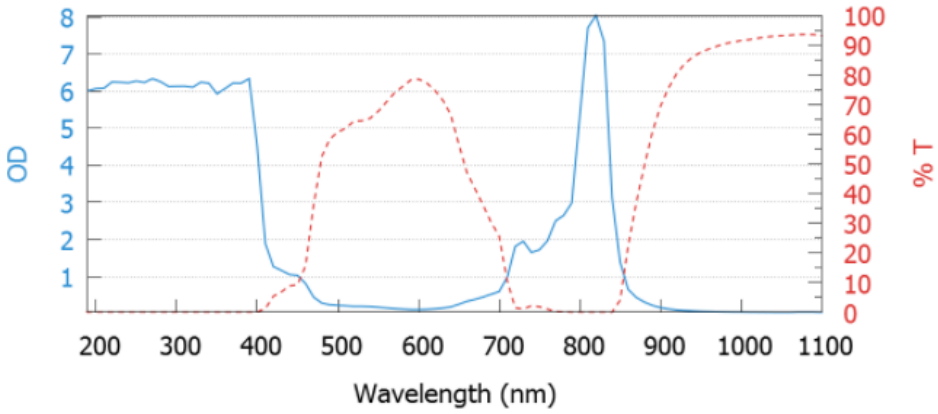

Figure 81: Absorption and Transmission characteristics of the filter used for calibration.

7.2 MEASUREMENT PROCEDURE AND SIGNAL PROCESSING.

The light signals reaching the detector (a silicon photomultiplier (SiPM) device, Excelitas, Waltham, MA, USA) revealed the intensity of each of the four temporarily modulated illumination components via Fourier transformations. Each set of recorded values for a given frequency was averaged, so that a complete measurement resulted in four intensity values describing the total light reflected from the two retinal areas at the two wavelengths. The four intensity values were used to extract the 1.4-degree average value of the MPOD normalized at 460 nm using the following expression:

$$D_{MP}(460) = \frac{0.5}{K_{MP}(\lambda_1) - K_{MP}(\lambda_2)}\left[log\frac{R_P(\lambda_1)}{R_P(\lambda_2)} + log\frac{R_F(\lambda_2)}{R_F(\lambda_1)}\right]$$

Equation 30

where R_F and R_P are the recorded total intensity at the fovea and the periphery respectively and K_{MP} the extinction coefficients of macular pigment for the measured wavelengths, normalized at 460 nm. An in-depth discussion on the derivation of the above formula can be found in (François C. Delori, Goger, Hammond, Snodderly, & Burns, 2001).

7.3 VALIDATION MEASUREMENTS

For the validation of the device's accuracy and sensitivity, twenty-four eyes from twelve young subjects (average age 31 ± 9 years), without any known ocular pathology, were measured. Each session consisted of three consecutive measurements, with the average value being used to estimate the MPOD for every eye. The MPOD values were similar in magnitude (0.43, S.D. ± 0.10) to those reported in previous large scale studies (François C. Delori et al., 2001; Van Der Veen et al., 2009) using different methods. Figure 82 shows the results of the MPOD for each measured eye.

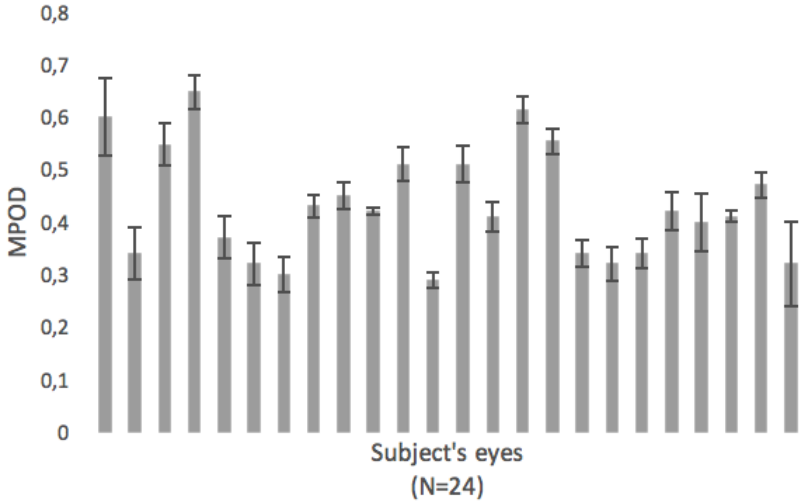

Figure 82: The results from the 24 eyes measured. Each estimated MPOD value reflects the average recorded value from three consecutive measurements. The range of each error bar equals to two standard deviations.

In each subject, the differences within eyes were relatively small (Pearson correlation coefficient for measurements in each eye for every subject: 0.90) (Figure 83).

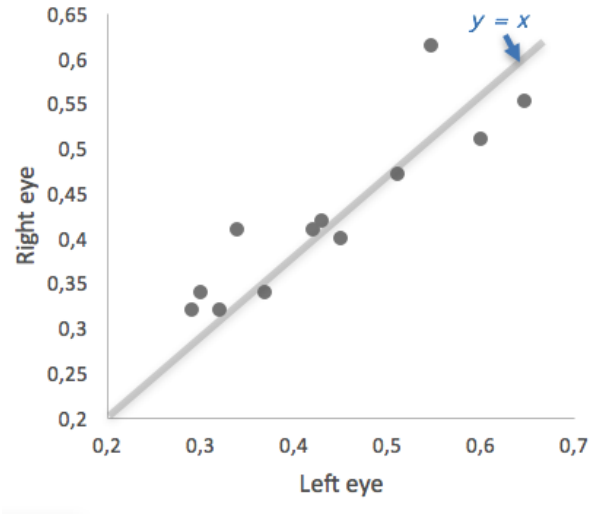

Figure 83: The estimated MPOD values for each eye of every participating subject.

This new instrument for the objective evaluation of the MPOD provides measurements in a small fraction of time, optically, without any preparation (i.e. pupil dilation) or participation of the subject. Its small size, compared to other optical instruments for the same type of measurements and its relatively low built-cost along with its ease of use provide a potential clinical instrument for measurements of MPOD. It should be noted, that the device is meant to provide a single value and not a spatial reconstruction of the MPOD, as is the case with other reflectometric devices. The extracted value expresses the MPOD for a disk of 0.7 degrees of radius, around the fovea. Although there is not a golden standard for the measurement of the MPOD this technique gives a good and representative estimation of the MPOD and could potentially detect even small changes in the MPOD.

8. CONCLUSIONS

In this thesis, we established new methods for the measurement of intraocular straylight and to correlate its effect with visual performance. The following afre the main conclusions of the work:

1. A new method for the reconstruction of the characteristic wide angle PSF of an optical system was developed. The method was evaluated by characterizing commercially available diffusers used for the simulation of the effects of intraocular scattering.
2. The method was initially applied on a "single pass" setup for measuring the scatter produced by optical samples, in particular different types of intraocular lenses.
3. The effect of increased hydration of the corneal stroma on intraocular scattering was evaluated. This increase maybe caused by the disruption of the organization of the stromal collagen.
4. The optical integration method was adapted to a double pass setup to perform measurements in human eyes in vivo.
5. We studied the dependence of intraocular scattering on the wavelength of the used light. Shorter wavelengths are affected more due to their comparable size with that of the scatterers, thus longer wavelengths, reaching the infrared part of the spectrum, are subject to other phenomena such as diffusion and absorption by deeper layers of the retina.
6. A compact prototype device was developed to perform fast and repetitive measurements of intraocular scattering in a clinical setup. A clinical study evaluated the repeatability and validated its results, through comparison with another device for the measurement of intraocular scattering.
7. A a new method to estimate scatter from differential measurement of contrast sensitivity was developed. The results of this method were compared with those from a commercially available subjective instrument for the estimation of the Straylight parameter and with those, measured optically by the own-developed compact double-pass prototype.
8. The differential CS measurement method was adapted for use in compact mobile devices (iPad tablet). This portable version of the method, made it more intuitive and accessible to the general population adding also a low-cost character to the method. A study confirmed its capability of fast and repetitive subjective measurements of intraocular straylight.
9. We developed a compact optical method to measure the Macular Pigment Optical Density. It is based on the reflectance and absorption characteristics of the central and the peripheral part of the retina, for specific wavelengths. The method provided similar MPOD values in young healthy subjects as those in the literature

BIBLIOGRAPHY

Abrahamsson, M., & Sjöstrand, J. (1986). Impairment of contrast sensitivity function (CSF) as a measure of disability glare. *Investigative Ophthalmology & Visual Science*, *27*(7), 1131–6.

Artal, P. (2015). Image Formation in the Living Human Eye. *Annual Review of Vision Science*, *1*(1), 1–17. http://doi.org/10.1146/annurev-vision-082114-035905

Artal, P., Benito, A., Pérez, G. M., Alcón, E., De Casas, A., Pujol, J., & Marín, J. M. (2011). An objective scatter index based on double-pass retinal images of a point source to classify cataracts. *PloS One*, *6*(2), e16823. http://doi.org/10.1371/journal.pone.0016823

Artal, P., & Navarro, R. (1994). Monochromatic modulation transfer function of the human eye for different pupil diameters: an analytical expression. *Journal of the Optical Society of America A*, *11*(1), 246. http://doi.org/10.1364/JOSAA.11.000246

Artal, P., & Tabernero, J. (2008). The eye ' s aplanatic answer. *Nat. Photonics*, *2*, (10)586-589 http://doi.org/10.1038/n.photon.2008.187

Asbell, P., & Brocks, D. (2010). Cornea Overview. In *Encyclopedia of the Eye* (pp. 522–531). http://dx.doi.org/10.1016/B978-0-12-374203-2.00058-0

Bassnett, S., Shi, Y., & Vrensen, G. F. J. M. (2011). Biological glass: structural determinants of eye lens transparency. *Philosophical Transactions of the Royal Society of London. Series B, Biological Sciences*, *366*(1568), 1250–64. http://doi.org/10.1098/rstb.2010.0302

Beatty, S., Boulton, M., Henson, D., Koh, H. H., & Murray, I. J. (1999). Macular pigment and age related macular degeneration. *The British Journal of Ophthalmology*, *83*(7), 867–77. http://doi.org/10.1136/BJO.83.7.867

Benedek, G. B. (1971). Theory of transparency of the eye. *Applied Optics*, *10*(3), 459–73. http://doi.org/10.1364/AO.10.000459

Berendschot, T. (2003). Fundus reflectance—historical and present ideas. *Progress in Retinal and Eye Research*, *22*(2), 171–200. http://doi.org/10.1016/S1350-9462(02)00060-5

Berendschot, T. T. J. M., & van Norren, D. (2004). Objective determination of the macular pigment optical density using fundus reflectance spectroscopy. *Archives of Biochemistry and Biophysics*, *430*(2), 149–155. http://doi.org/10.1016/j.abb.2004.04.029

Bok, D. (1993). The retinal pigment epithelium: a versatile partner in vision. *Journal of Cell Science. Supplement*, *17*, 189–95 .

Bone, R. A., Landrum, J. T., & Tarsis, S. L. (1985). Preliminary identification of the human macular pigment. *Vision Research*, *25*(11), 1531–1535. http://doi.org/10.1016/0042-6989(85)90123-3

Bone, R. A., & Sparrock, J. M. B. (1971). Comparison of macular pigment densities in human eyes. *Vision Research*, *11*(10), 1057–1064. http://doi.org/10.1016/0042-6989(71)90112-X

Bron, A. J., Tripathi, R. C., Tripathi, B. J., & Wolff, E. (1997). *Wolff's anatomy of*

the eye and orbit. Chapman & Hall Medical.

BROWN, P. K., & WALD, G. (1963). Visual Pigments in Human and Monkey Retinas. *Nature*, *200*(4901), 37–43. http://doi.org/10.1038/200037a0

Bueno, J. M., De Brouwere, D., Ginis, H., Sgouros, I., & Artal, P. (2007). Purkinje imaging system to measure anterior segment scattering in the human eye. *Optics Letters*, *32*(23), 3447–9. http://doi.org/10.1364/OL.32.003447

Campbell, F. W., & Robson, J. G. (1968). Application of fourier analysis to the visibility of gratings. *The Journal of Physiology*, *197*(3), 551–566. http://doi.org/10.1113/jphysiol.1968.sp008574

Carney, T., Klein, S. a, Tyler, C. W., Silverstein, a D., Beutter, B., Levi, D., … Chen, C. C. (1999). The development of an image/threshold database for designing and testing human vision models. *Human Vision, Visual Processing, and Digital Display IX, Proc. SPIE*, *3644*(January), 542–551. http://doi.org/10.1117/12.348473

Costello, M. J., Johnsen, S., Metlapally, S., Gilliland, K. O., Ramamurthy, B., Krishna, P. V., & Balasubramanian, D. (2008). Ultrastructural analysis of damage to nuclear fiber cell membranes in advanced age-related cataracts from India. *Experimental Eye Research*, *87*(2), 147–158. http://doi.org/10.1016/j.exer.2008.05.009

Cox, M. J. (2001). Optics of the Human Eye D.A. Atchison, G. Smith; Butterworth-Heinemann, Oxford, 2000, 269 pages, ISBN 0-7506-3775-7, f27.50. *Ophthalmic and Physiological Optics*, *21*(5), 426–426. http://doi.org/10.1046/j.1475-1313.2001.00577.x

Davison, P., Akkali, M., Loughman, J., Scanlon, G., Nolan, J., & Beatty, S. (2011). Macular Pigment: Its Associations with Color Discrimination and Matching. *Optometry and Vision Science*, *88*(7), 816–822. http://doi.org/10.1097/OPX.0b013e31821798ec

De Valois, R. L., Morgan, H., & Snodderly, D. M. (1974). Psychophysical studies of monkey Vision-III. Spatial luminance contrast sensitivity tests of macaque and human observers. *Vision Research*, *14*(1), 75–81. http://doi.org/10.1016/0042-6989(74)90118-7

De Waard, P. W. T., Ijspeert, J. K., Van den Berg, T. J. T. P., & De Jong, P. T. V. M. (1992). Intraocular light scattering in age-related cataracts. In *Investigative Ophthalmology and Visual Science* (Vol. 33, pp. 618–625).

Delori, F. C. (2004). Autofluorescence method to measure macular pigment optical densities fluorometry and autofluorescence imaging. *Archives of Biochemistry and Biophysics*, *430*(2), 156–162. http://doi.org/10.1016/j.abb.2004.05.016

Delori, F. C., Goger, D. G., Hammond, B. R., Snodderly, D. M., & Burns, S. A. (2001). Macular pigment density measured by autofluorescence spectrometry : comparison with reflectometry and heterochromatic flicker photometry. *Journal of the Optical Society of America A*, *18*(6), 1212–1230. http://doi.org/10.1364/JOSAA.18.001212

Delori, F. C., & Pflibsen, K. P. Spectral reflectance of the human ocular fundus., 28Applied optics 1061–1077 (1989). http://doi.org/10.1364/AO.28.001061

Edge, R., McGarvey, D. J., & Truscott, T. G. (1997). The carotenoids as anti-oxidants--a review. *Journal of Photochemistry and Photobiology. B, Biology*, *41*(3), 189–200.

Ehrenstein, W. H., & Ehrenstein, A. (1999). Psychophysical Methods. *Modern Techniques in Neuroscience Research*, 1211–1241. http://doi.org/10.1007/978-3-642-58552-4_43

Elliott, D. B., Fonn, D., Flanagan, J., & Doughty, M. (1993). Relative sensitivity of clinical tests to hydrophilic lens-induced corneal thickness changes. *Optometry and Vision Science : Official Publication of the American Academy of Optometry*. http://doi.org/10.1097/00006324-199312000-00009

Elliott, D. B., Hurst, M. a, & Weatherill, J. (1990). Comparing clinical tests of visual function in cataract with the patient's perceived visual disability. *Eye*, *4*(5), 712–717. http://doi.org/10.1038/eye.1990.100

Franssen, L., Coppens, J. E., & van den Berg, T. J. T. P. (2006). Compensation Comparison Method for Assessment of Retinal Straylight. *Investigative Opthalmology & Visual Science*, *47*(2), 768. http://doi.org/10.1167/iovs.05-0690

Gilliland, K. O., Freel, C. D., Johnsen, S., Craig Fowler, W., & Costello, M. J. (2004). Distribution, spherical structure and predicted Mie scattering of multilamellar bodies in human age-related nuclear cataracts. *Experimental Eye Research*, *79*(4), 563–576. http://doi.org/10.1016/j.exer.2004.05.017

Gilliland, K. O., Freel, C. D., Lane, C. W., Fowler, W. C., & Costello, M. J. (2001). Multilamellar bodies as potential scattering particles in human age-related nuclear cataracts. *Molecular Vision*, *7*, 120–130. http://doi.org/v7/a18 [pii]

Ginis, H., Pérez, G. M., Bueno, J. M., Artal, P., & Perez, G. M. (2012). The wide-angle point spread function of the human eye reconstructed by a new optical method Harilaos Ginis. *Journal of Vision*, *12*, 1–10. http://doi.org/10.1167/12.3.20.Introduction

Ginis, H. S., Perez, G. M., Bueno, J. M., Pennos, A., & Artal, P. (2013). Wavelength dependence of the ocular straylight. *Investigative Ophthalmology & Visual Science*, *54*(5), 3702–3708. http://doi.org/10.1167/iovs.13-11697

Ginis, H., Sahin, O., Pennos, A., & Artal, P. (2014). Compact optical integration instrument to measure intraocular straylight. *Biomed. Opt. Express*, *5*(9), 3036. http://doi.org/10.1364/BOE.5.003036

Ginsburg, A. P. (1984). A new contrast sensitivity vision test chart. *American Journal of Optometry and Physiological Optics*, *61*(6), 403–7.

Hemenger, R. P. (1988). Small-angle intraocular light scatter: a hypothesis concerning its source. *J Opt Soc Am [A]*, *5*, 577–582. http://doi.org/10.1364/JOSAA.5.000577

Hodgkinson, I. J., Molteno, A. C. B., Greer, P. B., & Molteno, A. C. B. (1994).

Point-spread function for light scattered in the human ocular fundus. *Journal of Optical Society of America A*, *11*(2), 479–486. http://doi.org/10.1364/JOSAA.11.000479

Holladay, L. L. (1926). The Fundamentals of Glare and Visibility. *Journal of the Optical Society of America*, *12*(4), 271. http://doi.org/10.1364/JOSA.12.000271

Hou, F., Huang, C. B., Lesmes, L., Feng, L. X., Tao, L., Zhou, Y. F., & Lu, Z. L. (2010). qCSF in clinical application: Efficient characterization and classification of contrast sensitivity functions in amblyopia. *Investigative Ophthalmology and Visual Science*, *51*(10), 5365–5377. http://doi.org/10.1167/iovs.10-5468

Howes, S. C., Caelli, T., & Mitchell, P. (1982). Contrast sensitivity in diabetics with retinopathy and cataract. *Australian Journal of Ophthalmology*, *10*(3), 173–8.

Hsueh, C. M., Lo, W., Chen, W. L., Hovhannisyan, V. A., Liu, G. Y., Wang, S. S., … Dong, C. Y. (2009). Structural characterization of edematous corneas by forward and backward second harmonic generation imaging. *Biophysical Journal*, *97*, 1198–1205. http://doi.org/10.1016/j.bpj.2009.05.040

IJspeert, J. K., de Waard, P. W. T., van den Berg, T. J. T. P., & de Jong, P. T. V. M. (1990). The intraocular straylight function in 129 healthy volunteers; Dependence on angle, age and pigmentation. *Vision Research*, *30*(5), 699–707. http://doi.org/10.1016/0042-6989(90)90096-4

Ijspeert, J. K., Van Den Berg, T. J. T. P., & Spekreijse, H. (1993). An improved mathematical description of the foveal visual point spread function with parameters for age, pupil size and pigmentation. *Vision Research*, *33*(1), 15–20. http://doi.org/10.1016/0042-6989(93)90053-Y

International Commission on Illumination. (1999). *CIE collection 1999 : vision and colour : physical measurement of light and radiation*. Commission internationale de l'eclairage.

Kilbride, P. E., Alexander, K. R., Fishman, M., & Fishman, G. A. (1989). Human macular pigment assessed by imaging fundus reflectometry. *Vision Research*, *29*(6), 663–74.

King-Smith, P. E., Grigsby, S. S., Vingrys, A. J., Benes, S. C., & Supowit, A. (1994). Efficient and unbiased modifications of the QUEST threshold method: Theory, simulations, experimental evaluation and practical implementation. *Vision Research*, *34*(7), 885–912. http://doi.org/10.1016/0042-6989(94)90039-6

Kling, S., Ginis, H., & Marcos, S. (2012). Corneal Biomechanical Properties from Two-Dimensional Corneal Flap Extensiometry: Application to UV-Riboflavin Cross-Linking. *Investigative Opthalmology & Visual Science*, *53*(8), 5010. http://doi.org/10.1167/iovs.12-9583

Koblova, E. V., Bashkatov, A. N., Genina, E. a., Tuchin, V. V., & Bakutkin, V. V. (2005). Estimation of melanin content in iris of human eye. *Proceedings of SPIE*, *5688*, 302–311. http://doi.org/10.1117/12.593651

Kontadakis, G. A., Ginis, H., Karyotakis, N., Pennos, A., Pentari, I., Kymionis, G. D., & Pallikaris, I. G. (2013). In vitro effect of corneal collagen cross-linking on corneal hydration properties and stiffness. *Graefe's Archive for Clinical and Experimental Ophthalmology*, *251*(2). http://doi.org/10.1007/s00417-012-2082-9

Krinsky, N. I. (1989). Antioxidant functions of carotenoids. *Free Radical Biology and Medicine*, *7*(6), 617–635. http://doi.org/10.1016/0891-5849(89)90143-3

Labin, A. M., Safuri, S. K., Ribak, E. N., & Perlman, I. (2014). Muller cells separate between wavelengths to improve day vision with minimal effect upon night vision. *Nat Commun*, *5*, 4319. http://doi.org/10.1038/ncomms5319

Lesmes, L. A., Lu, Z. L., Baek, J., & Albright, T. D. (2010). Bayesian adaptive estimation of the contrast sensitivity function: the quick CSF method. *Journal of Vision*, *10*(3), 17 1-21. http://doi.org/10.1167/10.3.17

Lesmes, L., Lu, Z., Baek, J., & Albright, T. (2010). Bayesian adaptive estimation of the contrast sensitivity function: the quick CSF method. *Journal of Vision*, *10*, 1–21. http://doi.org/10.1167/10.3.17.Introduction

Li, G., Macdonald, C., Mahajan, V., Eds, E. V. S., & Optics, H. (2010). Pelli, D. G., & Farell, B. (2010). Psychophysical methods. In M. Bass, C. DeCusatis, J. Enoch, V. Lakshminarayanan, G. Li, C. MacDonald, V. Mahajan & E. V. Stryland (Eds.),. *Handbook of Optics, Third Edition, Volume Iii: Vision and Vision Optics*, *III*, 3.1-3.12.

Loane, E., Kelliher, C., Beatty, S., & Nolan, J. M. (2008). The rationale and evidence base for a protective role of macular pigment in age-related maculopathy. *British Journal of Ophthalmology*, *92*(9), 1163–1168. http://doi.org/10.1136/bjo.2007.135566

Loughman, J., Akkali, M. C., Beatty, S., Scanlon, G., Davison, P. A., O'Dwyer, V., … Nolan, J. M. (2010). The relationship between macular pigment and visual performance. *Vision Research*, *50*(13), 1249–1256. http://doi.org/10.1016/j.visres.2010.04.009

Loughman, J., Davison, P. A., Nolan, J. M., Akkali, M. C., & Beatty, S. (2010). Macular pigment and its contribution to visual performance and experience. *Journal of Optometry*, *3*(2), 74–90. http://doi.org/10.1016/S1888-4296(10)70011-X

Loughman, J., Scanlon, G., Nolan, J. M., O'Dwyer, V., & Beatty, S. (2012). An evaluation of a novel instrument for measuring macular pigment optical density: the MPS 9000. *Acta Ophthalmologica*, *90*(2), e90–e97. http://doi.org/10.1111/j.1755-3768.2011.02294.x

Mei, M., & Leat, S. J. (2007). Suprathreshold Contrast Matching in Maculopathy. *Investigative Opthalmology & Visual Science*, *48*(7), 3419. http://doi.org/10.1167/iovs.06-0731

Michael, R., & Bron, A. J. (2011). The ageing lens and cataract: a model of normal and pathological ageing. *Philosophical Transactions of the Royal Society of London. Series B, Biological Sciences*, *366*(1568), 1278–92.

http://doi.org/10.1098/rstb.2010.0300

Michael, R., Van Marle, J., Vrensen, G. F. J. M., & Van Den Berg, T. J. T. P. (2003). Changes in the refractive index of lens fibre membranes during maturation - Impact on lens transparency. *Experimental Eye Research*, *77*(1), 93–99. http://doi.org/10.1016/S0014-4835(03)00065-4

Mura, M., Engelbrecht, L. A., de Smet, M. D., Papadaki, T. G., van den Berg, T. J., & Tan, H. S. (2011). Surgery for Floaters. *Ophthalmology*, *118*(9), 1894–1894.e1. http://doi.org/10.1016/j.ophtha.2011.05.020

Nickla, D. L., & Wallman, J. (2010). The multifunctional choroid. *Progress in Retinal and Eye Research*, *29*(2), 144–168. http://doi.org/10.1016/j.preteyeres.2009.12.002

Noll, R. J. (1976). Zernike polynomials and atmospheric turbulence. *Journal of the Optical Society of America*, *66*(3), 207. http://doi.org/10.1364/JOSA.66.000207

Owsley, C., Sekuler, R., & Siemsen, D. (1983). Contrast sensitivity throughout adulthood. *Vision Research*, *23*(7), 689–99.

Paulsson, L.-E., & Sjostrand, J. (1980). Contrast sensitivity in the presence of a glare light. *Invest. Ophthalmol. Vis. Sci.*, 401–406.

Pelli, D. G., & Robson, J. G. (1988). the Design of a New Letter Chart for Measuring Contrast Sensitivity. *Clinical Vision Science*, *2*(3), 187–199. http://doi.org/10.1016/j.parkreldis.2012.11.013

Pelli, D. G., & Bex, P. (2013). Measuring contrast sensitivity. *Vision Research*, *90*, 10–4. http://doi.org/10.1016/j.visres.2013.04.015

Qazi, Y., Wong, G., Monson, B., Stringham, J., & Ambati, B. K. (2010). Corneal transparency: Genesis, maintenance and dysfunction. *Brain Research Bulletin*. http://doi.org/10.1016/j.brainresbull.2009.05.019

Robson, J. G. (1966). Spatial and Temporal Contrast-Sensitivity Functions of the Visual System. *Journal of the Optical Society of America*, *56*(8), 1141. http://doi.org/10.1364/JOSA.56.001141

Ross, J. E., Bron, a J., & Clarke, D. D. (1984). Contrast sensitivity and visual disability in chronic simple glaucoma. *Br. J. Ophthalmol.*, *68*(11), 821–827.

Sabour-Pickett, S., Loughman, J., Nolan, J. M., Stack, J., Pesudovs, K., Meagher, K. a, & Beatty, S. (2013). Visual performance in patients with neovascular age-related macular degeneration undergoing treatment with intravitreal ranibizumab. *Journal of Ophthalmology*, *2013*, 268438. http://doi.org/http://dx.doi.org/10.1155/2013/268438

Schade, O. H. (1956). Optical and Photoelectric Analog of the Eye. *Journal of the Optical Society of America*, *46*(9), 721. http://doi.org/10.1364/JOSA.46.000721

Snodderly, D. M. (1995). Evidence for protection against age-related macular degeneration by carotenoids and antioxidant vitamins. *The American Journal of Clinical Nutrition*, *62*(6 Suppl), 1448S–1461S.

Snodderly, D. M., Auran, J. D., & Delori, F. C. (1984). The Macular Pigment. II.

Spatial Distribution in Primate Retinas. *Investigative Ophthalmology & Visual Science*, *25*, 674–685.

Steinberg, R. H. (1985). Interactions between the retinal pigment epithelium and the neural retina. *Documenta Ophthalmologica*, *60*(4), 327–346. http://doi.org/10.1007/BF00158922

Stiles, W. S. (1929). The Scattering Theory of the Effect of Glare on the Brightness Difference Threshold. *Proceedings of the Royal Society of London B: Biological Sciences*, *105*(735).

Taylor, M. M., & Creelman, C. D. (1967). PEST: Efficient Estimates on Probability Functions. *The Journal of the Acoustical Society of America*, *41*(4A), 782. http://doi.org/10.1121/1.1910407

Tomás-juan, J. (2014). Multifocal IOLs with apodized di ff ractive central zone and refractive periphery : optical performance and clinical outcomes, 155–166.

Trier, K. (2005). The Sclera. *Advances in Organ Biology*, *10*, 353–373. http://doi.org/10.1016/S1569-2590(05)10013-5

Tyler, C. W. (1997). Colour bit-stealing to enhance the luminance resolution of digital displays on a single pixel basis. *Spatial Vision*, *10*(4), 369–77.

Vaegan, & Halliday, B. L. (1982). A forced-choice test improves clinical contrast sensitivity testing. *The British Journal of Ophthalmology*, *66*(8), 477–91. http://doi.org/10.1136/BJO.66.8.477

van De Hulst, H. C. (2003). *Light scattering by small particles*. *Light Scattering by Small Particles*. http://doi.org/10.1007/BF00225274

van de Kraats, J., Berendschot, T. T. J. M., Valen, S., & van Norren, D. (2006). Fast assessment of the central macular pigment density with natural pupil using the macular pigment reflectometer. *Journal of Biomedical Optics*, *11*(6), 64031. http://doi.org/10.1117/1.2398925

van den Berg, T. J. (1991). On the relation between glare and straylight. *Documenta Ophthalmologica. Advances in Ophthalmology*, *78*(3–4), 177–181. http://doi.org/10.1007/BF00165678

van den Berg, T. J., Hwan, B. S., & Delleman, J. W. (1993). The intraocular straylight function in some hereditary corneal dystrophies. *Documenta Ophthalmologica. Advances in Ophthalmology*, *85*(1), 13–9.

van den Berg, T. J., & Spekreijse, H. (1997). Near infrared light absorption in the human eye media. *Vision Res.*, *37*(2), 249–253.

van den Berg, T. J. T. P., Franssen, L., & Coppens, J. E. (2010). Ocular Media Clarity and Straylight. *Encyclopedia of Eye*, *3*, 173–183. http://doi.org/http://dx.doi.org/10.1016/B978-0-12-374203-2.00230-X

van den Berg, T. J. T. P., Franssen, L., Kruijt, B., & Coppens, J. E. (2011). Psychophysics, reliability, and norm values for temporal contrast sensitivity implemented on the two alternative forced choice C-Quant device. *Journal of Biomedical Optics*, *16*(8), 85004. http://doi.org/10.1117/1.3613922

Van Den Berg, T. J. T. P., & Ijspeert, J. K. (1995). Light scattering in donor lenses. *Vision Research*, *35*(1), 169–177. http://doi.org/10.1016/0042-6989(94)00123-4

Van Der Veen, R. L. P., Berendschot, T. T. J. M., Hendrikse, F., Carden, D., Makridaki, M., & Murray, I. J. (2009). A new desktop instrument for measuring macular pigment optical density based on a novel technique for setting flicker thresholds. *Ophthalmic and Physiological Optics*, *29*(2), 127–137. http://doi.org/10.1111/j.1475-1313.2008.00618.x

Vaz, S., Falkmer, T., Passmore, A. E., Parsons, R., & Andreou, P. (2013). The Case for Using the Repeatability Coefficient When Calculating Test-Retest Reliability. *PLoS ONE*, *8*(9), 1–7. http://doi.org/10.1371/journal.pone.0073990

Veraart, H. G., van den Berg, T. J., IJspeert, J. K., & Cardozo, O. L. (1992). Stray light in radial keratotomy and the influence of pupil size and straylight angle. *American Journal of Ophthalmology*, *114*(4), 424–428.

Vos, J. (1984). Disability glare-a state of the art report. *Commision International de l'Eclairage Journal*, *3*, 39–53.

Vos, J., & Boogaard, J. (1963). Contribution of the cornea to entoptic scatter. *Journal of the Optical Society of America*, *53*(7), 869–873. http://doi.org/10.1364/JOSA.53.000869

Watson, A. B. (2000). Visual detection of spatial contrast patterns: Evaluation of five simple models. *Optics Express*, *6*(1), 12. http://doi.org/10.1364/OE.6.000012

Watson, A. B., Ahumada, A. J., J., A. A., N., G., G., H., F., Q. R., … J., Y. (2005). A standard model for foveal detection of spatial contrast. *Journal of Vision*, *5*(9), 6. http://doi.org/10.1167/5.9.6

Watson, A. B., & Pelli, D. G. (1983). Quest: A Bayesian adaptive psychometric method. *Perception & Psychophysics*, *33*(2), 113–120. http://doi.org/10.3758/BF03202828

Watt, R. J., & Andrews, D. P. (1981). APE: Adaptive probit estimation of psychometric functions. *Current Psychological Reviews*, *1*(2), 205–213. http://doi.org/10.1007/BF02979265

Wetherill, G. B., & Levitt, H. (1965). SEQUENTIAL ESTIMATION OF POINTS ON A PSYCHOMETRIC FUNCTION. *British Journal of Mathematical and Statistical Psychology*, *18*(1), 1–10. http://doi.org/10.1111/j.2044-8317.1965.tb00689.x

Wüstemeyer, H., Jahn, C., Nestler, A., Barth, T., & Wolf, S. (2002). A new instrument for the quantification of macular pigment density: first results in patients with AMD and healthy subjects. *Graefe's Archive for Clinical and Experimental Ophthalmology*, *240*(8), 666–671. http://doi.org/10.1007/s00417-002-0515-6

www.aao.org. (n.d.). Normal Crystalline Lens. Retrieved from https://www.aao.org/bcscsnippetdetail.aspx?id=f38d473f-c836-4fe6-8555-20d34ce19816

PEER-REVIEWED PUBLICATIONS RELATED TO THIS THESIS

A. PEER REVIEWED CONFERENCE PAPERS.

Straylight measurements in intraocular lenses with an optical integration method.

Alexandros Pennos; Harilaos S Ginis; Adrian Gambin; Pablo Artal

Invest. Ophthalmol. Vis. Sci.. 2016; 57(12):3116.

Macular pigment density estimated with Fourier-domain fundus reflectometry

Harilaos S Ginis; Alexandros Pennos; Juan Mompeán; Pablo Artal

Invest. Ophthalmol. Vis. Sci.. 2016; 57(12):5097.

Visual impact of artificially induced intraocular scatter with a liquid crystal phase modulator

Augusto Arias Gallego; Alexandros Pennos; Harilaos S Ginis; Pablo Artal

Invest. Ophthalmol. Vis. Sci.. 2016; 57(12):215.

Intraocular scattering shows low heritability

Antonio Benito; Lucia Hervella; Juan Tabernero; Alexandros Pennos; Harilaos S. Ginis; Juan Francisco Sánchez-Romera; Juan Ramón Ordoñana; Marcos Ruiz-Sánchez; Jose María Marín; Pablo Artal

Invest. Ophthalmol. Vis. Sci.. 2015; 56(7):1069.:

Clinical validation of a compact optical straylight meter in cataract patients

Harilaos S. Ginis; Alexandros Pennos; Lucia Hervella; Eloy A. Villegas; Onurcan Sahin; Belen Cañizares; Jose María Marín; Pablo Artal

Invest. Ophthalmol. Vis. Sci.. 2015; 56(7):1079.:

Intraocular scattering compensation in macular pigment density measurement

Dimitrios Christaras; Harilaos Ginis; Alexandros Pennos; Pablo Artal; Laboratorio de Optica Universidad de Murcia

Invest. Ophthalmol. Vis. Sci.. 2015; 56(7):4119.

Impact of scattering on accommodation responses

Alexandros Pennos; Emmanuel Chirre; Pedro M. Prieto; Ulrich Wildenmann; Frank Schaeffel; Pablo Artal

Invest. Ophthalmol. Vis. Sci.. 2015; 56(7):6002.:

Diffusers induced ocular light scattering measured by a psychophysical and an optical method.

Marrie Van der Mooren; Harilaos S Ginis; Robert Rosén; Antonio Benito; Luuk Franssen; Alexandros Pennos; Dimitrios Christaras; Patricia A Piers; Pablo Artal

Invest. Ophthalmol. Vis. Sci.. 2014; 55(13):3781.:

Impact of the Retinal Reflection on the Wide-Angle Point Spread Function of the Human Eye

Harilaos Ginis; Guillermo Perez; Alexandros Pennos; Juan Bueno; Pablo Artal

Invest. Ophthalmol. Vis. Sci.. 2013; 54(15):1285.:

B. PEER REVIEWED JOURNAL PUBLICATIONS.

Scattering contribution to the double-pass PSF using Monte Carlo simulations.

Dimitrios Christaras, Harilaos Ginis, Alexandros Pennos, Pablo Artal. Ophthalmic and Physiological Optics 05/2017; 37(3):342-346., DOI:10.1111/opo.12375

Performance of a differential contrast sensitivity method to measure intraocular scattering.

Alexandros Pennos, Harilaos Ginis, Augusto Arias, Dimitrios Christaras, Pablo Artal. Biomedical Optics Express 02/2017; 8(3)., DOI:10.1364/BOE.8.001382

Optical Measurement of Straylight in Eyes With Cataract.

Onurcan Sahin, Alexandros Pennos, Harilaos Ginis, Lucia Hervella, Eloy A. Villegas, Belen Cañizares, Jose Maria Marin, Ioannis Pallikaris, Pablo Artal. Journal of refractive surgery (Thorofare, N.J.: 1995) 12/2016; 32(12):846-850., DOI:10.3928/1081597X-20160920-02

Intraocular scattering compensation in retinal imaging.

Dimitrios Christaras, Harilaos Ginis, Alexandros Pennos, Pablo Artal. Biomedical Optics Express 10/2016; 7(10):3996-4006., DOI:10.1364/BOE.7.003996

Environmental and Genetic Factors Explain Differences in Intraocular Scattering.

Antonio Benito, Lucía Hervella, Juan Tabernero, Alexandros Pennos, Harilaos Ginis, Juan F Sánchez-Romera, Juan R Ordoñana, Marcos Ruiz-Sánchez, José M Marín, Pablo Artal. Investigative ophthalmology & visual science 01/2016; 57(1):163-168., DOI:10.1167/iovs.15-17897

Compact optical integration instrument to measure intraocular straylight.

Harilaos Ginis, Onurcan Sahin, Alexandros Pennos, Pablo Artal. Biomedical Optics Express 09/2014; 5(9):3036-3041., DOI:10.1364/BOE.5.003036

Wavelength Dependence of the Ocular Straylight.

Harilaos S Ginis, Guillermo M Perez, Juan M Bueno, Alexandros Pennos, Pablo Artal: Investigative ophthalmology & visual science 04/2013; 54(5)., DOI:10.1167/iovs.13-11697

ACKNOWLEDGMENTS

Every page of this thesis is a result of lots of dedicated effort. Nothing from all this work, required for this Ph.D. thesis, would be ever possible without the help and support from a big number of people that surrounded me all these five years.

Of course, nothing would be also possible, if I was not offered the opportunity, the position of the Ph.D. candidate and a prestigious Marie-Curie scholarship, from Pablo Artal, the director and supervisor of my thesis. Apart from his enormous scientific contribution, which was continuous, he also convinced me to trust myself, rely on my own capabilities and be the absolute responsible for my present and future course as a scientist, professional and as a person.

Several years before even getting here (writing the acknowledgments of my Ph.D. thesis), I began absorbing the influence of Harilaos Ginis; one of the brightest scientists I have ever known. I consider him as my mentor, not only for his tremendous amount of knowledge that he has transmitted to (and hopefully absorbed by) me, but because he also taught me how to behave and fight when confronting difficulties, of any nature.

The completion of this thesis is also attributed to the friends and colleagues (many of them were both) which I met in Murcia and chose to mention in this section, clearly by order of "appearance" to my life. So, the first words belong to Dimitrios Christaras. He was the first person I shared my first discussions with, during the very first days I arrived in Murcia, Spain and we kept sharing words and thoughts every single day since then. His advices and opinion on problems concerning physics, optics and computer science, were always very useful and important for me. He's proven to be a true friend in several occasions, when he was really needed.

Another friendship I gained, during this journey, was the one of Emmanuel Chirre. Another Ph.D. student from the "Laboratorio de Optica (LoUm)" family. Not only during the projects we had in common, but daily, Manu was always helpful and supportive. His expertise in complex optical setups has been an extra "tool" for my lab-life and his superb character made him the best company during almost every weekend.

The fourth that entered the LoUm Ph.D. club, was Martin Skorsetz. As with the other two (Manu and Dimitris), we have been close friends and he has also made my life significantly easier and more pleasant.

Last but definitely not least, I am really grateful to Augusto. Not only for his scientific contribution in many of the projects I am presenting on this thesis, but for his altruistic support and the determinant "boost" he gave me, especially during the last months of my stay in Murcia.

Being part of one of the best groups in visual optics, Lo.Um, was also a motivating force that kept me moving forward. I am honestly thankful to its senior members, Juanma Bueno, Antonio Benito, Josua Fernadez, Pedro Prieto, Eloy Villegas, Silvestre Manzanera, Esther Berrio for sharing their knowledge with me, especially to those who offered me the opportunity to collaborate with them in some of their porjects.

The contribution of the newest members of LoUm was equally important for me. I am also very thankful to Adrian Gambín and Juan Mompeán, for offering very responsibly their high-quality help on software and programming-nature problems that occurred. Additionally, I would like to thank Daniel Sola, Fran Ávila, Lucia Hervella, Consuelo Robles, Javier Roca Alcaraz, Alberto de Castro, Lucie Sawides, Dibyendu Pusti and Manto Chouliara along with the former LoUm members, Benjamin Lochocki, Juan Tabernero, Guillermo Perez, Luis Blanco and Bart Jaeken for all the good times during the daily coffee brakes, long lasting trips, conferences and especially for making our weekly meetings a lot more fun.

I also feel grateful to the European commission for offering me the scholarship to complete my Ph.D. making me also part of the Marie Curie IT network, OpAl, through which I had the opportunity to know, meet and elaborate my projects and ideas some of the most important people in visual optics: Frank Schaeffel, Susana Marcos and Linda Lundstrom. Special thanks to all of my fellow Marie Curie young researchers, Ulrich Wildenmann, Yohann Benard, Simon Winter, Mengchan Sun, Yun Chen, Mohammad Fathi, Aiswaryah Radhakrishnan, Abinaya Priya Venkataraman and my beloved friend Onurcan Sahin.

Some special thanks should be specially dedicated to Carmen Martinez, the heart and many times the brain of LoUm. She was also the one who helped me "un montón" to deal with the paper work for the submission of the thesis. I need to thank also, Fina Gracia Palma and Mercedes Paredes for their continuous efforts to put an order to our daily needs in the lab.

A lot of people was also supporting me despite being a bit far from Spain. I feel very thankful to all of my friends from Greece and the rest of the world, Thanasis Pouftas and his whole family, Nikos Exelzes, Michalis Kalloudis, Kostas Efstathiou, Kostas Kouroupis, Christos and Maria Prevyzis, Lefteris Tsanakas, Vaggelis Lanaras, Thanasis Charalambidis, Giorgos Tzitzis, Giannis Tragoudas, Kostas Raptopoulos, Grigoris Kokkinos, Christoforos and Lazaros Chistoforides and the whole Christoforides family and my finally cousins Sofia, Christos and Evgenios Papafilippou.

Of course, this very last lines, should be dedicated to thank Kleoniki, my companion in life, for all the support she offered and continues to offer me.

Σας ευχαριστώ πολύ όλους, για όλα!